Chem Soc Rev

REVIEW ARTICLE

View Article Online
View Journal | View Issue

Cite this: *Chem. Soc. Rev.*, 2022, **51**, 8300

Advances in metal–organic framework-based membranes

Youdong Cheng, Shuvo Jit Datta, Sheng Zhou, Jiangtao Jia, Osama Shekhah and Mohamed Eddaoudi *

Membrane-based separations have garnered considerable attention owing to their high energy efficiency, low capital cost, small carbon footprint, and continuous operation mode. As a class of highly porous crystalline materials with well-defined pore systems and rich chemical functionalities, metal–organic frameworks (MOFs) have demonstrated great potential as promising membrane materials over the past few years. Different types of MOF-based membranes, including polycrystalline membranes, mixed matrix membranes (MMMs), and nanosheet-based membranes, have been developed for diversified applications with remarkable separation performances. In this comprehensive review, we first discuss the general classification of membranes and outline the historical development of MOF-based membranes. Subsequently, particular attention is devoted to design strategies for MOF-based membranes, along with detailed discussions on the latest advances on these membranes for various gas and liquid separation processes. Finally, challenges and future opportunities for the industrial implementation of these membranes are identified and outlined with the intent of providing insightful guidance on the design and fabrication of high-performance membranes in the future.

Received 17th May 2022

DOI: 10.1039/d2cs00031h

rsc.li/chem-soc-rev

1. Introduction

Separation processes play important roles in diversified industrial applications and our daily lives due to their major functions of concentration, purification and fractionation. Although conventional separation technologies, such as distillation, filtration, condensation, extraction, crystallization, and evaporation, can fulfil separation tasks, their disadvantages of high energy demand, large carbon footprint, and complicated operation and maintenance impede their further development for next-generation separation applications. Membrane technology, which has been shown to be promising for various separation applications, is now considered as an energy-efficient

Functional Materials, Design, Discovery and Development (FMD3), Advanced Membrane & Porous Materials Center (AMPMC), Division of Physical Sciences and Engineering, King Abdullah University of Science and Technology, Thuwal, Saudi Arabia. E-mail: mohamed.eddaoudi@kaust.edu.sa

Youdong Cheng

Youdong Cheng received his PhD degree in Chemical Engineering under the supervision of Prof. Dan Zhao from the National University of Singapore in 2019. He is now a postdoctoral fellow in Prof. Mohamed Eddaoudi's Research Group in King Abdullah University of Science and Technology (KAUST). His research focuses on the design and fabrication of MOF-based membranes for gas separation.

Shuvo Jit Datta

Shuvo Jit Datta received his MSc from Rajshahi University and PhD in Inorganic Chemistry in 2011 from Sogang University, Seoul, Korea, where he continued as a postdoctoral researcher (2011–2013) and Research Professor (2013–2017). He is currently a Staff Scientist in the Advanced Membranes and Porous Materials Center at KAUST. His research interests focus on the rational design and development of mixed matrix MOF (MMMOF) membranes for energy-efficient molecular separation.

alternative to the above-mentioned conventional separation technologies.[1–3] Membranes work as semi-permeable barriers that control the selective transport of certain components over others in a mixture system, leading to an effective separation process with low energy costs. Moreover, membranes are also well-known for their small carbon footprint, low capital investment, environmental friendliness and simple operation process, which synergistically contribute to the rapid implementation of membranes for industrial separations.

Membranes can be mainly classified into three major categories based on membrane materials, including polymeric membranes, inorganic membranes, and mixed matrix membranes (MMMs). Among these membranes, polymeric membranes are most widely used in industry due to their good solution processability, high mechanical strength, relatively low cost, and acceptable separation performance. Nevertheless, the trade-off effect between permeability and selectivity in polymeric membranes highlights that these highly selective polymeric membranes are less permeable and *vice versa*.[4,5] Moreover, polymeric membranes also face other substantial challenges, such as the limited anti-fouling ability of reverse osmosis (RO) membranes and the fast-aging process of gas separation membranes. Apart from these, polymeric membranes generally exhibit limited stability under harsh conditions (*e.g.*, high temperature or polar solvents). Therefore, the quest for other membrane materials that outperform polymers in terms of separation performance and stability is urgent and of tremendous value.

Sheng Zhou

Sheng Zhou was born in Yantai, China (1994). He obtained his bachelor's/master's degree in Chemical Engineering under the supervision of Prof. Haihui Wang from South China University of Technology in 2018, and completed his PhD degree in Chemical Science under the supervision of Prof. Mohamed Eddaoudi from King Abdullah University of Science and Technology in 2022. His research focuses on the design and synthesis of MOF-based membranes for gas separation.

Jiangtao Jia

Jiangtao Jia received his PhD degree in Inorganic Chemistry in 2014 under the supervisor of Prof. Guangshan Zhu from Jilin University. From August 2014 to August 2015, he was a postdoctoral fellow with Prof. Kimoon Kim at Pohang University of Science and Technology. In November 2015, he joined Prof. Mohamed Eddaoudi's Research Group in King Abdullah University of Science and Technology as a postdoctoral fellow (2015–2020) and a research scientist (2020–current). His current research interests focus on the design and preparation of mixed matrix membranes and pure MOF membranes.

Osama Shekhah

Osama Shekhah received his PhD in Physical and Surface Chemistry in 2001 from Freie Universität Berlin and Fritz-Haber institute MPG under the supervision of Prof. R. Schlögl. He then worked for one year as a postdoc at Fritz-Haber Institute in Berlin. In 2005 he joined the Prof. C. Wöll Physical Chemistry Group at Ruhr-Universität Bochum and in 2009 he moved to Karlsruhe Institute of Technology as a group leader. He joined Prof. Mohamed Eddaoudi's group at KAUST as a group leader in 2011, and his research interests include the growth of MOFs and COFs thin films and their various applications for separations, sensing, catalysis, and energy storage.

Mohamed Eddaoudi

Mohamed Eddaoudi was born in Agadir, Morocco. He is currently Distinguished Professor of Chemical Science and Director of the Advanced Membranes and Porous Materials Center, King Abdullah University of Science and Technology (KAUST, Kingdom of Saudi Arabia). He received his PhD degree in Chemistry from Université Denis Diderot (Paris VII), France. After postdoctoral research (Arizona State University, University of Michigan), he started his independent academic career as Assistant Professor, University of South Florida (2002), Associate Professor (2008), and Professor (2010). His research focuses on developing strategies, based on (super)-molecular building approaches (MBB, SBB, SBL), for rational construction of MOFs for energy and environmental sustainability applications.

Inorganic membranes have drawn considerable attention as promising membranes for both gas and liquid separations owing to their excellent thermal and chemical stability, good operational stability and impressive separation performance. A wide range of materials, including metals,[22] ceramics,[23] silicas,[24] carbons,[25] zeolites,[26] and metal–organic frameworks (MOFs),[27] have been processed into inorganic membranes for task-specific separation applications. Among them, MOFs have attracted much attention as membrane materials owing to their large surface area, rich chemical functionality, tunable pore system, and good thermal stability. MOF-based polycrystalline membranes have experimentally demonstrated impressive separation performance for both gas and liquid separation applications. Moreover, two-dimensional (2D) MOF membranes fabricated by the assembly of ultrathin MOF nanosheets have aroused great interest due to their ultrasmall membrane thicknesses, providing new strategies to construct high-performance membranes. Considering that 2D MOF nanosheet membranes are still in their infancy, opportunities and challenges coexist in the future development of this novel class of MOF membranes.

To overcome the shortcomings of polymeric and inorganic membranes, MMMs have been creatively proposed by incorporating organic/inorganic fillers into continuous polymeric matrixes. MMMs can demonstrate both good processability, originating from their continuous polymeric phase, and attractive separation performance originating from the dispersed filler phase. Thus far, a great number of materials, such as carbon materials,[28,29] silicas,[30] metal oxides,[31] zeolites,[32] and MOFs,[33] have been examined as filler materials in MMMs. Among them, MOFs have received tremendous attention due to their inorganic–organic hybrid nature that improves their compatibility with the polymeric phase. Their tunable pore system and rich chemical functionality offer great potential to boost the membrane selectivity through a molecular sieving effect. Moreover, the well-defined pores in MOFs can provide fast transport pathways for permeation in resultant MMMs, leading to enhanced membrane permeability. As shown in Fig. 1, tremendous efforts have been put into the design and application of MOF-based membranes for separation over the past decade. A soaring increase in the number of publications in this field over the last few years highlights the great potential of MOF-based membranes. To offer a better understanding on various types of MOF-based membranes, a brief summary on the timeline of their development for separation applications is presented in Fig. 2.

The past two decades have witnessed significant advances in the MOF field, and MOFs with new structures and novel functionalities have been applied for diversified applications. The continuous research efforts from both academia and industry facilitate the scale-up synthesis of MOFs in an economic and environmentally friendly way, leading to the commercialization of several typical MOFs.[34] Nevertheless, to the best of our knowledge, the separation applications of MOF-based membranes are still remaining in the research stage although some MOF-based membranes demonstrate excellent separation performance. Therefore, grand challenges still exist in the development of MOF-based membranes for industrial applications. Several excellent reviews have summarized the progress of MOF-based membranes for gas and liquid separations over the past few years and provided guidance on the deployment of these membranes for real-life applications.[35–40] However, with the rapid development of chemistry and materials science, novel MOF membrane design strategies, such as electrochemical synthesis for polycrystalline membranes and *in situ* filler generation for MMMs, and new membrane types, such as 2D MOF membranes, offer exciting opportunities for the design and scale-up preparation of MOF-based membranes with notable looked-for separation performances. It is therefore of great importance to provide an updated summary of the advances in this field. Herein, we present a comprehensive review of the literature on MOF-based membranes, with a special focus on membrane design strategies and state-of-the-art separation applications.

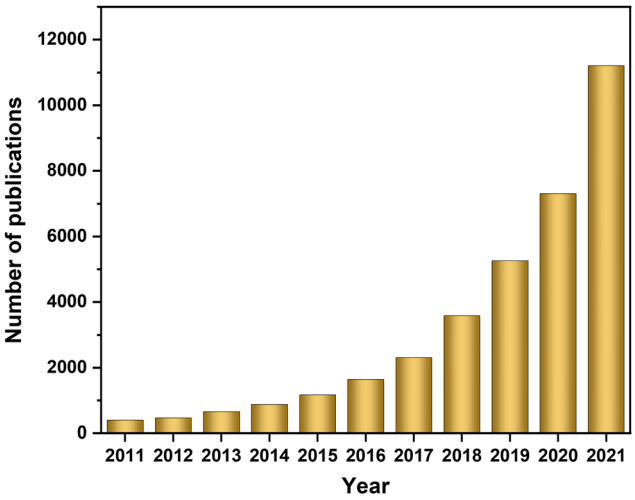

Fig. 1 The number of publications on MOF-based membranes for separation applications for the past 10 years (2011–2021). The data are retrieved from the Google Scholar website.

To facilitate our discussions and analyses, this review has been divided into three parallel sections based on membrane types, including MOF polycrystalline membranes, MOF-based MMMs and MOF nanosheet-based membranes. For the first two sections, specific membrane design strategies will be outlined, accompanied by a detailed discussion on the merits and limits of each strategy. Correspondingly, particular emphasis will be given to the latest applications of these MOF-based membranes for gas and liquid separations. For MOF nanosheet-based membranes, special attention will be given to the efforts on obtaining high-quality MOF nanosheets in both top-down and bottom-up strategies, followed by a discussion on potential applications of MOF nanosheet-based membranes with impressive separation performance. Finally, a concise perspective on opportunities and challenges toward the design of MOF-based membranes with separation performance that can meet industrial demands will be given, hoping to facilitate the implementation of these membranes for real-life applications.

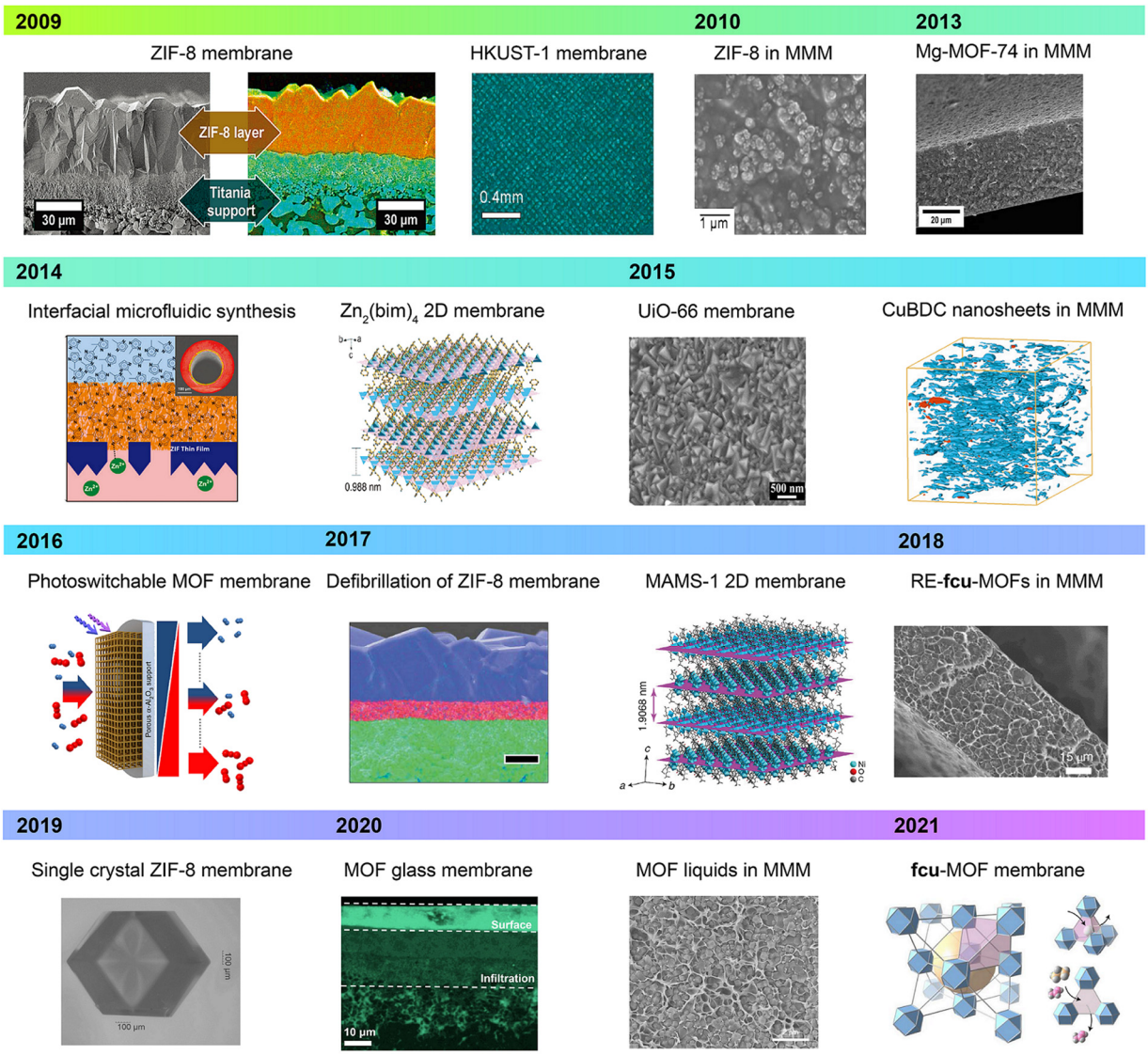

Fig. 2 A timeline for the development of MOF-based membranes for separation applications. All figures are reproduced from the literature with copyright permissions from the respective publishers. From top left: 2009 – the figure of a zeolitic imidazolate framework-8 (ZIF-8) membrane is reproduced from ref. 6, Copyright 2009 American Chemical Society; and the figure of a Hong Kong University of Science and Technology-1 (HKUST-1) membrane is reproduced from ref. 7, Copyright 2009 American Chemical Society; 2010 – the figure of ZIF-8 in MMMs is reproduced from ref. 8, Copyright 2010 Elsevier; 2013 – the figure of Mg-MOF-74 in MMMs is reproduced from ref. 9, Copyright 2013 The Royal Society of Chemistry; 2014 – the scheme of interfacial microfluidic synthesis is reproduced from ref. 10, Copyright 2014 AAAS; and the structure of a $Zn_2(bim)_4$ MOF is reproduced from ref. 11, Copyright 2014 AAAS; 2015 – the figure of a UiO-66 membrane is reproduced from ref. 12, Copyright 2015 American Chemical Society; and the figure of copper 1,4-benzene dicarboxylate (CuBDC) nanosheets in an MMM is reproduced from ref. 13, Copyright 2015 Nature Publishing Group; 2016 – the schematic illustration of a photoswitchable MOF membrane is reproduced from ref. 14, Copyright 2016 Nature Publishing Group; 2017 – the figure of a ZIF-8 membrane is reproduced from ref. 15, Copyright 2017 AAAS; and the crystal structure of Mesh Adjustable Molecular Sieve-1 (MAMS-1) is reproduced from ref. 16, Copyright 2017 Nature Publishing Group; 2018 – the figure of a face-centered cubic topology (RE-**fcu**-MOFs) in an MMM is reproduced from ref. 17, Copyright 2018 Nature Publishing Group; 2019 – the figure of a single crystal ZIF-8 membrane is reproduced from ref. 18, Copyright 2019 Elsevier; 2020 – the figure of a MOF glass membrane is reproduced from ref. 19, Copyright 2020 Wiley-VCH; and the figure of MOF liquids in MMM is reproduced from ref. 20, Copyright 2020 Nature Publishing Group; 2021 – the figure of an **fcu**-MOF membrane is reproduced from ref. 21, Copyright 2021 Nature Publishing Group.

2. MOF polycrystalline membranes

2.1 Membrane fabrication strategies

Membranes with well-intergrown MOF crystals as selective layers are entitled as MOF polycrystalline membranes. MOF polycrystalline membranes often exhibit impressive separation performance for diversified applications owing to their high porosity and well-defined pore-aperture sizes. Nevertheless, it remains a grand challenge to develop compact and defect-free MOF polycrystalline membranes on porous supports. The existence of intercrystalline defects will largely undermine the intrinsic separation performance of MOF polycrystalline

membranes and sometimes can even render these membrane nonselective.[41] Therefore, tremendous efforts and remarkable advances have been made towards the development of various membranes fabrication methods during the last decade, enabling the preparation of MOF polycrystalline membranes with minimized defects. Moreover, due to the large variety of MOF structures and their synthetic conditions, each of the established membrane preparation methodologies is indispensable and can be applied in different scenarios. Additionally, it is of great importance to improve the adhesion/bonding between the MOF selective layer and the porous support to ensure the good mechanical stability of the resultant membranes. In the following sections, we will briefly describe different methodologies that have been developed and rationalized for the fabrication of high-quality MOF polycrystalline membranes.

2.1.1 *In situ* solvothermal growth. As a mimic of the growth of MOF crystals, *in situ* solvothermal growth of polycrystalline membranes usually requires identical conditions to those used for MOF crystallization. With the immersion of porous supports inside the precursor solution, heterogeneous nucleation happens on the support surface, and thus the growth of MOF layers continues. It is worth noting that the *in situ* solvothermal growth is applicable to a wide variety of MOF membranes. For example, Liu *et al.* applied the *in situ* solvothermal method to grow the MOF-5 membrane on a porous alumina support, which is now regarded as the first reported continuous MOF polycrystalline membrane.[42] Moreover, the first highly water-stable UiO-66 membranes on alumina supports were prepared by *in situ* solvothermal growth in 2015.[12] Despite the several examples of success, direct growth of continuous, crack-free MOF layers on bare, unmodified supports remains challenging due to insufficient nucleation sites on the support surface. One effective solution is to deliberately modify the substrates prior to the solvothermal growth in order to promote and enhance the heterogeneous nucleation. Moreover, an essential understanding towards the nature of MOFs allows researchers to design different strategies, such as metal-targeted modification and ligand-targeted modification, to grow defect-free MOF polycrystalline membranes on various supports, which will be described in the following part.

As a class of hybrid materials comprising metal nodes and organic linkers, MOFs tend to grow on the top of the support when the interactions between the support surface and MOF building blocks are promoted. Metal-targeted modification has been proven to be useful in enhancing these interactions. This strategy involves the use of organic modifiers encompassing preselected functional terminal moieties that can eventually attract metal ions in the MOF precursor solution, which will boost the nucleation and growth of MOF crystals on supports. One typical example is the preparation of ZIF-90 membranes by using 3-aminopropyltriethoxysilane (APTES) as an organic, metal-targeted modifier (Fig. 3a).[43] The ethoxy end groups of APTES first reacted with hydroxyl groups on the alumina surface to form a monolayer, allowing other terminal amino groups to point to the precursor solution. In the course of the membrane growth, the aldehyde groups from ligands would react with these amino groups *via* imine condensation to form a ligand layer on the support surface. This ligand layer attracted metal ions in the solution and promoted the nucleation and crystallization of ZIF-90. Continuous ZIF-90 membranes were obtained by *in situ* solvothermal growth at 100 °C for 18 hours, with a thickness of around 20 μm. Another versatile platform for metal-targeted modification is polydopamine,[45] which exposes sufficient amounts of surface hydroxyl groups that can actively coordinate with metal ions. The polydopamine modification is applicable to various MOF membranes, such as ZIF-8,[45] ZIF-90,[45] ZIF-100,[46] and Materials Institute Lavoisier-160 (MIL-160).[47]

Another strategy to enhance the interaction between MOF crystals and the support is ligand-targeted modification. This strategy involves the use of inorganic modifiers encompassing the same type of metal ion with targeted MOFs. The porous

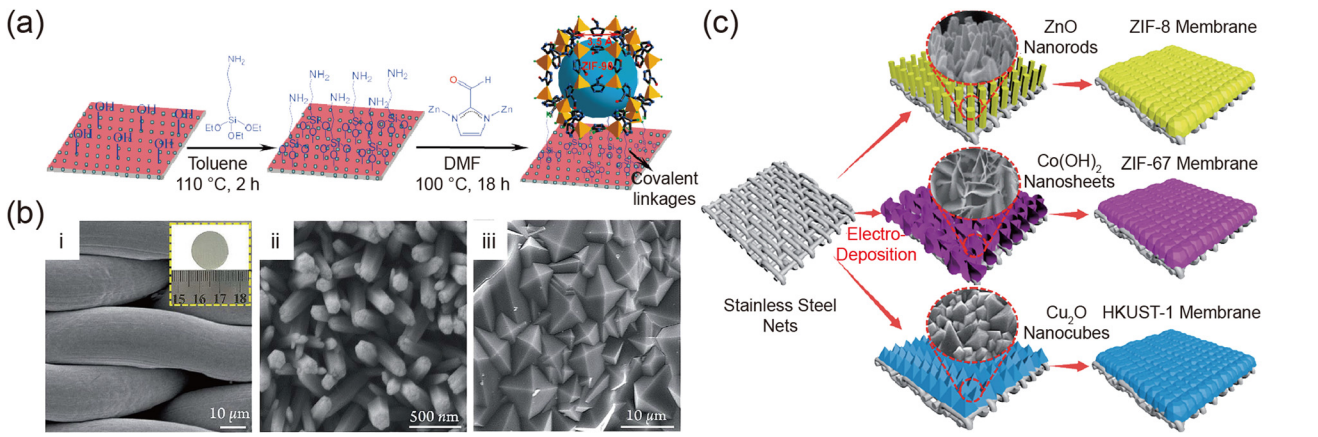

Fig. 3 (a) Schematic illustration of the preparation of ZIF-90 membranes by using APTES as a covalent linker. (b) Microstructure images of (i) bare stainless-steel nets; (ii) ZnO nanorods; and (iii) the ZIF-8 membrane. (c) Schematic illustration of the preparation of different MOF polycrystalline membranes on supports modified by electrodeposition. Reprinted with permission from ref. 43. Copyright 2010 American Chemical Society, ref. 44. Copyright 2017 The Royal Society of Chemistry, respectively.

support is pre-treated with these inorganic modifiers that can actively interact with MOF ligands from the precursor solution. Therefore, the nucleation and growth of MOF crystals on the support surface is largely promoted. By introducing inorganic modifiers containing Zn^{2+}, Co^{2+}, and Cu^{2+} ions, ZIF-8, ZIF-67, and HKUST-1 membranes could be successfully prepared on supports, respectively (Fig. 3b and c).[44] Specifically, inexpensive stainless-steel net supports were coated with ZnO nanorods, $Co(OH)_2$ nanosheets and Cu_2O nanocubes by electrodeposition. These coating materials would offer active sites for the crystallization and growth of continuous ZIF-8, ZIF-67 and HKUST-1 membranes *via* an *in situ* growth strategy.

In situ solvothermal growth is the most straightforward route to prepare MOF polycrystalline membranes, and it has been widely proven to be successful in obtaining a large number of high-quality MOF polycrystalline membranes. Nevertheless, from the perspective of engineering, it is challenging to use this strategy to mass-produce large-area MOF polycrystalline membranes due to the limitations of membrane growth reactors, a slow membrane growth process, and harsh synthesis conditions.

2.1.2 Seed-assisted secondary growth. *In situ* solvothermal growth usually results in relatively thick membrane layers (*e.g.*, >1 μm) due to the low concentration of nucleation sites. These thick MOF polycrystalline membranes often exhibit limited gas/liquid permeance owing to their large transport resistance. Consequently, another strategy known as seed-assisted secondary growth has been developed to fabricate MOF polycrystalline membranes with reduced membrane thicknesses. In a typical seed-assisted secondary growth process, MOF seed crystals are first introduced on the top of porous supports. Subsequently, these seeded supports are immersed in the MOF mother solution for a secondary growth. Notably, an appropriate seeding strategy can provide uniformly distributed seeds on the support surface to offer abundant nucleation sites for the growth of homogeneous and continuous MOF polycrystalline membranes.

Traditional seeding procedures, such as manually rubbing and dip-coating, have been proven to be effective for the fabrication of high-quality MOF polycrystalline membranes. Li *et al.* adopted a dip-coating method to transfer ZIF-7 nanoseeds onto a porous support and prepared ZIF-7 membranes with a thickness of 1.5 μm by a microwave-assisted solvothermal secondary growth approach.[50] Interestingly, applying the same concept to ZIF-8 membranes resulted in continuous ZIF-8 layers with preferred orientation, which could be explained with the van der Drift competitive growth model induced by the enhanced concentration of nucleation sites from seeding layers.[51]

The quality of the seeding layer is also vital to the membrane structure and the seeds should be anchored firmly on the supports. The use of a crosslinking agent, such as polyethylenimine (PEI), has been shown to be useful in promoting interactions between MOF seeds and porous supports. PEI may form hydrogen bonds with both organic linkers in MOF seeds and free functional groups (*e.g.*, hydroxyl groups) on the support surface. As a result, different MOFs, including Cu-MOF,[52] ZIF-7,[50,53] and ZIF-8,[51] have been made into polycrystalline membranes by using PEI as the crosslinking agent.

Recently, He *et al.* developed an electrophoretic method to produce nanoseeds in several minutes, which is much faster than previous routes (Fig. 4a).[48] Dense and continuous MOF membranes could be obtained based on these nanoseeds with an ultrathin thickness (*e.g.*, 500 nm). These MOF membranes could be synthesized on various supports, including anodic aluminium oxide (AAO), porous polyacrylonitrile, nanoporous carbon, and even graphene (Fig. 4b). Another advantage of seed-assisted secondary growth is the straightforward orientation control over membranes by controlling the orientation of seeding layers, which can be helpful for MOFs with one dimensional (1D) pores or channels. For example, Sun *et al.* developed a dynamic air–liquid interface-assisted self-assembly strategy to prepare oriented MIL-125-NH_2 nanoseed monolayers (Fig. 4c).[49] Subsequently, a secondary growth was used to heal intercrystalline defects and prepare highly oriented polycrystalline membranes (Fig. 4d).

Seed-assisted secondary growth is a delicate strategy for the fabrication of MOF polycrystalline membranes, but its procedures are more intricate than *in situ* solvothermal growth. Typically, nano-sized MOF crystals are required to get a good seeding layer, which may be problematic for some MOFs that are only reported as large crystals in the literature. Similar to *in situ* solvothermal growth, seed-assisted secondary growth is a powerful tool for academic exploration of certain MOF polycrystalline membranes. Nevertheless, it still remains a grand challenge to directly apply this strategy to produce large-area membranes with good quality.

2.1.3 Counter-diffusion growth. Counter-diffusion growth is a relatively mild route to fabricate polycrystalline membranes based on interfacial engineering. The metal sources and ligand sources are provided separately from two opposite sides of the porous support. It is worth mentioning that the MOF layer growth happens on one side of the support, which can be, in general, controlled by adjusting the reagent concentrations.

Yao *et al.* reported the first example of ZIF-8 films on nylon supports by the counter-diffusion concept, which was named the contra-diffusion method in their report.[57] A homemade H-shaped cell was used, and the porous support was fixed in the middle of the cell. The metal solution and ligand solution were introduced from one side of the H-shaped cell, respectively, and would diffuse to the other side, driven by the concentration gradient. The porous support in the middle provided an interface for the reaction of two precursors to produce MOF films. However, membrane-quality layers could not be obtained on bare supports. A subsequent study from the same group demonstrated that the pre-treatment of supports by introducing seeds or extra nucleation sites was helpful to get high-quality ultrathin ZIF-8 membranes.[58]

To apply the counter-diffusion concept to hollow fiber supports, Brown *et al.* developed an interfacial microfluidic membrane processing (IMMP) method by dissolving metal salts and ligands in two immiscible solvents, respectively, and pumping them into the core or shell side of the hollow fiber

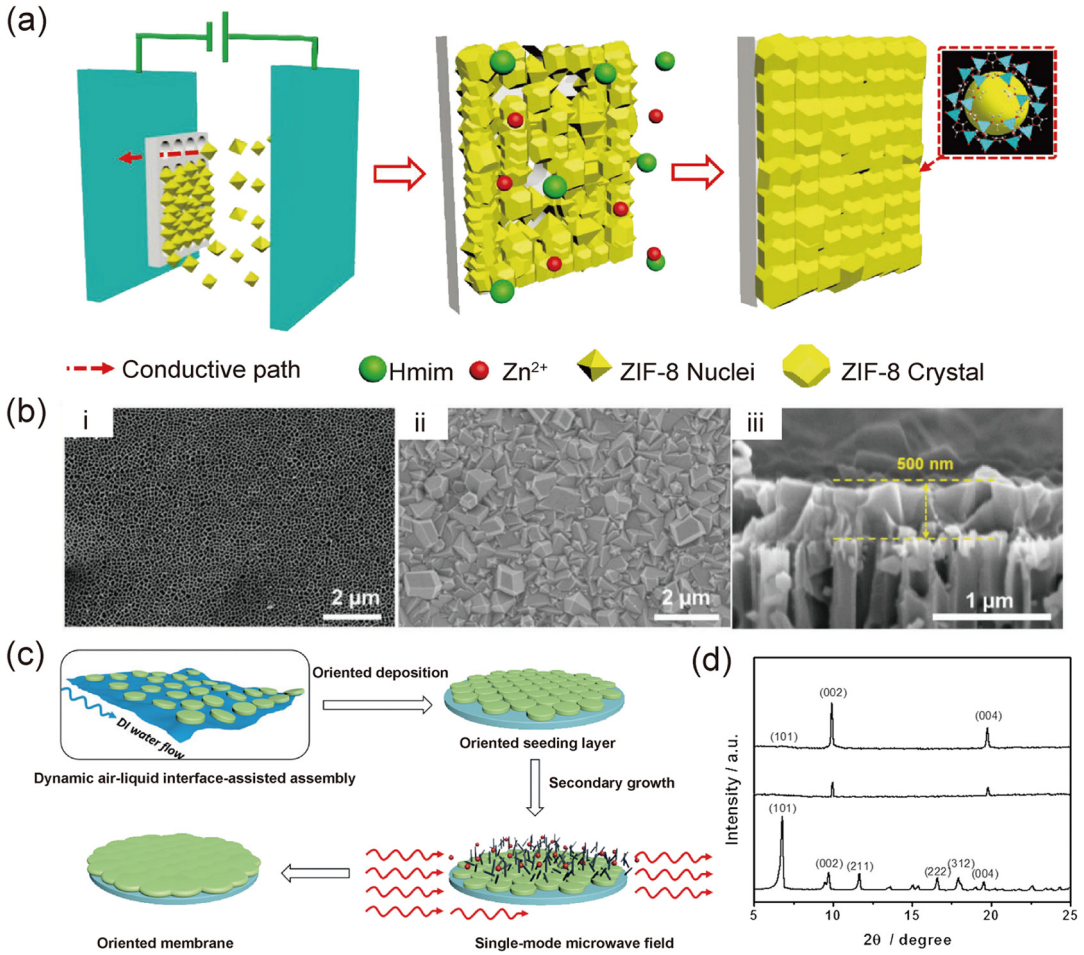

Fig. 4 (a) Schematic illustration of the preparation of nanoseeds by electrophoretic deposition and MOF membranes on various supports. (b) Surface/cross-sectional morphologies of (i) an AAO support and (ii and iii) a ZIF-8/AAO membrane. (c) Schematic illustration of the preparation of highly c-oriented MIL-125-NH_2 membranes. (d) X-ray diffraction patterns of MIL-125-NH_2 powder (bottom), a MIL-125-NH_2 seed layer (middle), and a MIL-125-NH_2 membrane (top). Reprinted with permission from ref. 48. Copyright 2018 Wiley-VCH, ref. 49. Copyright 2018 Wiley-VCH, respectively.

support, respectively.[10] Similar to the mechanism of the above-mentioned reports, the diffusion of the two precursors allowed them to meet at the support interface and form MOF membranes on the support surface.

Counter-diffusion growth is considered as an important technical improvement for the fabrication of MOF polycrystalline membranes with thinner thicknesses. The IMMP method also sheds light on mass membrane production. However, the versatility of this strategy for the preparation of different MOF polycrystalline membranes remains unclear, as indicated by the fact that most of the reported examples are based on ZIF-8 membranes. For other types of MOFs that require relatively harsh synthesis conditions (*e.g.*, high temperature and high pressure), the application of counter-diffusion growth to fabricate good membranes may be challenging. Consequently, continuous efforts are still needed to explore the applicability of this strategy for the fabrication of more MOF polycrystalline membranes.

2.1.4 Layer-by-layer growth. Layer-by-layer (LBL) growth, also known as liquid phase epitaxy growth, is a useful method for the preparation of MOF films and membranes. In a typical LBL growth process, the support surface is alternatively exposed to MOF precursor solutions with a rinsing step in between to remove excess/unreacted precursors. This unique approach offers the opportunity to accurately adjust membrane growth parameters, such as precursor concentrations and the number of growth cycles, enabling precise control over the membrane thickness.

Our group demonstrated the first successful example of homogeneous, continuous ZIF-8 membranes using the LBL approach, and the membrane thickness was determined by the number of growth cycles.[61] For instance, 150 and 300 growth cycles led to membranes with thicknesses of ~0.5 μm and ~1.6 μm, respectively. Moreover, these growth cycles could be performed using programmed machines, making the entire membrane fabrication process easy and convenient. For instance, Hurrle *et al.* combined the LBL concept with the automated spraying technique with moving spray nozzles (Fig. 5a),[54] overcoming the limitations on the reactor scale and thus enabling the preparation of large-area membranes.

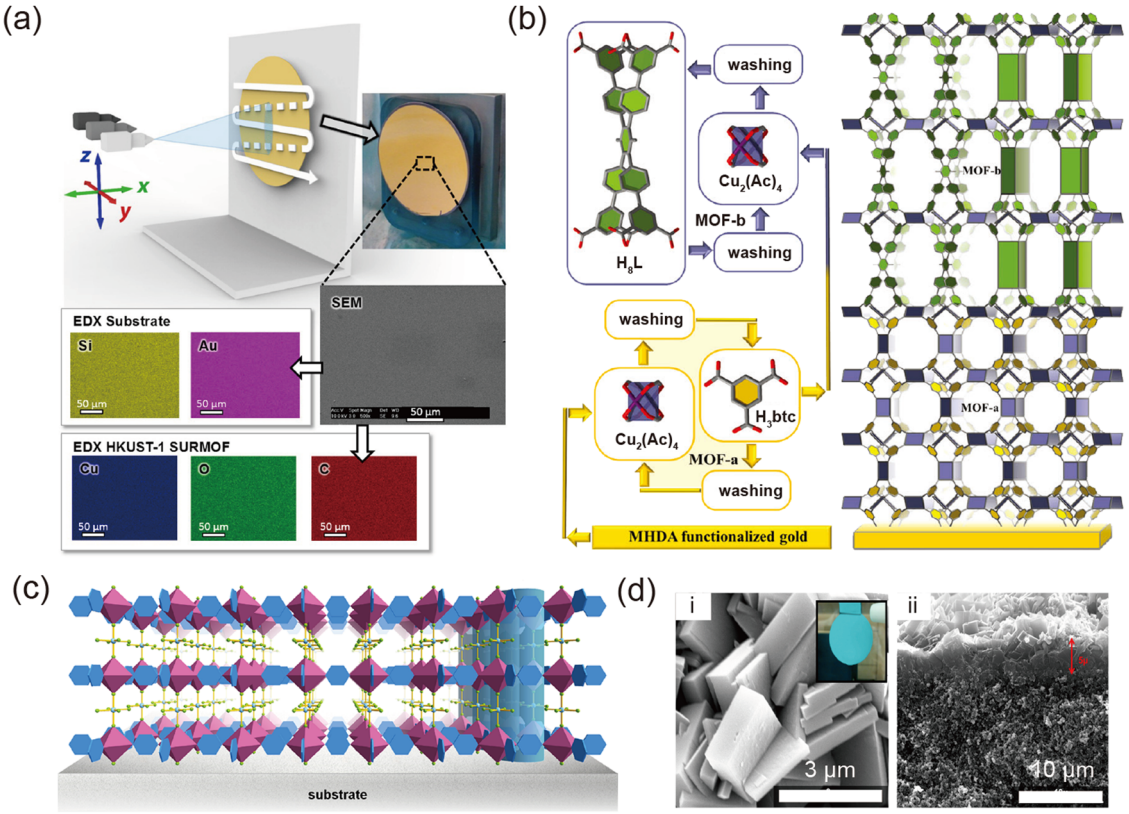

Fig. 5 (a) Schematic illustration of the preparation of MOF films/membranes by the LBL concept with the automated spraying technique. (b) Schematic illustration of the preparation of ordered hierarchical tbo-type MOF films. (c) Scheme of a **SIFSIX**-3 membrane on a substrate. (d) Microscopy images of a **SIFSIX**-3-Ni membrane, (i) top view, (inset) optical image of the membrane, and (ii) cross-section. Reprinted with permission from ref. 54. Copyright 2017 Wiley-VCH, ref. 55. Copyright 2017 The Royal Society of Chemistry, ref. 56. Copyright 2020 American Chemical Society, respectively.

As a deliberately designed process for membrane growth, the LBL approach permits fine control over the orientation of MOF layers by modifying the support with self-assembled monolayers (SAMs) encompassing different terminal groups. Our group reported the first (110)-oriented ZIF-8 thin films *via* the LBL approach on OH-terminated SAM modified substrates.[62] The same concept was further extended to prepare ordered hierarchical **tbo**-type MOF films, and the preformed orientation was maintained in heterostructured layers (Fig. 5b).[55] Moreover, the LBL approach can be coupled with the Langmuir–Blodgett or Langmuir–Schaefer method to prepare ultrathin MOF films with the preferred orientation.[63,64] Synchrotron X-ray diffraction measurements validated the high crystallinity of the as-prepared MOF films in both the in-plane and out-of-plane orientations. These seminal contributions provide insightful guidance on the rational preparation of MOF polycrystalline membranes with desired orientations for separation applications.

Our group successfully reported the fabrication of **SIFSIX**-3-M (M = Ni or Cu) membranes as highly CO_2 selective MOF membranes for CO_2/H_2 separation (Fig. 5c).[56] By alternatively immersing the support into the pillar salt solution and the ligand solution for 30 cycles, a continuous **SIFSIX**-3-Ni or **SIFSIX**-3-Cu membrane could be obtained (Fig. 5d).

The LBL growth approach represents one of the most promising methods for the scale-up production of MOF polycrystalline membranes. The whole membrane growth process can be completed using automated machines using this approach. One major challenge that restricts the further development of this approach is that large amounts of organic solvents are consumed during the membrane growth process, suggesting to some extent a plausible increase in the membrane production cost. Another issue is that the LBL growth approach is hardly practicable for those MOFs that need to be synthesized under harsh conditions (*e.g.*, high temperature and high pressure). One possible solution can be the design of temperature- and pressure-controlled apparatus, which may require collaborative efforts from chemists, materials scientists, and chemical engineers.

2.1.5 Solvent-free conversion. The use of organic solvents during the growth of MOF polycrystalline membranes not only increases the capital cost, but also generates large amounts of waste that are harmful to the environment. In the MOF community, several solvent-free methods have been proposed for the mass production of MOFs in a green pathway.[34] Similarly, considerable efforts have been devoted to the solvent-free fabrication of MOF polycrystalline membranes. One widely explored solvent-free membrane fabrication method is to coat reactive metal precursors on the support surface in the first step. Next, the resultant support is exposed to melted or vaporized ligands to afford well-intergrown MOF membranes.[66]

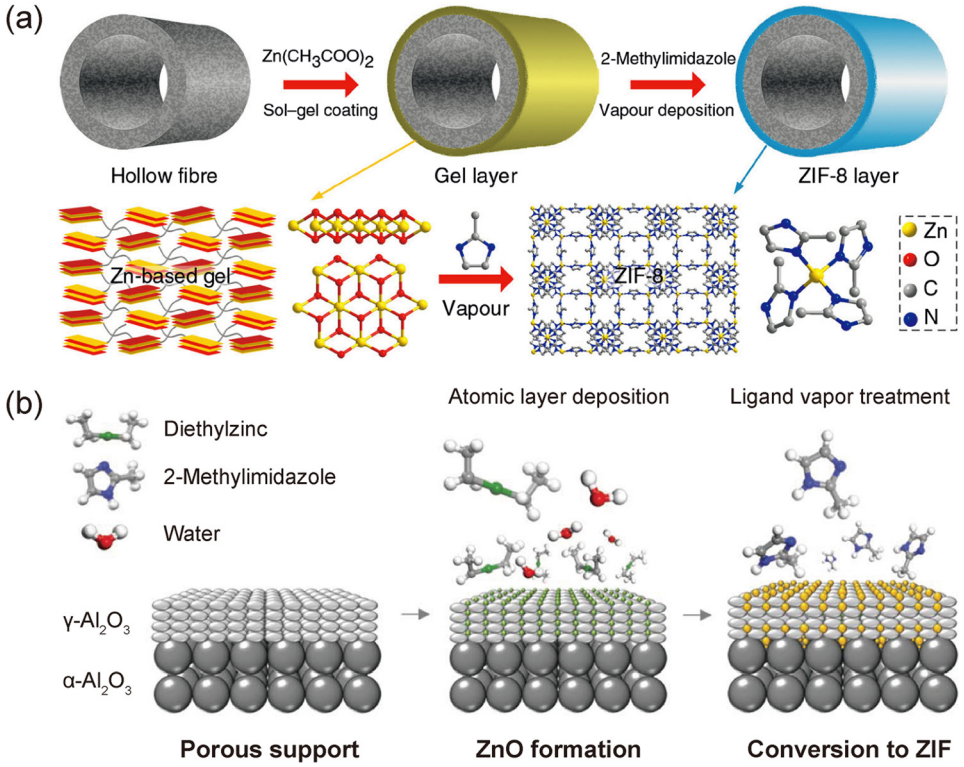

Fig. 6 (a) Schematic illustration of the preparation of ZIF-8 membranes by a gel-vapor deposition method. (b) Schematic illustration of the preparation of ZIF membranes by a solvent-free conversion method. Reprinted with permission from ref. 59. Copyright 2017 Nature Publishing Group, ref. 60. Copyright 2018 AAAS, respectively.

Li *et al.* demonstrated a gel-vapor deposition method for the fabrication of ZIF-8 membranes on a hollow fiber support, where the support was first coated with gels containing metal sources.[59] Subsequently, the resultant support was placed together with the ligand powder in an autoclave. During the heating process, the ligand powder vaporized and reacted with metal salts in gels, leading to the formation of continuous ZIF-8 layers (Fig. 6a). Notably, the layer thickness could be controlled by varying the reaction time and the gel concentration.

Previous strategies towards the fabrication of MOF membranes mainly focus on preventing the penetration of MOF powders into pores of the porous support, enabling the formation of continuous MOF membranes only on the support surface. Ma *et al.* presented a different approach for the fabrication of high-quality ZIF-8 membranes (Fig. 6b).[60] In their report, the pores in the support were first filled with nonporous ZnO *via* atomic layer deposition (ALD), after which the support was placed with the ligand powder in autoclaves. The ligand powder vaporized and reacted with the ZnO to form porous ZIF-8 crystals at high temperatures. As a result, the pores in the support were reopened and allowed gas molecules to permeate.

Compared with conventional solvothermal strategies, the solvent-free conversion strategy is more environmentally friendly and promising for the mass production of MOF polycrystalline membranes. However, this method has only been explored on ZIF membranes, mainly ZIF-8 membranes. To promote the vaporization of the ligand, the whole reaction system should be heated to high temperatures. Even though the melting point of the ligand for ZIF-8 is relatively low, the autoclaves still need to be heated above 125 °C. For other ligands with higher melting points, the required temperature should be much higher.[67]

2.1.6 Fast current-driven synthesis. Fast current-driven synthesis (FCDS) is an emerging interdisciplinary strategy for the fabrication of MOF polycrystalline membranes, where electrochemical principles are employed as efficient tools for promoting the ligand deprotonation process, thus boosting the formation of continuous MOF selective layers in an extremely short period of time. Conventional methods to promote reactions between metal ions and deprotonated ligands rely on increasing the ligand/metal ratio or heating solvents to generate bases. This FCDS strategy offers another route for the ligand deprotonation by external electrons. The unique current-driven growth process permits the realization of continuous MOF membranes composed of ultrathin defect-free layers due to the self-healing and self-inhibited growth characteristics of this method.

In 2018, Zhou *et al.* reported the first example of current-driven synthesis of ZIF-8 membranes within 20 minutes at room temperature (Fig. 7a).[65] A two-electrode system based on an H-shaped electrolytic cell was used for the membrane growth, where the conductive porous support worked as the cathode and the carbon rods worked as the counter electrode.

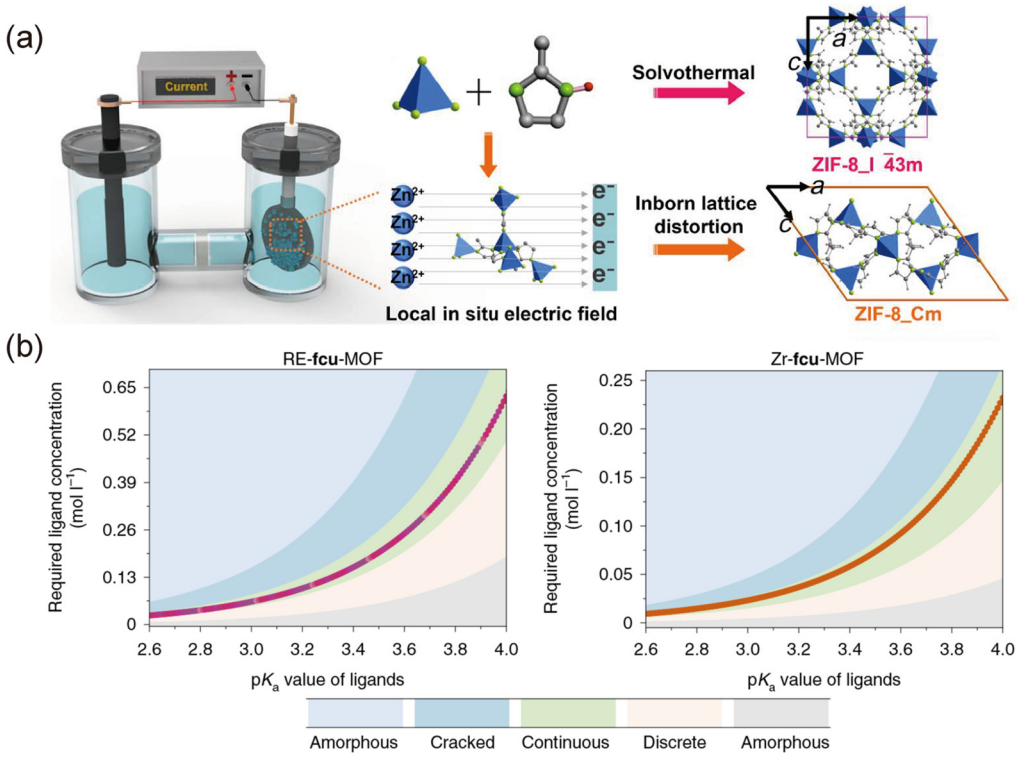

Fig. 7 (a) Schematic illustration of the synthesis of ZIF-8 membranes by the FCDS strategy (left) and different phases for membranes obtained by different membrane fabrication strategies (right). (b) Guidelines that permit the discovery of optimal conditions for synthesis of continuous **fcu**-MOF membranes. Reprinted with permission from ref. 65. Copyright 2018 AAAS, ref. 21. Copyright 2021 Nature Publishing Group, respectively.

During the membrane growth process, Zn^{2+} ions were attracted by the electric field to move towards the cathode and accumulated at the support surface. Meanwhile, the ZIF-8 ligands were deprotonated quickly by the external current. Consequently, the deprotonated ligands with negative charges immediately reacted with Zn^{2+} ions to form ZIF-8 crystals at the support surface. This process enables the self-elimination of defects to afford high-quality membranes, because any existing defects will expose the bare and conductive areas of supports to the precursor solution, which can allow the further formation of ZIF-8 crystals at these bare locations. Moreover, due to the insulating properties of ZIF-8, the well-intergrown ZIF-8 membrane will hinder the contact between external electrons (on the support) and precursors, thus preventing the further increase of the membrane thickness. Therefore, ultrathin ZIF-8 membranes could be easily obtained even under a prolonged reaction time.

Recently, our group pioneered the electrochemical synthesis of a series of defect-free **fcu**-MOF polycrystalline membranes with molecular sieving abilities for hydrocarbon separations.[21] We discovered that the use of pre-assembled hexanuclear clusters and the continuous supply of deprotonated organic linkers during the membrane growth process play pivotal roles in producing high-quality **fcu**-MOF membranes. Importantly, guidelines that facilitate the discovery of good conditions for synthesis of continuous and well-intergrown **fcu**-MOF membranes were proposed and proved to be successful in this study (Fig. 7b). Moreover, our group extended this strategy to mixed-linker MOF polycrystalline membranes based on fumarate (fum) and mesaconate (mes) linkers with an irregular pore shape effective for nitrogen removal from raw natural gas.[71] Ultrathin (~30 nm) MOF membranes with varying fum to mes ratios could be prepared on AAO and carbon nanotube (CNT)-modified stainless steel net supports. Two-dimensional magic-angle spinning solid-state nuclear magnetic resonance (NMR) results confirmed the co-existence of two types of linkers within one window of the MOF structure in the resultant membranes. Impressively, owing to the rigid structure of the framework, the optimized membrane demonstrated outstanding and stable nitrogen rejection performance even after a continuous permeation test over 150 days. This work will definitely inspire the design and fabrication of MOF polycrystalline membranes with intricate structures for challenging separations in the future.

The FCDS strategy is facile for the fabrication of MOF polycrystalline membranes in a short period of time, representing a new route to use electricity as the driving force for membrane growth. It shows great promise for large-scale membrane production, because it is applicable on various commercially available and cheap supports, such as stainless-steel nets and nickel foams.[65] Moreover, this ultrafast membrane fabrication process can also provide a convenient platform for the replacement or repair of damaged membranes in industry.

2.1.7 Membrane post-modification. Post-modification of MOF polycrystalline membranes is considered as an effective

route to improve the membrane separation performance. It provides a powerful tool for sealing defects in membranes, leading to greatly enhanced membrane separation performance. To be specific, it is quite challenging to directly grow defect-free MOF polycrystalline membranes. Nevertheless, the existence of intercrystalline defects can severely deteriorate the membrane selectivity. It is therefore of great importance to develop some post-modification approaches to seal these defects. Polymer coating represents a good post-modification strategy to achieve this goal. Sheng *et al.* demonstrated that by coating dimethylsiloxane (PDMS), poly(1-trimethylsilyl-1-propyne) (PTMSP) or polymer of intrinsic microporosity-1 (PIM-1) on the top of defective ZIF-8 membranes, they could achieve a more than tenfold increase in the membrane propylene/propane (C_3H_6/C_3H_8) selectivity.[41] Recently, Wu *et al.* reported that the polydopamine layer deposited on defective UiO-66 membranes was helpful to improve the membrane separation performance (Fig. 8a).[68] Polydopamine could penetrate into nano-sized pinholes and grain boundary voids in defective UiO-66 membranes, therefore efficiently sealing these defects and enhancing the membrane selectivity.

For MOF polycrystalline membranes without noticeable intercrystalline defects, their structures can still be further post-modified in order to enhance their separation capability. Lee *et al.* reported a ligand exchange strategy for the post-modification of continuous ZIF-8 membranes.[69] In their report, the ligands of ZIF-90 (imidazole-2-carbaldehyde) with a smaller bulkiness were employed to partially replace the ligands of ZIF-8 (2-methylimidazole) to effectively enlarge the aperture size of the resultant membranes (Fig. 8b). The ligand exchange process mainly happened at the membrane top layer, while the bottom ZIF-8 layer still demonstrated a good C_3H_6/C_3H_8 separation ability. Due to relatively larger pore-aperture size of ZIF-90, the resultant membranes showed decreased gas transport resistance and a largely increased C_3H_6 permeance, with a slightly decreased C_3H_6/C_3H_8 selectivity. Similarly, ZIF-94 polycrystalline membranes with abundant aldehyde groups in MOF linkers can be post-functionalized with long-chain amines.[72] This aldehyde–amine condensation process can partially change the MOF membrane from the **sod** structure to a less dense **rho** structure with a larger window size. Consequently, the amine-functionalized membrane showed a largely increased CO_2 permeability and a slightly reduced CO_2/CH_4 selectivity.

Post-modification has also been identified to be able to hinder the linker mobility in MOF membranes and further improve the membrane sieving ability. For example, a polymer-coated UiO-66 polycrystalline membrane showed much higher gas selectivity compared to a pristine UiO-66 membrane.[73] A closer examination by ^{2}H NMR spectroscopy revealed that when UiO-66 crystals were wrapped with polymers, the 2-site 180° flips (π-flips) of their aromatic ring would be hindered.[74] This provides strong evidence on the restricted linker mobility in MOF polycrystalline membranes induced by the polymer coating. Recently, Babu *et al.* also reported that a quick heat treatment to ZIF-8 membranes would result in restricted lattice flexibility and thus an enhanced gas sieving ability (Fig. 8c and d).[70] Notably, this facile heat treatment process could be finished within a few seconds.

Despite the effectiveness in improving the membrane sieving ability, post-modification is hardly to be considered as the first choice for membrane design. This strategy requires extra procedures and sometimes can be time-consuming. Moreover,

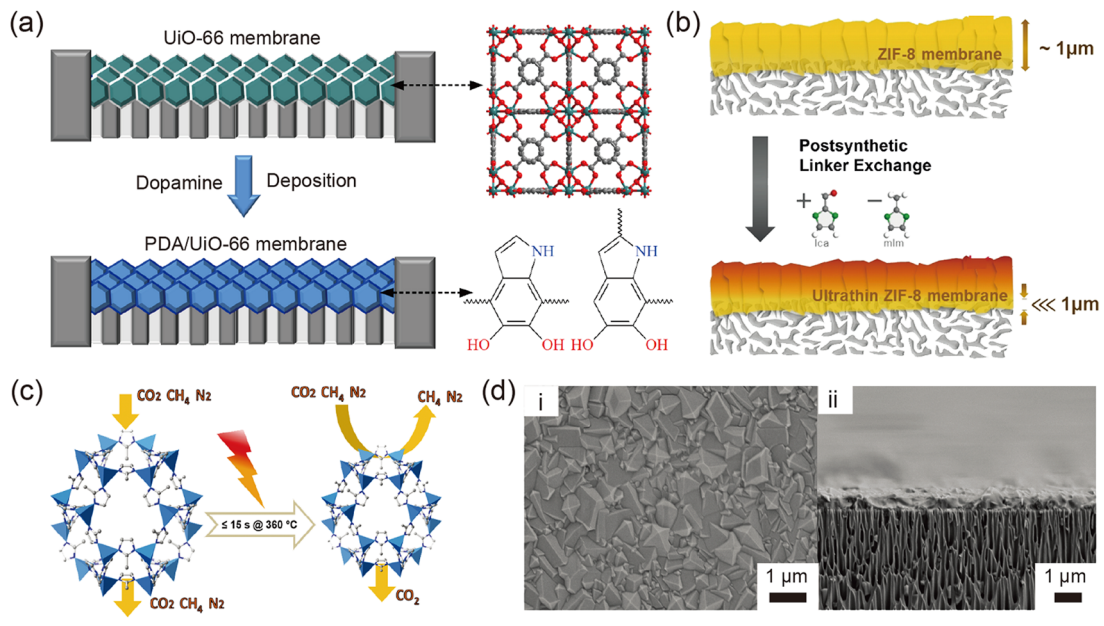

Fig. 8 Schematic illustration of the post-modification of (a) the UiO-66 membrane with polydopamine, (b) the ZIF-8 membrane by a ligand exchange strategy, and (c) the ZIF-8 membrane by the quick heat treatment process. (d) SEM images of ZIF-8 membranes – (i) top view and (ii) cross-sectional view. Reprinted with permission from ref. 68. Copyright 2019 American Chemical Society, ref. 69. Copyright 2018 Wiley-VCH, ref. 70. Copyright 2019 Wiley-VCH, respectively.

Table 1 Comparison of main strategies for the fabrication of MOF polycrystalline membranes

Fabrication strategy	Advantages	Disadvantages	Typical MOF types	Membrane thickness	Common support types
In situ solvothermal growth	• Straightforward synthesis procedure • Applicable to many MOFs	• Slow membrane growth rate • Harsh synthesis conditions	ZIFs, MILs, MOF-5, UiO-66, *etc.*	1–30 μm	α-Al_2O_3
Seed-assisted secondary growth	• Beneficial for the formation of continuous membranes • Better control on membrane orientation	• Demand on high-quality MOF seeds • High membrane fabrication costs	ZIFs, MILs	0.5–12 μm	α-Al_2O_3
Counter-diffusion growth	• Allow the self-elimination of defects • Suitable for large-scale production of membranes (IMMP)	• Mainly limited to ZIFs • Lack of precise control on membrane thickness	ZIFs	0.1–20 μm	α-Al_2O_3, polymer
Layer-by-layer growth	• Precise control on membrane thickness and orientation • Can be completed using automated machines	• Limited to MOFs synthesized at room temperature • Consume large amounts of solvents	ZIF-8, HKUST-1, **SIFSIX**-3-Ni	0.5–5 μm	α-Al_2O_3
Solvent-free conversion	• Avoid using organic solvents • Enable the fabrication of ultrathin membranes	• Mainly limited to ZIFs	ZIFs	50–100 nm	α-Al_2O_3, polymer
Fast current-driven synthesis	• Fast membrane growth rate • Enable the fabrication of ultrathin membranes	• Need a conductive support	ZIFs, Zr-**fcu**-MOF	30–200 nm	AAO
Membrane post-modification	• Produce membranes with improved quality	• High membrane fabrication cost • High operational complexity	ZIFs, UiO-66	0.8–2 μm	α-Al_2O_3, AAO

in some cases, post-modification can lead to an obvious decrease in membrane permeance, which may largely undermine the potential of the resultant membranes for industrial applications.

2.1.8 Other strategies. The design or fabrication strategies for MOF polycrystalline membranes are far beyond what we have listed above, and there are also a number of less commonly used but still effective methods, such as spin coating, rapid thermal deposition, and microfluidic growth. Specifically, our group reported the spin coating method for the fabrication of various MOF polycrystalline membranes based on the LBL concept, which could help to greatly reduce the consumption of chemicals and solvents.[75] Moreover, Hou *et al.* also demonstrated the fabrication of ZIF-8/g-C_3N_4 hybrid membranes by the spin coating approach.[76] G-C_3N_4 nanosheets functioned as good hosts to immobilize Zn^{2+} *via* coordination interactions. During the membrane fabrication process, the Zn^{2+}/g-C_3N_4 nanosheet suspension and the ligand (2-methylimidazole) solution were alternatively spin coated on the porous support, which promoted the *in situ* formation of ZIF-8 crystals on g-C_3N_4 nanosheets and eventually the growth of continuous ZIF-8 membranes. Shah *et al.* developed a rapid thermal deposition approach to fabricate MOF polycrystalline membranes, where the porous support was soaked in the MOF precursor solution and subjected to thermal treatment at elevated temperatures.[77] Microfluidic growth is somehow similar to the *in situ* growth, except that the MOF precursor solution keeps flowing during the growth.[78]

The exploration of advanced methods for the fabrication of high-quality MOF polycrystalline membranes has been one of the most popular topics over the past decade. Facile and efficient approaches that can be adopted for mass membrane production are highly desired for the industrial implementation of MOF polycrystalline membranes. The characteristics of major membrane fabrication strategies discussed in this section are summarized in Table 1. It is clear that some strategies, such as *in situ* solvothermal growth and seed-assisted secondary growth, are less likely to be used in industry due to either their limited ability to produce ultrathin membranes or high operational costs. On the other hand, several other strategies, such as solvent-free conversion and FCDS, demonstrate the ability to mass-produce ultrathin membranes with high-quality, are therefore worth exploring in the near future.

2.2 Gas separation

MOF-based membranes exemplify a long-term effort to transform MOFs from bulk crystals synthesized in the laboratory to more valuable products that are of great potential for industry-available commodities, which provide a more promising future for energy-efficient separation applications. Recently, MOF-based membranes have paved their way as promising candidates for many essential gas separation applications. In this section, specific prominent examples on high-performance MOF polycrystalline membranes will be outlined and discussed in detail with an emphasis on the membrane design and performance evaluation.

2.2.1 H_2 purification. H_2 has aroused great interest as a green energy source over the past decades owing to its high energy density, good sustainability, and clean combustion process. In recent years, there has been continuously growing demands for H_2, and these demands are expected to grow even more in the future.[79] H_2 is always present with other light gases such as CO_2, N_2, and CH_4, which are coproducts, by-products, and residual reactants generated during different industrial production processes. The efficient separation of H_2 from these gas mixtures, mainly H_2/CO_2 mixtures, is of great importance in industry. MOF polycrystalline membranes with pore-aperture

sizes comparable to the kinetic diameter of the H_2 molecule have attracted considerable attention as potential candidates for this important application. Hitherto, a series of MOFs, including ZIFs,[80–82] MILs,[83,84] MOF-74 series,[85] and UiO-66 series,[73,86] have been shown to be promising for the fabrication of polycrystalline membranes with notable H_2 purification performance.

ZIF-8 polycrystalline membranes are one class of the most widely explored MOF membranes for H_2 purification mainly due to their small pore-aperture size, good chemical stability, and facile synthesis procedure. To advance their industrial implementation, it is crucial to develop reliable and eco-friendly membrane fabrication methods to produce high-quality ZIF-8 membranes with good mechanical strength. Considering that a large number of MOF membranes were grown on expensive and brittle inorganic porous supports, Hou *et al.* explored the fabrication of ultrathin ZIF-8 membranes on relatively cheap and flexible polymeric supports.[87] Specifically, polyvinylidene fluoride (PVDF) hollow fiber supports were first coated with TiO_2 nanoparticles and then treated with APTES. Subsequently, ZIF-8 membranes were deposited onto the modified PVDF supports *via* a direct immersion strategy (Fig. 9a and b). Ultrathin ZIF-8 membranes with a selective layer thickness of 400 nm showed a high H_2 permeance of 60 000 GPU (GPU = Gas Permeation Unit) and an ideal H_2/CO_2 selectivity of 7. It is worth noting that GPU is one of the most widely used units of gas permeance: 1 GPU = 10^{-6} cm^3(STP) cm^{-2} s^{-1} cm_{Hg}^{-1} = 3.344 × 10^{-10} mol m^{-2} s^{-1} Pa^{-1}. Similarly, ultrathin ZIF-8 membranes could also be grown on ethylenediamine (EDA)-modified polymeric supports for H_2/CO_2 separation.[88] The resultant membrane demonstrated a H_2 permeance of 6120 GPU and an ideal H_2/CO_2 selectivity of ~13, outperforming most of the other ZIF-8 membranes reported in the literature.

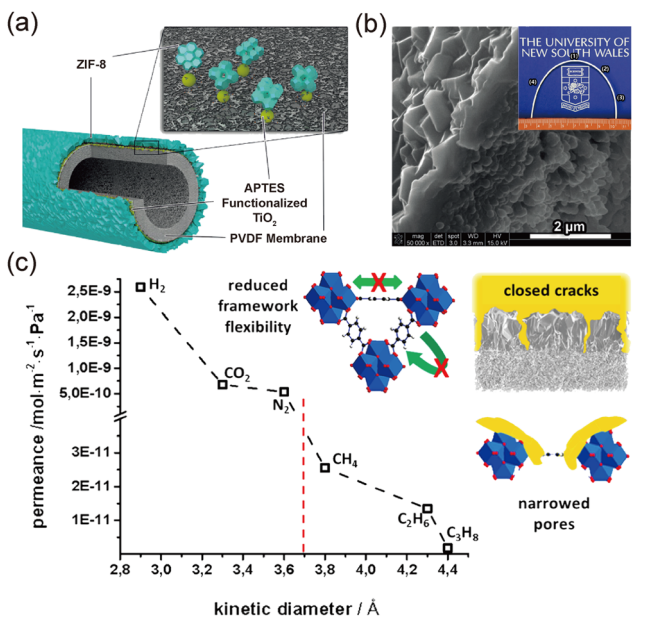

Fig. 9 (a) Schematic representation of the composite membrane. (b) Cross-sectional SEM images of the ZIF-8 layer. The inset shows the optical image of the bent ZIF-8 membrane. (c) Gas separation performance of the Matrimid-coated UiO-66 membrane. The insert shows the possible reason for enhanced membrane performance. Reprinted with permission from ref. 87. Copyright 2016 Wiley-VCH, ref. 73, Copyright 2017 American Chemical Society, respectively.

UiO-66 and its derivatives have also been explored as promising membrane materials for H_2 purification mainly owing to their excellent chemical stability. Given the harsh separation conditions in industry, these robust UiO-66 series membranes can have higher chances of maintaining their separation performance compared to their fragile counterparts. Nevertheless, the pore-aperture size of UiO-66 is larger than kinetic diameters of small gas molecules, including H_2, CO_2, N_2, and CH_4, making it difficult to realize molecular sieving separation in UiO-66 polycrystalline membranes. Therefore, it is demanding to develop efficient strategies to improve the gas selectivity of UiO-66 series membranes. Friebe *et al.* proposed to enhance the gas discrimination ability of UiO-66 membranes by coating them with a thin layer of Matrimid polymer.[73] This polymer coating not only helped to seal possible defects in UiO-66 membranes, but also hindered the free rotation of benzene moieties in the MOF structure, resulting in narrowed MOF pore-aperture size. Moreover, the authors mentioned that polymer chains might penetrate into membrane pores to a certain degree, leading to enhanced membrane gas selectivity (Fig. 9c). The Matrimid-coated UiO-66 membranes demonstrated a H_2/CH_4 selectivity of 80, which is much higher than those of the pristine UiO-66 membrane (13) and the neat Matrimid membrane (~17).

Recently, stimuli-responsive membranes have aroused great interest owing to their ability to adjust their separation performance, including permeance and selectivity, under external stimuli. MOFs offer great opportunities in the design and fabrication of smart membranes. One typical example of smart MOF polycrystalline membrane was reported by Wang *et al.* in 2016 (Fig. 10).[14] In this work, MOFs containing light-responsive azobenzene side groups were processed into membranes with a thickness of 2 μm. The azobenzene moieties in the MOFs could be switched from the *trans* phase to *cis* phase under 365 nm light irradiation and *vice versa* under 455 nm light irradiation. The resultant MOF membranes demonstrated photoswitchable performance for the separation of the equimolar H_2/CO_2 mixture. Their CO_2 permeance decreased from *ca.* 300 to 120 GPU and the H_2/CO_2 selectivity increased from 3 to 8 when they were switched from the *trans* phase to *cis* phase. Remarkably, the membrane performance could be easily changed back under 455 nm light irradiation without noticeable loss in gas permeance or selectivity. Similar results have been found in β-cyclodextrin-capped UiO-68 membranes containing azobenzene side groups.[89] Considering that there are many other stimuli-responsive MOFs reported in the literature, these pioneering studies will definitely inspire the design of more MOF smart membranes with interesting and valuable separation performance for H_2 purification.

2.2.2 CO_2/N_2 separation. The rapid increase of CO_2 emissions from anthropogenic activities constitutes a grand challenge

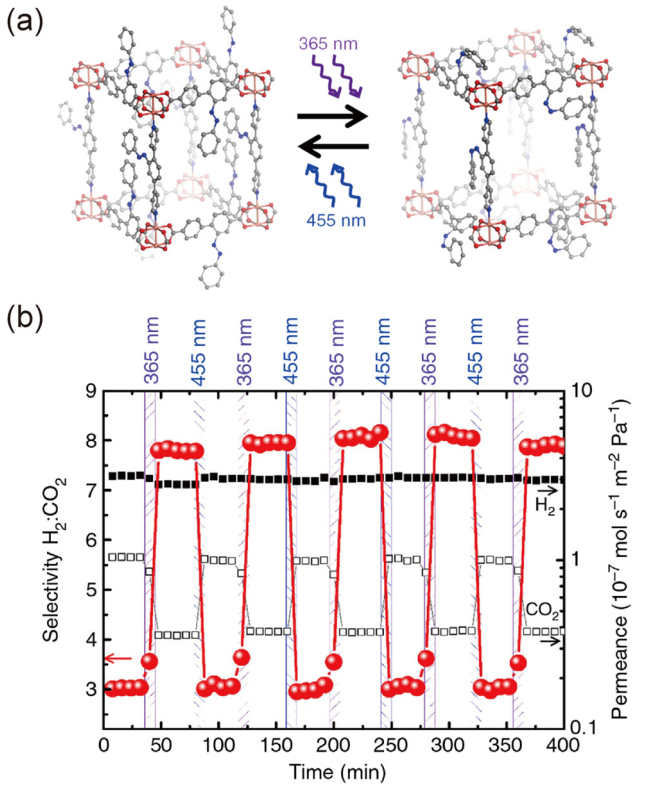

Fig. 10 (a) Illustration of the structural change of MOFs with azobenzene moieties. (b) H_2/CO_2 separation performance of photoswitchable MOF membranes. Reprinted with permission from ref. 14. Copyright 2016 Nature Publishing Group.

for the sustainable development of human society. It has been widely accepted that the continuous increase of the atmospheric concentration of greenhouse gases, such as CO_2, can lead to global warming and climate change. The development of efficient separation technologies to remove CO_2 from flue gas mixtures (CO_2/N_2 separation) generated during the post-combustion process is of great importance in mitigating the global warming effect. MOFs with suitable pore-aperture sizes and high CO_2 affinity are attractive candidates for membrane-based CO_2/N_2 separation. The amino-decorated MOF, CAU-1 (CAU = Christian-Albrechts-University), is one of the most promising membrane materials for efficient CO_2 capture. This MOF consists of distorted octahedral and tetrahedral cages, which are interconnected by triangular windows with an aperture size of 3–4 Å. Yin *et al.* reported the growth of dense CAU-1 membranes on Al_2O_3 tube supports by the seeded growth method.[92] The abundant amino groups in CAU-1 membranes could favorably interact with acidic CO_2 molecules owing to strong acid–base interactions, leading to improved membrane CO_2/N_2 separation performance. CAU-1 membranes showed a high CO_2 permeance of 3940 GPU and an ideal CO_2/N_2 selectivity of 26, highlighting their good potential for industrial CO_2/N_2 separation.

ZIFs represent one class of MOFs with high potential for CO_2/N_2 separation. Despite the exciting advances in ZIF membranes grown on inorganic supports with good separation performance, it is still rather challenging to grow defect-free ZIF membranes on relatively cheap polymeric supports. Zhu *et al.* tried to grow two-component ZIF-L membranes on poly(acrylonitrile) (PAN) supports *via* a heteroepitaxial growth approach and explored their potential for CO_2/N_2 separation.[90] PAN supports were hydrolyzed and coated with poly(sodium-4-styrene sulfonate)-modified halloysite nanotubes (PSS-HNTs) to allow the control of the growth orientation of ZIF-L membranes. Horizontally aligned PSS-HNTs with ample hydrophilic functional groups acted as templates to guide the growth of ZIF-L membranes in a vertical direction. As a result, well-intergrown and vertically aligned ZIF-L membranes were successfully fabricated on polymeric supports (Fig. 11a). Single-component ZIF-L (Co-ZIF-L) membranes exhibited a low ideal CO_2/N_2 selectivity of 3.2 owing to defects in crystal boundaries, induced by fast crystal nucleation rates. In contrast, two-component ZIF-L (Co/Zn-ZIF-L) membranes synthesized by the heteroepitaxial growth strategy showed improved grain boundary structures. Consequently, Co/Zn-ZIF-L membranes demonstrated a CO_2 permeance of 245 GPU and a high CO_2/N_2 selectivity of 18, outperforming many ZIF-8-based membranes reported in the literature.

Membranes made from MOFs with large pores usually demonstrate super-high gas permeability and low selectivity, precluding them from being directly applied for CO_2/N_2 separation. Considering their good mechanical stability, these highly porous membranes can be used as gutter layers for the deposition of ultrathin polymeric membranes with impressive separation performance. For instance, Xie *et al.* prepared a dense and continuous MIL-53-NH_2 membrane as the gutter layer for the deposition of an ultrathin poly(ethyl glycol) (PEG)-based polymeric membrane for CO_2/N_2 separation (Fig. 11b).[91] Compared to the conventional gutter layer prepared from PDMS, this MOF-based gutter layer could afford more than 15 times higher permeance owing to its intrinsic pores. It is worth mentioning that in this MOF-based composite membrane structure, the MOF gutter layer functions as a porous support. while the ultrathin selective polymeric layer (~30 nm) offers high CO_2/N_2 selectivity. The resultant composite membrane demonstrated a high CO_2 permeance of 3000 GPU and an ideal CO_2/N_2 selectivity of 34. This performance falls in the range of economically attractive area for post-combustion CO_2 capture applications (Fig. 11c).

2.2.3 CO_2/CH_4 separation. Efficient CO_2/CH_4 separation is of great importance in the purification of natural gas and biogas. The concentration of CO_2 in these gases needs to be maintained at a low level to meet the pipeline specifications.[94] Notably, membrane technology is now commercially available for the natural gas purification in industry with a market share of around 10%. The development of novel membranes with higher permeance and selectivity will definitely increase the competitiveness of membrane technology over energy-intensive amine absorption for natural gas and biogas purification.

Considerable efforts have been made to fabricate good MOF membranes for efficient CO_2/CH_4 separation in laboratories. For instance, a number of MOFs, such as ZIF-8,[95] isoreticular MOF-1 (IRMOF-1),[96] MIL-53-NH_2,[97] CAU-1,[97] and UiO-66,[68]

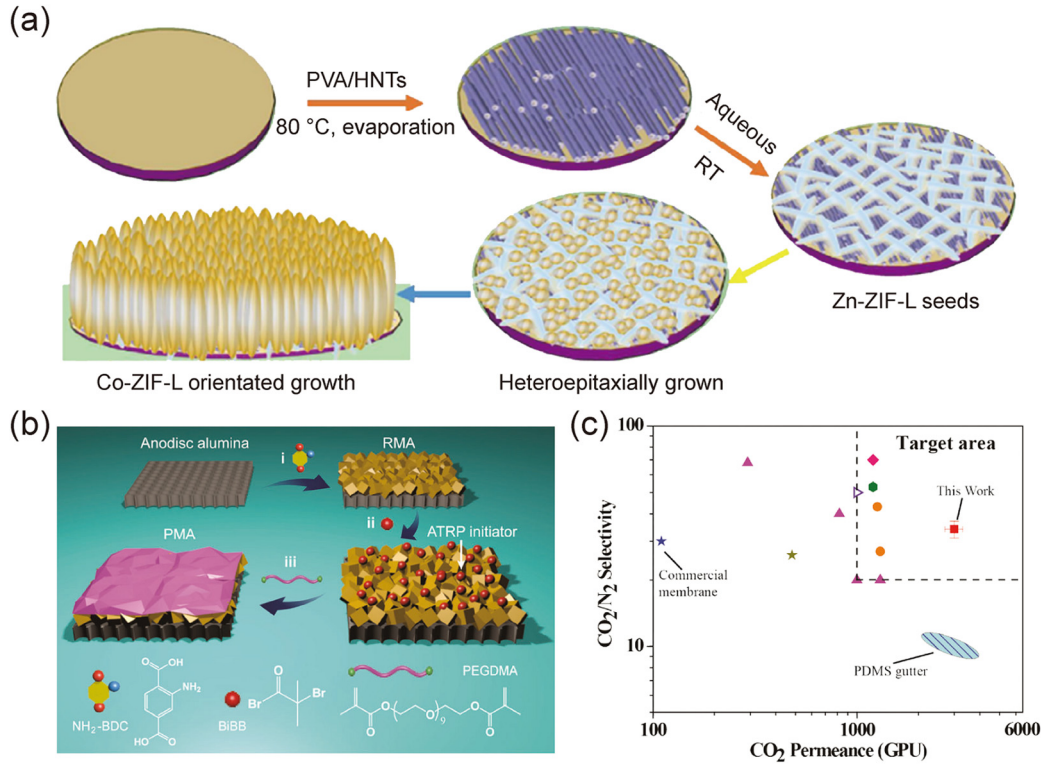

Fig. 11 (a) Schematic illustration of the preparation of Zn/Co-ZIF-L membranes on PSS-HNT coated PAN substrates. (b) Schematic illustration of the preparation of the composite membrane with the MOF as a gutter layer. (c) CO_2/N_2 selectivity *versus* permeance diagram comparing the as-prepared composite membrane with other high-performance membranes reported in the literature. Reprinted with permission from ref. 90. Copyright 2020 American Institute of Chemical Engineers, ref. 91, Copyright 2018 The Royal Society of Chemistry, respectively.

have been processed into polycrystalline membranes for CO_2/CH_4 separation. Owing to their intrinsic pores, MOF membranes usually exhibit much higher permeability compared to polymeric membranes. However, it should be pointed out that a large number of MOF membranes only showed rather low CO_2/CH_4 selectivities (*e.g.*, <15) in the literature. It is highly desired to realize molecular sieving separation in MOF membranes to achieve an ultrahigh CO_2/CH_4 selectivity. Rui *et al.* reported the preparation of dense and thick MOF-5 membranes on porous alumina supports and explored their CO_2/CH_4 separation performance.[96] They discovered that for mixed gas test at a low CO_2 concentration ($<60\%$), CO_2 molecules were strongly adsorbed within MOF-5 pores, which helped to reduce the concentration gradient of CH_4 in the mixture across the membrane. Meanwhile, the slow diffusion of CH_4 would hinder the diffusion of CO_2, leading to reduced CO_2 permeance in the membrane. At a higher CO_2 concentration, CO_2 adsorption layers would form in MOF-5 pores, which eventually blocked the diffusion of CH_4 molecules and led to the molecular sieving effect. As a result, MOF-5 membranes displayed an ultrahigh CO_2/CH_4 selectivity of 328 and a good CO_2 permeance of 760 GPU for a CO_2/CH_4 (81.5/18.5) mixture at 5 bar and 298 K.

ZIF-8 has been considered as a good membrane candidate for CO_2/CH_4 separation owing to its small crystallographic pore size. However, its actual pore-aperture size is slightly larger than the ideal value owing to its flexible lattice, which often leads to a low CO_2/CH_4 selectivity for membrane-based gas separation. Hou *et al.* proposed a mixed-linker strategy to restrict the lattice flexibility and reduce the pore-aperture size in ZIF-8 membranes (Fig. 12).[93] A series of ZIF-7_x-8 hybrid membranes were prepared from benzimidazole/2-methylimidazole mixtures as mixed ligands and Zn^{2+} cations *via* the FCDS approach (where x represents the molar percentage of benzimidazole in the MOF structure). With the increase of molar percentage of benzimidazole in the hybrid structure, the resultant membrane afforded contracted pore-aperture sizes. The optimal ZIF-7_{22}-8 hybrid membranes showed a CO_2/CH_4 selectivity of 25, much higher than that of pristine ZIF-8 membranes (<5). Moreover, these hybrid membranes could maintain their separation performance during a 180 h temperature swing separation test, confirming their good structural stability.

Recently, MOF glass membranes have also gained considerable attention for efficient CO_2/CH_4 separation. Conventional MOF polycrystalline membranes often demonstrate limited CO_2/CH_4 selectivity partly due to their grain boundary defects. It is well-known that some MOFs can demonstrate solid–liquid–glass transition at different temperatures, which makes it possible to fabricate MOF glass membranes from defective MOF polycrystalline membranes under heating.[19,98] It is worth mentioning that grain boundary defects will be eliminated when the MOF membranes are melted at a high temperature, leading to high-quality membranes with impressive separation

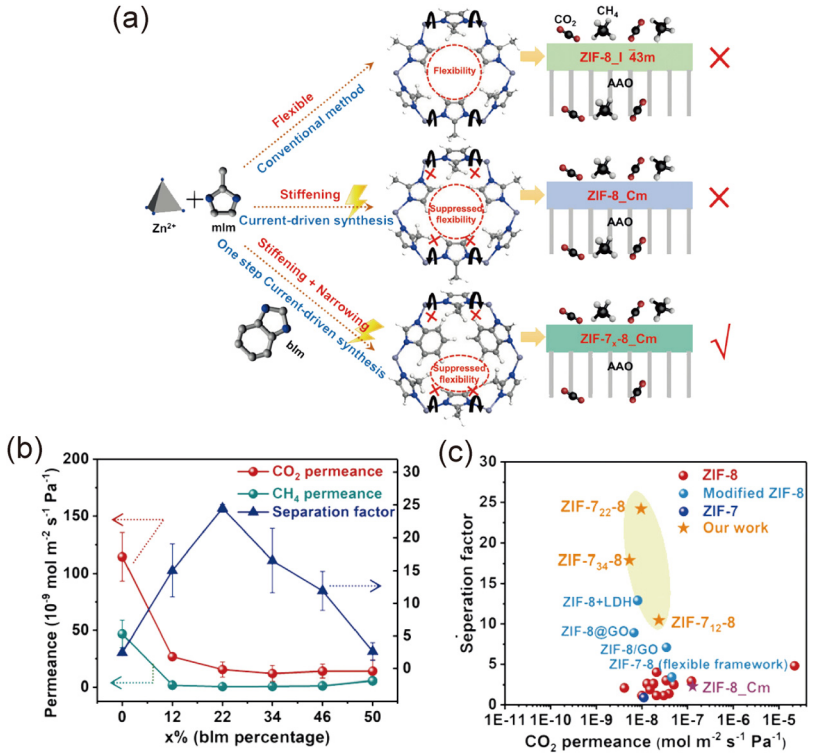

Fig. 12 (a) Schematic illustration of the synthesis of different ZIF-8 membranes on AAO supports by different strategies. (b) CO_2/CH_4 separation performance of the mixed-linker ZIF-7_x-8 membranes. (c) Comparison of the CO_2/CH_4 separation performances of ZIF-7_x-8 membranes with other ZIF membranes. Reprinted with permission from ref. 93. Copyright 2019 Wiley-VCH.

performance. For example, a dense and defect-free ZIF-62 glass membrane was successfully prepared by a melt-quenching treatment of a defective ZIF-62 polycrystalline membrane on a porous alumina support.[19] The resultant ZIF-62 glass membrane exhibited an excellent CO_2/CH_4 selectivity of 37 and a CO_2 permeability of 2602 barrer (1 barrer = 10^{-10} cm^3(STP) cm cm^{-2} s^{-1} cm_{Hg}^{-1} = 3.344 × 10^{-16} mol m m^{-2} s^{-1} Pa^{-1}), far exceeding the Robeson upper bounds. Similarly, a series of tetrahedral imidazolate framework-4 (TIF-4) glass membranes with different ratios of mixed linkers were prepared and tested for CO_2/CH_4 separation.[98] The optimal membrane showed a CO_2/CH_4 selectivity of 30, confirming its defect-free structure. Notably, this membrane also exhibited an excellent long-term stability of up to 10 months, validating its potential for industrial CO_2 separation.

2.2.4 C_3H_6/C_3H_8 separation. C_3H_6/C_3H_8 separation is a necessary yet energy-intensive process to produce high-purity C_3H_6, which is essential for the manufacturing of various valuable chemicals, including polypropylene. Industrial purification of C_3H_6 relying on the distillation technique requires a double-column system, which usually ranges from 70 to 90 m in height and 2 to 6 m in diameter.[65] The kinetic diameters of C_3H_6 and C_3H_8 are 4.0 and 4.2 Å, respectively. The slight difference of 0.2 Å offers the possibility, although challenging, to discriminate this mixture using MOF polycrystalline membranes based on the size sieving mechanism.

ZIF-8 shows a theoretical pore-aperture size of 3.4 Å based on its crystallographic data. Due to their framework flexibility, molecules with kinetic diameters larger than 3.4 Å are also allowed to pass through the apertures in ZIF-8. In fact, experimental studies have revealed that the effective pore-aperture size of ZIF-8 falls in the range of 4.0 to 4.2 Å, which permits the separation of the C_3H_6/C_3H_8 mixture based on the difference in diffusion kinetics.[100] Therefore, ZIF-8 membranes have been extensively studied for C_3H_6/C_3H_8 separation. Nevertheless, their separation performance can be totally different when prepared by different methods owing to their high sensitivity to grain boundary voids and intercrystalline defects. As a result, the preparation of high-quality ZIF-8 membranes without defects sets the foundation for the exploration of these membranes for efficient C_3H_6/C_3H_8 separation.

Notably, the framework flexibility of ZIF-8 defines the upper limit of membrane selectivity for C_3H_6/C_3H_8 separation, which is around 145 at maximum.[100] Consequently, it remains a big challenge for pristine ZIF-8 membranes to exhibit an even higher C_3H_6/C_3H_8 selectivity that goes beyond this limit. To overcome this challenge, the framework flexibility of ZIF-8 must be suppressed. Zhou *et al.* prepared a new class of ZIF-8 membranes with the polymorph of ZIF-8_Cm as the major membrane composition (~70%) (Fig. 13a).[65] The ZIF-8_Cm polymorph is more rigid compared with the normal ZIF-8, and the molecular dynamic simulation showed that the maximum C_3H_6/C_3H_8 selectivity of pure ZIF-Cm polymorph membranes could reach more than 500. The resultant ZIF-8_Cm-dominated membranes (70% in composition) showed an exceptionally C_3H_6/C_3H_8 selectivity of 304, with a C_3H_6 permeance of 52 GPU (Fig. 13b).

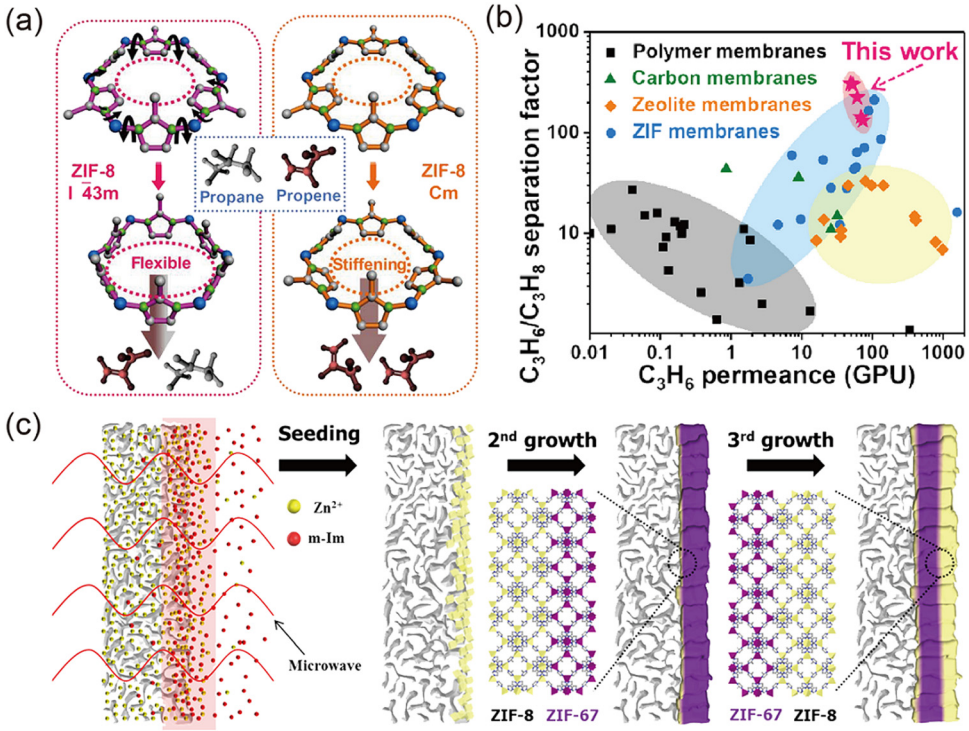

Fig. 13 (a) Schematic illustration of differences between normal ZIF-8 with a flexible structure and ZIF-8_Cm with a rigid structure for C_3H_6/C_3H_8 separation. (b) Comparison of the C_3H_6/C_3H_8 separation performance of ZIF-8_Cm-dominated membranes with other membranes reported in the literature. (c) Schematic illustration of the membrane preparation by heteroepitaxial growth. Reprinted with permission from ref. 65. Copyright 2018 AAAS, ref. 99, Copyright 2015 American Chemical Society, respectively.

Meanwhile, Kwon *et al.* reported that the Co–N bond in ZIF-67 were more rigid than the Zn–N bond in ZIF-8, which indicated that the intrinsic separation ability of ZIF-67 membranes should be higher than that of ZIF-8 membranes.[99] They prepared the ZIF-8-on-ZIF-67-on-ZIF-8 triple-layer membranes for C_3H_6/C_3H_8 separation (Fig. 13c), and the final membrane selectivity was higher than 200. The authors attributed this good selectivity to the more selective middle layer of ZIF-67, highlighting the huge potential of ZIF-67 membranes for C_3H_6/C_3H_8 separation. However, many other reports revealed opposite experimental conclusions that pristine ZIF-67 membranes always showed inferior C_3H_6/C_3H_8 separation performance compared with ZIF-8 membranes.[102–104] Consequently, more efforts are still needed to prepare high-quality ZIF-67 membranes and explore their potential for C_3H_6/C_3H_8 separation in the future.

2.2.5 Other gas separation applications. Besides the above-mentioned gas separations, there are also some other gas separations achieved using MOF polycrystalline membranes in the literature, such as the separation of butane/iso-butane isomers and helium extraction. The kinetic diameters of butane and iso-butane are 4.3 and 5.0 Å, respectively. Similar to ZIF-8, ZIF-90 also demonstrates framework flexibility with an effective aperture size of 5.0 Å. Therefore, ZIF-90 has the potential to discriminate butane/iso-butane isomers based on the difference in their gas diffusivity coefficients.[105] Eum *et al.* reported that ZIF-90 polycrystalline membranes showed a selectivity of 12 for the separation of a butane/iso-butane mixture.[106] The obtained selectivity was much lower than the theoretical value, indicating the existence of potential defects in their ZIF-90 membranes.

Helium (He) extraction from raw natural gas (He/CH_4 separation) is one of the most important processes to produce high-purity He. However, due to the low abundance of He in raw natural gas, a promising He extraction membrane should be highly selective even at a low He partial pressure. Currently, MOF polycrystalline membranes suitable for the He extraction process are not frequently reported mainly due to their moderate or even poor separation performance. For instance, Yoo *et al.* reported that IRMOF-3 membranes showed a good He permeance of *ca.* 2400 GPU and a low He/CH_4 selectivity of only 1.3.[107] Cao *et al.* reported that Cu-BTC membranes could separate the He/CH_4 mixture with a selectivity of ~2 and a high He permeance of 4180 GPU.[108] Considering the rich chemical functionality and adjustable pore sizes of MOFs, it is still promising to design and prepare MOF polycrystalline membranes with impressive He/CH_4 separation performance in the future. Notably, due to the low abundance of He in raw natural gas, these membranes should be tested at a low He partial pressure in order to provide useful data for accurately evaluating their potential for industrial applications.

2.3 Liquid separation

MOF polycrystalline membranes have found a wide range of applications in different liquid separations, including water

treatment, pervaporation, and organic solvent nanofiltration (OSN), owing to their well-defined and tailorable pore structures, high porosity, and diversified chemical functionality. Notably, the intrinsic separation performance of MOF membranes can sometimes largely surpass that of conventional polymeric membranes for liquid separation. Moreover, for some separation applications under harsh conditions, such as OSN, MOF polycrystalline membranes can outperform polymeric membranes attributed to their high solvent resistance and good anti-swelling ability. In this section, the emerging applications of MOF polycrystalline membranes for liquid separation are elaborated along with detailed discussions about challenges that hinder the potential commercialization of these membranes.

2.3.1 Water treatment. With the increase of population and rapid progress of urbanization, water scarcity has been identified as one of the most crucial issues for sustainable socioeconomic development. Membrane-based water treatment technology is an energy-efficient process to produce fresh water, offering a good solution to the challenge of water scarcity. Despite the fact that polymeric membranes dominate the current membrane separation market, MOF polycrystalline membranes still hold great promise to compete with polymeric membranes for liquid separation due to their outstanding separation performance. The thriving exploitation of water-stable MOFs with appropriate pore sizes has set a solid foundation for the swift development of MOF polycrystalline membranes for efficient separation based on the molecular sieving mechanism.

One important factor that deserves special attention is the stability of MOFs in water or even acidic/basic environments. MOFs generally exhibit good stability in common organic solvents, while only a few types of judiciously designed MOFs can demonstrate impressive water stability. It is now widely accepted that the relatively labile metal–ligand bonds in the MOF structure are responsible for the limited water stability of MOFs. Basic principles for designing water-stable MOFs are highlighted here and a detailed list of stable MOFs can be found elsewhere.[112–115] MOFs with excellent water stability normally have strong coordination bonds to survive from the attack of water molecules (thermodynamic stability) or have large steric hindrance to prevent the diffusion of water molecules to the metal nodes (kinetic stability). Pearson's hard/soft acid/base (HSAB) principle has been shown to be useful in guiding the design of MOFs with strong coordination bonds.[116] Therefore, water-stable MOFs can be roughly categorized into three major types: (1) MOFs consisting of high-valent metal ions (*e.g.*, Zr^{4+}, Ti^{4+}, Al^{3+}, Fe^{3+}, and Cr^{3+}, hard Lewis acids) and carboxylate-based ligands (hard Lewis bases). Typical examples are UiO series and MIL series MOFs.[117–119] It is worth noting that UiO-66 shows remarkable stability in water and even under acidic conditions, which make it a promising membrane candidate for water-related applications.[117] (2) MOFs containing azolate ligands (*e.g.*, imidazolates, pyrazolates, triazolates, and tetrazolates, and soft Lewis bases) and low-valency transition metal ions (*e.g.*, Zn^{2+}, Ni^{2+}, and Mn^{2+}, and soft Lewis acids). The most well-known examples of this class are ZIFs constructed with Zn^{2+} and imidazolate linkers.[120] (3) MOFs with hydrophobic pore/channel surfaces or blocked metal ions. To increase the pore/channel hydrophobicity or steric hindrance can keep water molecules away from metal ions, elevating the overall water stability of MOF structures. Typical examples of this class are fluorinated MOFs containing fluoride anions in their contracted 1D channels reported by our group, including NbOFFIVE-1-Ni and AlFFIVE-1-Ni.[121,122] Importantly, these fluorinated MOFs also show impressive stability toward corrosive H_2S, making them promising for natural gas purification (see Section 4.3.1).

Recently, MOF polycrystalline membranes have been mainly applied for two water treatment processes: dye removal and desalination. Considering that the dimensions of molecules or ions can vary in different water treatment processes, it is therefore of great importance to choose suitable MOFs for different separation applications.

The discharge of industrial dye effluents has always been a severe environmental problem. A large number of dyes are considered to be toxic and even carcinogenic, and therefore should be removed from wastewater to minimize their impact on the aquatic ecosystem.[124] MOF polycrystalline membranes have demonstrated great potential for dye removal from wastewater because their pores can be easily adjusted to allow the passage of water while blocking the passage of large dye molecules. For example, high-quality ZIF-8 membranes were successfully prepared on poly(ether sulfone) (PES) supports *via* a phase transformation interfacial growth strategy (Fig. 14a).[101]

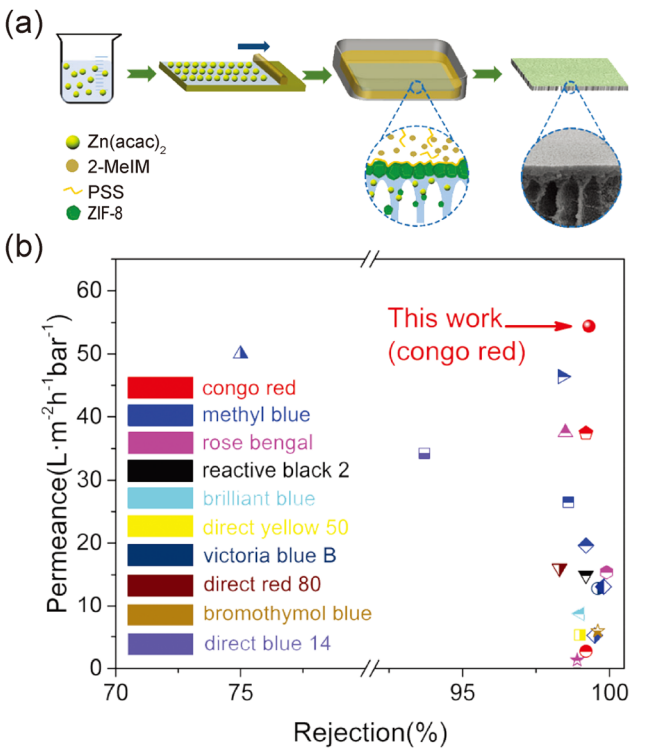

Fig. 14 (a) Schematic illustration of the ZIF-8 membrane preparation process. (b) Comparison of dye removal performances between the as-prepared ZIF-8 membrane and other studies. Reprinted with permission from ref. 101. Copyright 2018 The Royal Society of Chemistry.

The resultant membranes exhibited a good water permeance of 54 L m^{-2} h^{-1} bar^{-1} and a high rejection of 99% for Congo red (Fig. 14b). The dye adsorption experiment showed that only 6% of Congo red was adsorbed by the membrane. This confirmed that the efficient dye removal process in ZIF-8 membranes was mainly based on the size-sieving mechanism. Similar results have been found in another robust ZIF membrane, JUC-160 (JUC = Jilin University China), which demonstrated excellent rejections (>99%) for different dyes, including Congo red, Coomassie Brilliant Blue R250, and rhodamine B.[125] Recently, HKUST-1 polycrystalline membranes were prepared on PES supports *via* an electrochemically assisted interfacial growth strategy and applied for dye removal in a dead-end filtration system (Fig. 15a).[109] The resultant membranes exhibited an excellent rejection of >99% for Rose Bengal (M = 1017 g mol^{-1}) and a poor rejection of 44% for rhodamine B (M = 479 g mol^{-1}). However, HKUST-1 often demonstrates poor water stability due to strong interaction between its open copper sites and water molecules, therefore undergoing an irreversible structure degradation when continuously contacting with liquid water.[126] Consequently, water-stable MOFs with appropriate pore sizes are recommended for future dye removal studies.

Another important application of MOF polycrystalline membranes for water treatment is desalination. The pore sizes, pore volumes and functionalities of MOFs can be judiciously tailored for the efficient separation of water and ions. Interestingly, a simulation study by Lyu *et al.* suggested that MOF membranes with judiciously designed defects could exhibit an order of magnitude higher water permeance and similar ion rejections compared to defect-free MOF membranes (Fig. 15b).[110] Considerable efforts have been devoted to the experimental exploration of MOF polycrystalline membranes for desalination. Liu *et al.* successfully prepared continuous UiO-66 membranes on alumina hollow fibers.[12] The resultant membranes showed good rejection rates for multivariant ions, such as Ca^{2+} (86%), Mg^{2+} (98%), and Al^{3+} (99%), and relatively poor rejection rates for monovalent ions, such as K^{+} (46%) and Na^{+} (47%) (Fig. 15c). Interestingly, the pore size of UiO-66 was estimated to be around 6.0 Å, which is slightly smaller than the kinetic diameters of hydrated ions (6.6 Å for K^{+} and 7.2 Å for Na^{+}). This poor rejection performance of UiO-66 polycrystalline membranes for

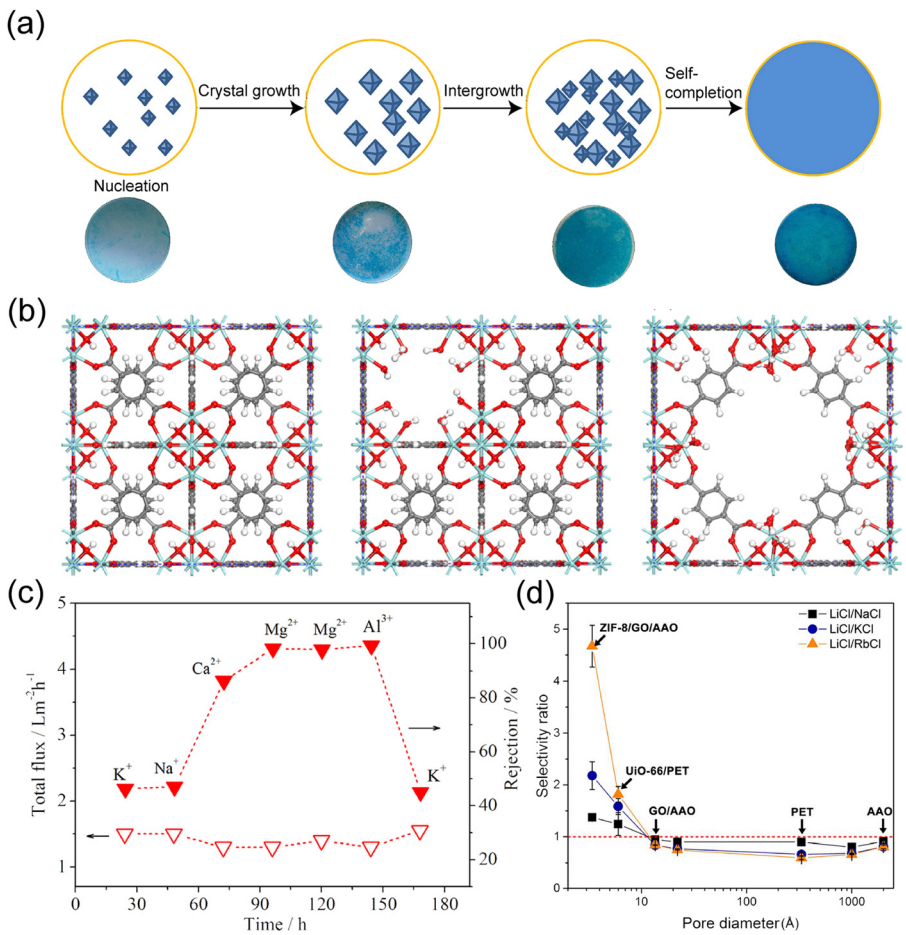

Fig. 15 (a) Schematic illustration of the MOF membrane preparation by the electrochemically assisted interfacial growth strategy. (b) Illustration of defect-free (left) and defective (middle and right) UiO-66 structures. (c) Desalination performance of UiO-66 membranes. (d) The relationship between alkali metal ion selectivity and pore sizes in different nanoporous membranes. Reprinted with permission from ref. 109. Copyright 2019 Elsevier, ref. 110. Copyright 2019 American Chemical Society, ref. 12. Copyright 2015 American Chemical Society and ref. 111. Copyright 2018 AAAS, respectively.

monovalent ions might be due to the existence of missing-ligand defects in UiO-66 crystals. To mitigate these missing-ligand defects in zirconium-based MOFs, Wang *et al.* proposed a post-synthetic defect healing (PSDH) strategy to improve the membrane desalination performance.[127] The original UiO-66 polycrystalline membrane demonstrated a rejection rate of 26% for Na^+, which could be increased to 45% after the PSDH treatment. Nevertheless, this improved rejection rate is still far from the desired value (>99%) for commercial desalination membranes.

ZIF-8 has also been experimentally explored as membrane material for desalination. Although the pore size of ZIF-8 is suitable for this application, the relatively poor long-term water stability of ZIF-8 may be a grand challenge.[129] The ion transport properties through ZIF-8 membranes were explored by Zhang *et al.* who prepared ultrathin ZIF-8 membranes by a nanoporous GO-assisted interfacial growth method.[111] The angstrom-sized aperture windows of ZIF-8 could work as ion filters to differentiate alkali metal ions based on their size differences (Fig. 15d). Moreover, the nanometer-sized cavities in ZIF-8 could act as ion conductive pores for fast ion transport. Notably, the pore-aperture size (3.4 Å) of ZIF-8 is between the hydrate ionic diameters (6–8 Å) and dehydrated ionic diameters (<3 Å) of alkali metal ions. Therefore, the fast and selective transport of ions through ZIF-8 membranes is associated with a partial ion dehydration process, as confirmed by molecular dynamics simulations. Nevertheless, the long-term stability of these ZIF-8 membranes remains elusive, which largely limits their implementation for real-life applications.

2.3.2 Pervaporation. Pervaporation is an important technology for molecular-level liquid/liquid separations in the petrochemical and pharmaceutical industries. There are three major types of pervaporation, namely hydrophilic pervaporation, organophilic pervaporation, and organic/organic pervaporation, depending on the exact composition of the feed solution. MOFs have gained considerable attention for membrane-based pervaporation owing to their well-defined pore size and geometry, large surface area, and tunable adsorption capacity.

Dense and continuous ZIF-8 polycrystalline membranes were fabricated and tested for seawater desalination by pervaporation in 2016.[130] The resultant ZIF-8 membranes showed high ion rejections of over 99% and a good water flux of ~6 kg m^{-2} h^{-1} at 25 °C, validating the ion sieving ability of ZIF-8. Moreover, these ZIF-8 membranes could maintain their good separation performance during a stability test of up to 7 days. Subsequently, Zhao *et al.* prepared well-intergrown ZIF-8 polycrystalline membranes on polymeric supports with imidazole-2-carboxaldehyde (ICA) as the linker between ZIF-8 membranes and supports.[131] The resultant ZIF-8 membranes showed impressive pervaporation performance for isopropanol dehydration with a flux of ~70 g m^{-2} h^{-1} and a water/isopropanol separation factor of higher than 600. The grain boundaries in the as-fabricated ZIF-8 membranes could be mitigated with PDMS or polydopamine coatings, leading to further enhanced membrane performance. Despite these advances, it is still worth mentioning that ZIFs are not the optimum membrane materials for water-related pervaporation separations owing to their moderate water stability.

Compared to ZIFs, Zr-MOFs (*e.g.*, UiO-66, UiO-66-OH, and UiO-67) show much better water stability, therefore having greater potential for organic dehydration by pervaporation. For instance, in 2017, Liu *et al.* prepared continuous UiO-66 polycrystalline membranes on pre-structured yttria-stabilized zirconia hollow fiber supports (Fig. 16a).[123] An on-stream activation procedure was adopted to remove guest molecules trapped in cavities to open the hydrophilic adsorption sites in the MOF structure, resulting in enhanced membrane flux and selectivity. The resultant UiO-66 membranes demonstrated an excellent water flux of 6 kg m^{-2} h^{-1} and impressive separation factors of over 45 000 for removing water from i-butanol, furfural, and tetrahydrofuran (Fig. 16b). Remarkably, these membranes could maintain their separation performance during a 300 h stability test and remain robust even in harsh environments (*e.g.*, boiling water, boiling benzene, and sulfuric acid) where some commercial polymeric and zeolite membranes cannot maintain their structural integrity (Fig. 16c). Similarly, RE-MOFs have also gained attention as pervaporation membrane materials due to their excellent water stability and rich chemical functionality. Moreover, 12-connected RE-**fcu**-MOFs often feature fewer missing-ligand defects compared to Zr-MOFs, therefore showing a better size sieving ability for membrane-based pervaporation.[132]

The efficient separation of organic/organic mixtures is of great importance in several chemical processes, such as the recovery of aromatics from a naphtha stream, the removal of methanol from methanol/toluene mixtures, and the reduction of the benzene content in C6 reformates. The application of polymeric membranes for organic/organic pervaporation is quite challenging owing to the limited chemical stability of some commercial polymers in aggressive organic mixtures. Owing to their high chemical resistance to common organic liquids, MOF membranes have been widely explored for organic/organic pervaporation. For instance, Kasik *et al.* fabricated continuous ZIF-68 polycrystalline membranes on ZnO-modified α-alumina supports *via* a modified reactive seeding approach.[133] The resultant ZIF-68 membranes demonstrated a much higher permeation flux (492×10^{-5} mol m^{-2} s^{-1}) for *p*-xylene compared to 1,3,5-triisopropylbenzene (flux: 30×10^{-5} mol m^{-2} s^{-1}) and 1,3-di-*tert*-butylbenzene (flux: $\sim 5 \times 10^{-5}$ mol m^{-2} s^{-1}) owing to the smallest kinetic diameter of *p*-xylene among the three. The pervaporation results ruled out possible defects in the as-prepared ZIF-68 membranes.

2.3.3 Other liquid separation applications. MOF polycrystalline membranes have also aroused great interest in other liquid separation applications, mainly including OSN and chiral separation. OSN is an emerging membrane-based process for molecular separation and purification in a variety of organic solvents that efficiently differentiate molecules in the 200–1000 g mol^{-1} range at mild temperature and sometimes even low pressure. Organic solvents are used worldwide on a megaton-scale annually, and OSN is an energy efficient process for purifying and recovering these organic solvents in an

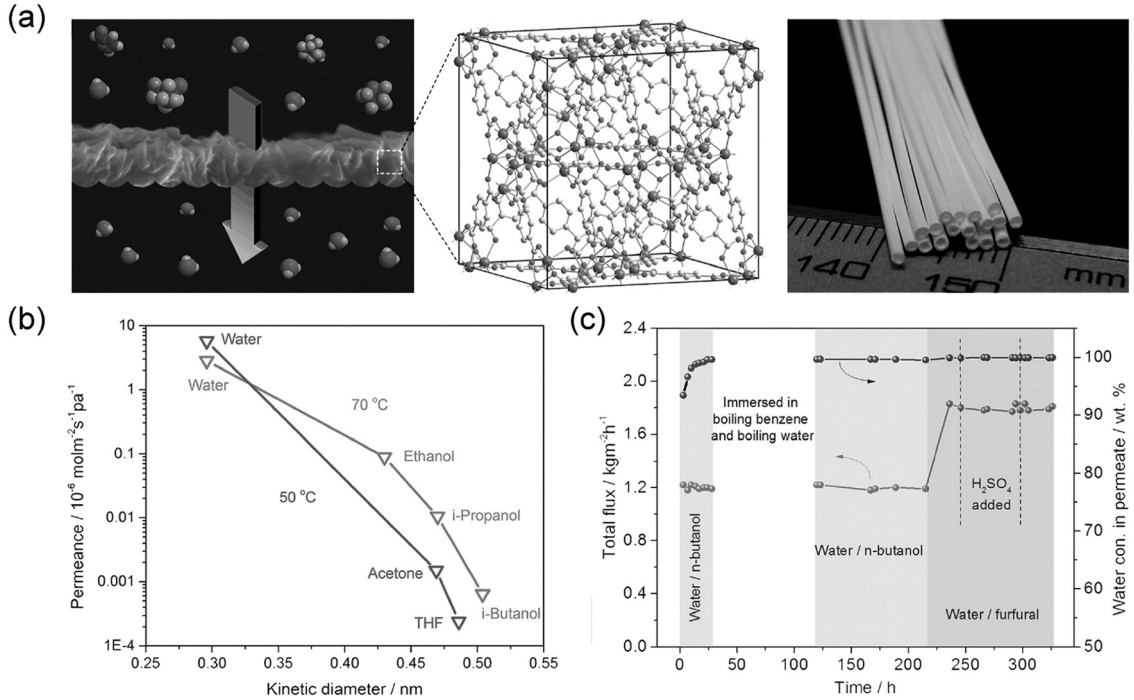

Fig. 16 (a) Schematic illustration of organic dehydration by using a UiO-66 membrane (left), and a photo of the yttria-stabilized zirconia hollow fiber support. (b) Permeance of water and organic compounds with different kinetic diameters in UiO-66 membranes. (c) The pervaporation performance of UiO-66 membranes for removing water from *n*-butanol and furfural. Reprinted with permission from ref. 123. Copyright 2017 Wiley-VCH.

economic way. Currently, the major challenge for OSN is the development of suitable membrane materials that are chemically stable in a great variety of solvents. MOFs usually exhibit good stability in common organic solvents, therefore attracting practical interest as promising OSN membrane materials.

The potential of MOF polycrystalline membranes for OSN was demonstrated by Tham *et al.* who prepared continuous Zn-benzene-1,4-dicarboxylic acid (Zn(BDC)) polycrystalline membranes on chemically modified PAN supports.[134] The as-prepared Zn(BDC) membranes demonstrated impressive OSN performance with a dye (Brilliant Blue R) rejection of 86% and an isopropyl alcohol (IPA) permeance of $\sim$2 L m^{-2} h^{-1} bar^{-1}. It is worth noting that Zn(BDC) could maintain its good crystallinity after being soaked in IPA for one week, highlighting its good chemical stability in simple alcoholic solvents. Subsequently, Ma *et al.* fabricated UiO-66-NH_2 polycrystalline membranes on polymeric supports *via* an *in situ* solvothermal synthesis approach for OSN.[135] The resultant UiO-66-NH_2 membranes exhibited a high Rose Bengal rejection of 96% and a good ethanol permeance of $\sim$1 L m^{-2} h^{-1} bar^{-1} owing to its size-sieving and electrostatic repulsion mechanisms. These seminal contributions have set a solid foundation for the development of more MOF polycrystalline membranes with good separation performance and long-term stability for OSN applications.

Chiral separation is of great significance in various fields, such as the pharmaceutical, agrochemical, and food industries. Great research efforts have been devoted to developing homochiral microporous materials for chiral separation over the past decade. In particular, homochiral MOFs have been recognized as some of the most promising materials for chiral separation. For instance, Huang *et al.* prepared novel homochiral [Ni_2(L-asp)$_2$(bipy)] (Ni-LAB, L-asp = L-aspartic acid, bipy = 4,4′-bipyridine) polycrystalline membranes on porous ceramic supports and applied them for enantioselective separation of racemic diols.[136] The homochiral Ni-LAB crystals showed enantioselective sorption performance for chiral diols owing to the chiral adsorption sites in their channels. The resultant Ni-LAB membranes exhibited an enantiomeric excess (e.e.) value of 36 $\pm$ 3% for the separation of racemic 2-methyl-2,4-pentanediol (MPD) at a feed concentration of 1.0 mmol L^{-1}. Notably, the chiral separation process of racemic MPD through the Ni-LAB membranes is governed by a preferential sorption mechanism. Following this work, Chan *et al.* fabricated homochiral L-His-ZIF-8 (L-His = L-histidine) polycrystalline membranes on porous AAO supports *via* an *in situ* growth approach (Fig. 17a).[128] It is worth mentioning that the natural amino acid L-His was added in a solution containing MOF precursors during the membrane preparation process. L-His was incorporated into the ZIF-8 framework, which eventually led to a chiral environment in the resultant membranes. Consequently, the L-His-ZIF-8 membranes showed good performance for the separation of the *R*-enantiomer and *S*-enantiomer for racemic 1-phenylethanol (Fig. 17b and c). The resultant membranes allowed preferential permeation of the *R*-enantiomer of racemic 1-phenylethanol with a high e.e. value of 76%. These studies shed light on the prospects of rational design of homochiral MOF polycrystalline membranes with high selectivity for real-life chiral separation applications.

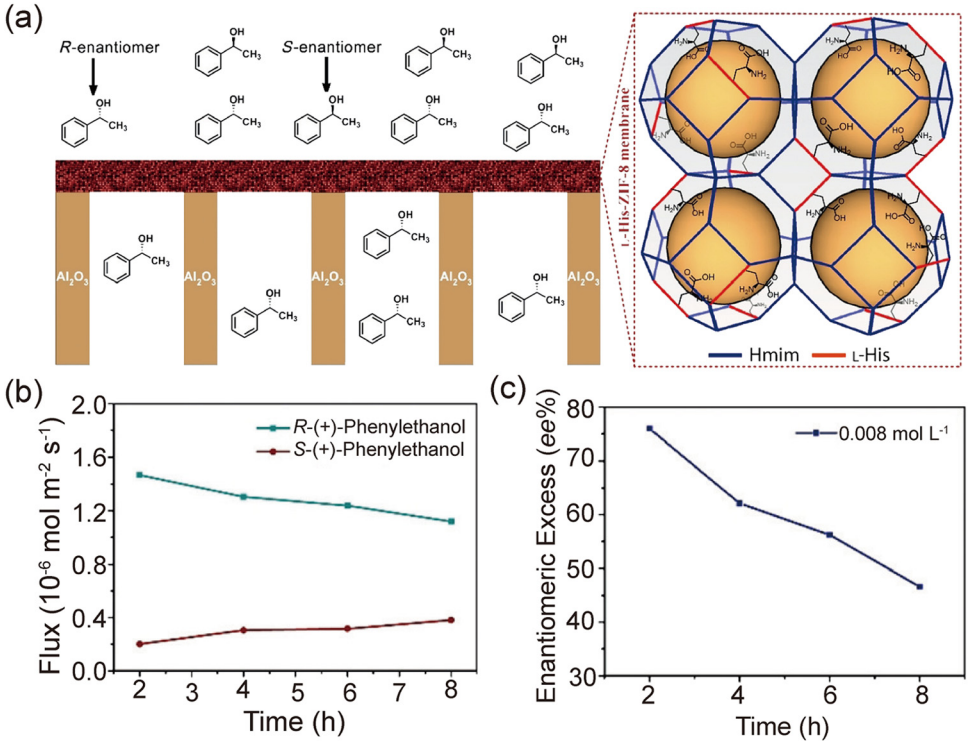

Fig. 17 (a) Schematic illustration of a homochiral L-His-ZIF-8-membrane for separating the *R*-enantiomer of 1-phenylethanol from the *S*-enantiomer. (b) Concentration of each enantiomer on the permeate side and (c) enantiomeric excess (ee%) as a function of time. Reprinted with permission from ref. 128. Copyright 2018 Wiley-VCH.

3. MOF-based MMMs

3.1 Design strategies

MMMs are hybrid membranes consisting of the dispersed filler phase and the continuous polymer phase. A perfect match between the filler and the polymeric matrix is highly desired to achieve defect-free MMMs with impressive separation performance. Compared to some conventional inorganic fillers, such as zeolites and mesoporous silica, MOF fillers demonstrate better compatibility with the polymeric matrix owing to their organic–inorganic hybrid properties. Moreover, owing to the rich chemistry of MOFs, it is relatively easy to design favorable interactions, including hydrogen bonding, covalent bonding, and π–π interactions, at filler–polymer interfaces in MOF-based MMMs. Another appealing feature of MOFs is their highly tunable pore structure, which can enable them to be customized for different separation processes. Nevertheless, in some cases, MOF-based MMMs still demonstrate undesired microstructures that will undermine the membrane performance (Fig. 18). An ideal MOF-based MMM should consist of homogenously dispersed fillers at their maximum loadings. Nano-sized MOF crystals are preferred over their micron-sized counterparts in MMMs due to their higher surface area-to-volume ratios and better interactions with the polymer matrix. Moreover, MMMs with high filler loadings (*e.g.*, >30 wt%) often demonstrate undermined separation performance and reduced mechanical properties because of severe filler aggregation. To prevent filler aggregation and maximize filler loadings, great efforts have been made towards enhance the filler–polymer affinity. Various strategies have been proposed to address the compatibility issue in MOF-based MMMs, which eventually help to facilitate the development of high-performance membranes for different separation applications. In this section, these effective strategies will be outlined and discussed, hoping to provide guidance on the rational design of high-quality MOF-based MMMs.

3.1.1 MOF modification. Favorable filler–polymer interfacial interactions play significant roles in the formation of defect-free MMMs. The choices of MOFs with functional groups, such as $-NH_2$, $-SO_3H$, and –OH groups, can facilitate the formation of hydrogen bonding between MOF fillers and the polymeric matrix, which in turn helps to improve the interfacial compatibility and prevent possible defects in the final membranes. Specifically MOFs including UiO-66-NH_2,[137] ZIF-8-NH_2,[138] ZIF-7-NH_2,[139] MIL-53-NH_2,[140] MIL-53-SO_3H,[141] BUT-203-SO_3H (BUT = Beijing University of Technology),[142] UiO-66(Hf)-$(OH)_2$,[143] and MOF-74 series MOFs[144] have been demonstrated to be useful in the preparation of MMMs with good interfacial affinity. Moreover, these MOFs with functional groups can sometimes exhibit high affinity with certain permeate molecules, such as CO_2 and H_2S, leading to enhanced adsorption uptake of these molecules in membranes. For example, Xiang *et al.* synthesized ZIF-7-NH_2 nanoparticles by an *in situ* substitution strategy and incorporated them into a crosslinked poly(ethylene oxide) rubbery polymer matrix to

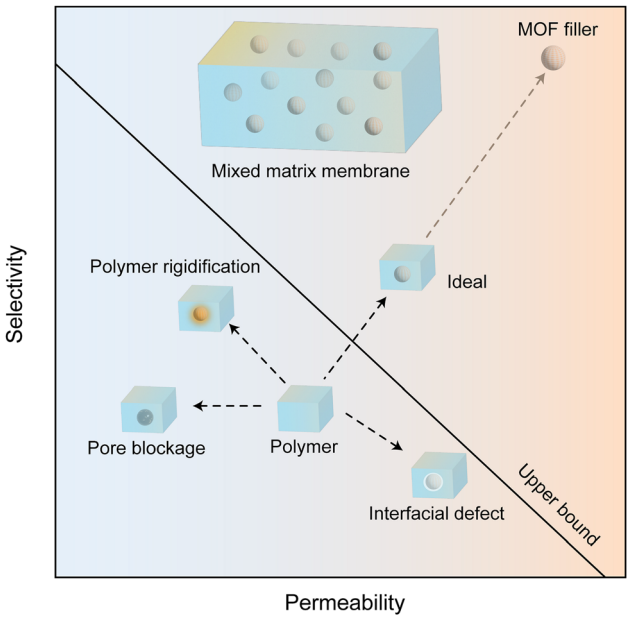

Fig. 18 Schematic illustration of the relationship between MOF filler dispersion states in MMMs and the corresponding membrane performance.

prepare MMMs (Fig. 19a).[145] ZIF-7-NH_2 showed larger aperture windows compared to pristine ZIF-7, which could be favorable for the fast diffusion of gases inside the framework. Moreover, a chelating effect between metal nodes in ZIF-7-NH_2 fillers and ester groups in the polymeric matrix could help to improve filler–polymer interactions.

Another strategy to impart MOFs with desired properties is to coat them with other functional materials, such as polymers,[146,147] other MOFs,[148] and even covalent organic frameworks (COFs).[149] These coating materials can exhibit high affinity with the polymeric matrix, resulting in improved filler–polymer interactions in MMMs. Xin *et al.* adopted a vacuum-assisted diffusion method to decorate MIL-101(Cr) with PEI to obtain PEI@MIL-101(Cr) nanoparticles and applied them in MMMs for CO_2 capture.[146] PEI could not only decorate the surface of MIL-101(Cr) but also penetrate into MOF pores owing to the large pore size of MIL-101(Cr). When embedded in MMMs, PEI@MIL-101(Cr) showed high affinity with the polymeric matrix owing to the electrostatic interaction and hydrogen bonding between abundant amino groups in PEI and sulfonic acid groups in the polymeric matrix.

To further promote the interfacial compatibility, Qian *et al.* proposed to coat the MOF surface with oligomers of identical chemical compositions to the polymeric matrix (Fig. 19b).[150] UiO-66-NH_2 was chosen as the filler material owing to its suitable pore size, high gas affinity, and good chemical stability. The amino functional groups in UiO-66-NH_2 functioned as crosslinking sites to react with dianhydride groups in oligomers of the polyimide matrix to form MOF–oligomer hybrid nanoparticles with a core–shell structure. These MOF–oligomer

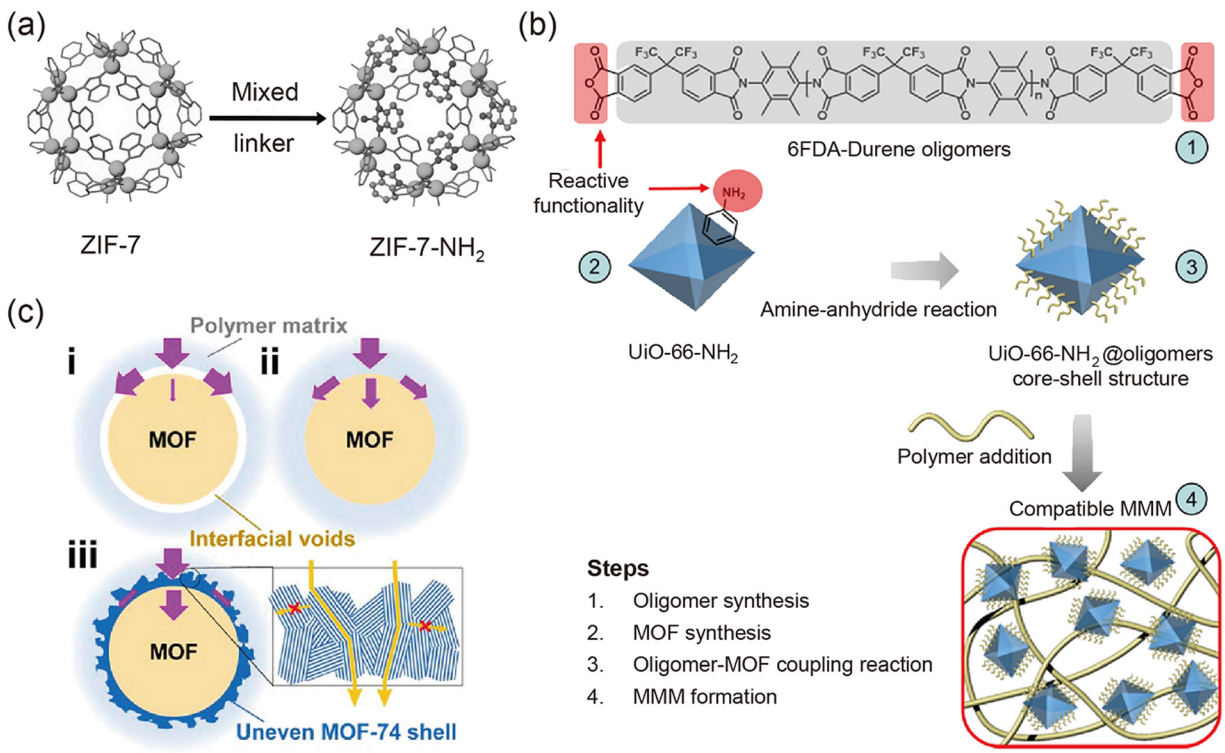

Fig. 19 (a) Schematic illustration of the synthesis of ZIF-7-NH_2 by a ligand substitution strategy. (b) Schematic illustration of the synthesis of UiO-66-NH_2@oligomers and preparation of MMMs. (c) Schematic demonstration of gas transport processes in MMMs with a defective interface (i), a defect-free interface (ii), and Ni-MOF-74 (iii) as the interphase. Reprinted with permission from ref. 145. Copyright 2017 Wiley-VCH; ref. 150. Copyright 2019 American Chemical Society; ref. 148. Copyright 2020 American Chemical Society.

hybrid nanoparticles demonstrated the same chemical composition as the polyimide matrix, leading to excellent interfacial compatibility in the corresponding MMMs. Consequently, defect-free MMMs with a filler loading of up to 40 wt% could still be achieved by using these MOF–oligomer hybrid nanoparticles as fillers. Similarly, good interfacial compatibility in another UiO-66-NH_2/polyimide system has also been realized by grafting polyimide brushes on to UiO-66-NH_2 fillers.[147] These two examples validate that this strategy can be applied to other MOF and polymer systems for the fabrication of good membranes with improved interfacial affinity.

Inspired by the coating of polymer chains, Wu *et al.* adopted a dual-interfacial engineering approach to coat the size-selective MOF core with a thin layer of polycrystalline MOF-74 shell to obtain MOF–MOF core–shell nanoparticles as fillers (Fig. 19c).[148] This MOF-74 coating layer showed larger external surface area due to its rough structure. Moreover, the abundant unsaturated open metal sites in the MOF-74 layer could form strong coordination bonds with oxygen atoms in polymer chains, leading to the fabrication of defect-free MMMs. Similarly, ZIF-93 nanoparticles can be post-synthetically modified with benzimidazole to form ZIF-93/11 hybrid nanoparticles.[151] The percentage of ZIF-11 in the hybrid material can be controlled by adjusting the reaction time and solvents. These ZIF-93/11 hybrid nanoparticles were incorporated into the polybenzimidazole (PBI) matrix to fabricate MMMs. These hybrid fillers showed good interfacial compatibility with the PBI matrix owing to the existence of benzimidazole moieties in both phases. Moreover, MOFs can be also coated with highly porous COF layers to form MOF@COF hybrid materials, which are also suitable to be used as fillers in MMMs.[149]

3.1.2 Polymer modification. For most MMMs reported in the literature, their optimum filler loadings are still relatively low (*e.g.*, $\leq$30 wt%), suggesting that the major part in MMMs is still the continuous polymer phase. For selected MOF fillers with fixed structures, it is of high importance to choose or design polymers that demonstrate high affinity with MOF fillers as the matrix for the preparation of good MMMs. One effective strategy to improve the filler–polymer interfacial compatibility is to modify polymer chains with organic chemicals that resemble MOF precursors. For instance, Fan *et al.* reported the introduction of imidazole groups into polyimide chains in ZIF-8-based MMMs.[152] Moreover, these MMMs were soaked in zinc(II) acetylacetonate solutions. The imidazole groups both in ZIF-8 fillers and the modified polyimide matrix were crosslinked by Zn^{2+} ions, leading to enhanced filler–polymer interactions. Therefore, the resultant MMMs demonstrated higher glass transition temperature, improved thermal stability, better stability in organic solvents, and better gas separation performance.

Polymers can also be modified with functional groups to promote their compatibility with MOF fillers *via* the formation of hydrogen bonding. Tien-Binh *et al.* reported the introduction of hydroxyl groups into polyimide chains to promote filler–polymer interactions in MMMs.[153] These hydroxyl groups in the polymeric matrix could form hydrogen bonding with amino groups in MIL-53-NH_2 MOF fillers, leading to homogenous filler distribution in the final MMMs. On the contrary, MIL-53-NH_2 nanoparticles could easily agglomerate in the non-hydroxyl-functionalized polyimide matrix owing to the lack of favorable filler–polymer interactions. Notably, the introduction of functional groups, such as –COOH, –NH_2, and –OH, into polymers have been widely reported in the literature.[154] Therefore, polymers modified with functional groups should deserve more attention as promising matrix materials compared to their non-functionalized counterparts in the future.

In order to fully exploit the potential of MOF fillers, the MOF filler loading should be maximized in MMMs. Nevertheless, at a high filler loading, fillers tend to agglomerate in the membranes, leading to reduced membrane mechanical properties and separation performance. Some MOF-based MMMs will become too brittle to be tested for separation when the filler loading reaches a certain content (*e.g.*, $>$34.5 wt% for ZIF-67/6FDA-DAM, 6FDA: (4,4′-hexafluoroisopropylidene)diphthalic anhydride; DAM: diaminomesitylene).[20] For the polyimide matrix with rigid polymer chains, it is possible to incorporate soft rubbery segments in these chains to enhance their interactions with MOF fillers and improve overall membrane mechanical properties. These soft rubbery segments can firmly wrap MOF fillers, leading to good interfacial compatibility.[155]

3.1.3 *In situ* synthesis. To prepare MOF-based MMMs, it is a common practice to synthesize MOF particles in hydrothermal or solvothermal reactions. Subsequently, these MOF particles are mixed with the polymer solution to prepare suspensions for membrane casting. A novel *in situ* filler synthesis strategy has been developed to combine the MOF synthesis and filler–polymer blending into one step, which may facilitate the fabrication of MMMs at a large-scale. In a typical procedure, MOF building blocks are directly mixed with the polymer solution. MOF crystals can *in situ* grow in the polymer matrix under a continuous stirring or membrane drying process.[156,157] Seoane *et al.* reported the *in situ* synthesis of MIL-68(Al) in polysulfone/tetrahydrofuran solution to prepare MMMs.[157] This one-pot synthesis method avoids the steps of MOF crystal separation from the mother liquor, drying, and redispersion in the polymer solution, largely promoting the homogeneous distribution of MOF fillers in the MMMs. Owing to the constraints of polymer chains, the size of the *in situ* synthesized MOF crystals is often limited within the nanometer range. These MOF nanoparticles can homogeneously distribute in the polymeric matrix and favorably interact with polymer chains. It is crucial to choose suitable solvents that can simultaneously dissolve the polymer and facilitate the MOF crystallization.

To further promote the homogeneous distribution of the *in situ* synthesized MOF fillers in MMMs at a high filler loading, Park *et al.* proposed a polymer-modification-enabled *in situ* MOF formation (PMMOF) strategy to enhance filler–polymer interactions in the MMMs.[158] This PMMOF strategy includes four major steps, including polymer hydrolysis, ion-exchange, ligand treatment, and imidization. These *in situ* synthesized ZIF-8 fillers exhibited an average particle size of $\sim$100 nm. Moreover, these ZIF-8 fillers demonstrated high affinity with

the polyimide matrix owing to their favorable filler–polymer interactions. Their loading could reach ~33 vol% in the MMMs without noticeable interfacial defects. Notably, this PMMOF strategy could also be applied to prepare thin selective layers for asymmetric mixed matrix hollow fiber membranes.

Similar to the *in situ* synthesis of MOF fillers, it is also possible to *in situ* synthesize the polymeric matrix in the presence of MOF fillers to prepare MMMs. During the *in situ* polymerization, functional groups in polymer monomers can favorably interact with MOF nanocrystals, leading to good adhesion between the polymeric matrix and MOF fillers in the MMMs. As a proof of concept, Lin *et al.* adopted this *in situ* polymerization strategy to prepare MMMs with improved interfacial compatibility for CO_2 capture.[159] Polymer monomers were added into a suspension containing MOF micron-sized crystals to start the *in situ* polymerization process. During the polymerization, the $-NH_2$ groups at the terminal of polyimide chains could form strong interactions with –COO– groups on the surfaces of the MOF crystals, leading to remarkable filler–polymer adhesion in the final MMMs.

3.1.4 Filler–polymer covalent crosslinking. The simple physical blending of MOF fillers with the polymeric matrix can occasionally lead to filler aggregation and interfacial nonselective voids in MMMs owing to the lack of strong filler–polymer interactions. The covalent crosslinking between MOF fillers and polymer chains has been demonstrated to be powerful in promoting filler dispersion and enhancing interfacial compatibility. For MMMs with covalent crosslinking, it is possible to incorporate MOF fillers at a considerably high loading (*e.g.*, >30 wt%) without deteriorating the membrane mechanical integrity. MOFs with functional groups, such as $-NH_2$,[160] –OH,[161] $-CH{=}CH_2$,[162] and –CN,[163] have been explored to be covalently crosslinked with polymer chains to prepare defect-free MMMs. Notably, this covalent crosslinking strategy is often coupled with the *in situ* polymerization strategy because of richer crosslinking sites in polymer monomers compared to existing polymers. For example, Tien-Binh *et al.* reported the preparation of covalently crosslinked MMMs with Mg-MOF-74 fillers and the PIM-1 matrix.[161] The hydroxyl groups in Mg-MOF-74 were crosslinked with fluoride groups in PIM-1 under thermal treatment. No "sieve-in-a-cage" morphology was observed in crosslinked MMMs, confirming that Mg-MOF-74 fillers were tightly wrapped by PIM-1 chains. Similarly, the same group explored to covalently crosslink UiO-66-NH_2 fillers with PIM-1 during the *in situ* PIM-1 polymerization process to prepare MMMs for carbon capture (Fig. 20a).[160] The amino groups in UiO-66-NH_2 could selectively react with the fluorine groups in the PIM-1 monomers under optimized conditions. The crosslinked MMMs demonstrated improved interfacial compatibility, higher gas permeability and selectivity, and better anti-aging performance compared to the pristine PIM-1 membrane and traditionally made MMMs.

The covalent crosslinking between MOF fillers and the polymeric matrix can also help to increase the rigidity of polymer chains and reinforce the chain orientation at the interface. Yu *et al.* demonstrated that thermally treated PIM-1 (sPIM-1) could be covalently crosslinked with UiO-66-CN nanoparticle fillers to prepare UiO-66-CN@sPIM-1 membranes for fast gas separation.[163] Cyano groups in both PIM-1 chains and UiO-66-CN nanoparticles were crosslinked to form triazine

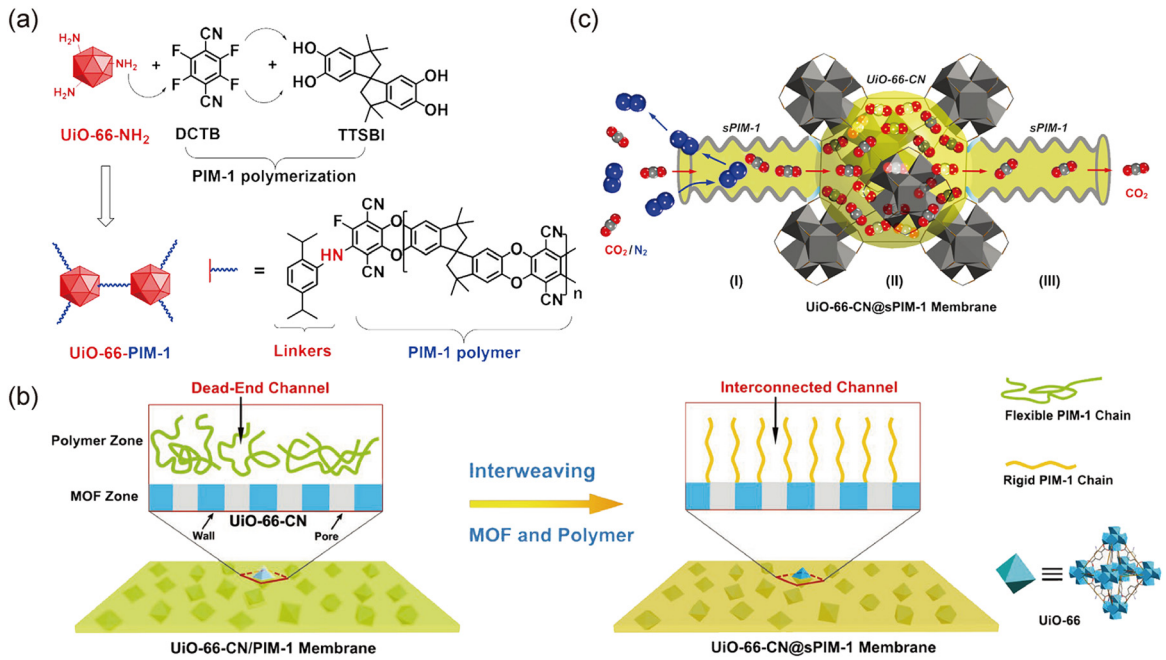

Fig. 20 (a) Schematic illustration of the covalent crosslinking between UiO-66-NH_2 and PIM-1. (b) Conceptual scheme for building CO_2 transport freeways through interweaving UiO-66 and PIM-1. (c) Schematic illustration of CO_2 and N_2 transport across the UiO-66-CN@sPIM-1 membrane. Reprinted with permission from ref. 160. Copyright 2018 Elsevier; ref. 163. Copyright 2019 Wiley-VCH.

structures at high temperatures. These UiO-66-CN nanoparticles were homogeneously dispersed in the crosslinked MMMs owing to the strong filler–polymer interaction. Moreover, this strong interaction resulted in polymer chain rigidification and better chain alignment at the surfaces of the MOF nanoparticles, which facilitated the formation of more open channels in the membrane (Fig. 20b). Consequently, gas molecules could diffuse freely through these open channels in the polymer zone and reach intrinsic pores in the MOF fillers. Competitive adsorption for CO_2 over N_2 occurred within MOF cavities, leading to narrowed MOF pores. Therefore, these narrowed pores could efficiently sieve CO_2 from N_2 (Fig. 20c). The resultant UiO-66-CN@sPIM-1 MMMs exhibited greatly enhanced permeability and good selectivity for CO_2/N_2 separation. Similarly, other MOF/polymer systems with covalent filler–polymer crosslinking, such as UiO-66-allyl-C (C = corona)/PDMS,[164] vinyl-functionalized UiO-66/PEO-based polymer,[165] trimethoxysilan-functionalized UiO-66/PDMS,[166] amino-functionalized ZIF-8/PDMS,[167] and UiO-66-NH_2/acid-functionalized polyimide (PI-COOH),[168] have also been explored for diversified separation applications.

3.1.5 Priming and wet fillers. To reduce the affinity among MOF fillers and enhance their interactions with polymer chains, one of the easiest methods is to physically introduce a thin layer of polymer on the outer surface of MOF fillers in the membrane casting suspension. This method is known as ''priming'' and it can largely improve the filler dispersion and enhance filler–polymer compatibility in MMMs. In a typical priming procedure, a desired amount of MOF fillers is weighed and dispersed in the organic solvent under sonication or mechanical stirring. Meanwhile, the matrix polymer is dissolved in the same solvent. Next, a certain amount of the polymer solution (*e.g.*, 20 wt%) is added into the MOF suspension. The resultant suspension is stirred or sonicated for a sufficiently long time (0.5–2 h). This process can be repeated until the desired amount of polymer is added into the filler suspension. The resultant suspension is poured into a petri dish or cast on a glass plate to prepare MMMs. This strategy is quite useful in preventing filler aggregation and avoiding interfacial defects in MMMs. Shahid *et al.* adopted the priming protocol to improve the filler–polymer interfacial microstructure in Fe(BTC)/Matrimid MMMs.[169] SEM images showed that Fe(BTC) particles were completely enfolded by the matrix in the MMM with a 30 wt% filler loading. Moreover, no interfacial defects were observed in that membrane. Similarly, this priming strategy can also be applied to other MOF-based MMMs, such as Bio-MOF-1/polysulfone,[170] ZIF-8/polyimide,[171] CuBDC/PVDF,[172] and MIL-53(Al)-NH_2/polyimide,[153] with improved filler–polymer interfacial compatibility.

Filler aggregation is one of the most difficult challenges in MOF-based MMMs with high filler loadings. Nowadays, MOF nanoparticles are preferred as good fillers compared to micron-sized crystals because these nanoparticles demonstrate higher surface area to volume ratios, which can help to improve the effective contact area between fillers and the polymeric matrix. In a typical MMM preparation process, these MOF nanoparticles are dried and activated at high temperatures before being mixed with the polymer solution. Nevertheless, these MOF nanoparticles tend to form stable aggregates to reduce their surface energies during the drying process. These MOF aggregates can be hardly redispersed in the polymer solution even under vigorous stirring or sonication. Therefore, in recent years, a new trend has emerged in which wet fillers instead of dried fillers are used for the fabrication of MMMs with improved filler dispersion. These MOF nanoparticles are synthesized by solvothermal or hydrothermal reactions, purified by solvent washing, activated by solvent exchange, and dispersed in the solvent which is used to dissolve the matrix polymer. Consequently, these wet fillers can remain their good dispersion states in solvents during the whole process. Finally, the filler suspension can be directly mixed with the polymer solution to prepare MMMs. For instance, Deng *et al.* prepared ZIF-8 nanoparticles and directly incorporated them into a polyvinyl alcohol (PVA) matrix without a filler drying process (Fig. 21a).[173] These ZIF-8 nanoparticles were synthesized in deionized water and purified by repeated washing with deionized water. The high stability of the as-prepared ZIF-8 suspension was validated by the good transmittance recorded using a UV spectrophotometer. In contrast, ZIF-8 particles prepared with a drying process could easily aggregate and float on top of the suspension (Fig. 21b). Subsequently, wet ZIF-8 nanoparticles were mixed with an aqueous solution of PVA to prepare MMMs. Meanwhile, dried ZIF-8 nanoparticles were also prepared and added into the PVA matrix to prepare MMMs as comparisons. MMMs with wet ZIF-8 nanoparticles were transparent and crack-free, while MMMs with dried ZIF-8 nanoparticles showed cracks and obvious phase separation. The strategy of directly using wet MOF nanoparticles or nanosheets as fillers can also be found in other MOF/polymer systems, including CuBDC/polyimide,[13] ZIF-8/PDMS,[174] and N-heterocyclic carbene-functionalized ZIF-8/polyimide.[20] It is anticipated that more wet MOF fillers will be explored in MMMs for better filler dispersion in the future.

3.1.6 Other strategies. To promote filler dispersion in the polymeric matrix in MMMs, it is crucial to design good MOF fillers with suitable particle size, morphology, and surface chemistry. During the initial development stage of MOF-based MMMs, micron-sized MOF crystals have been commonly used as fillers, which can easily lead to serious filler sedimentation and a ''sieve-in-a-cage'' morphology. As mentioned previously, nano-sized MOF particles with high surface area-to-volume ratios are preferred as promising fillers owing to their large contact area with the polymeric matrix.[148,174,175] Therefore, MMMs with nano-sized MOF particles can demonstrate enhanced filler–polymer compatibility compared to their counterparts with micron-sized fillers. Similarly, 2D MOF nanosheets with even higher surface area to volume ratios exhibit huge potential in promoting filler–polymer interactions in MMMs.[13,176–178] Notably, the new trend of using 2D MOF nanosheets as fillers will be elaborately discussed in the following section. MOFs with desired particle size and morphology can be obtained by both bottom-up and top-down strategies.[179,180] Several different bottom-up strategies that have been proved to be useful to produce MOF nanoparticles are

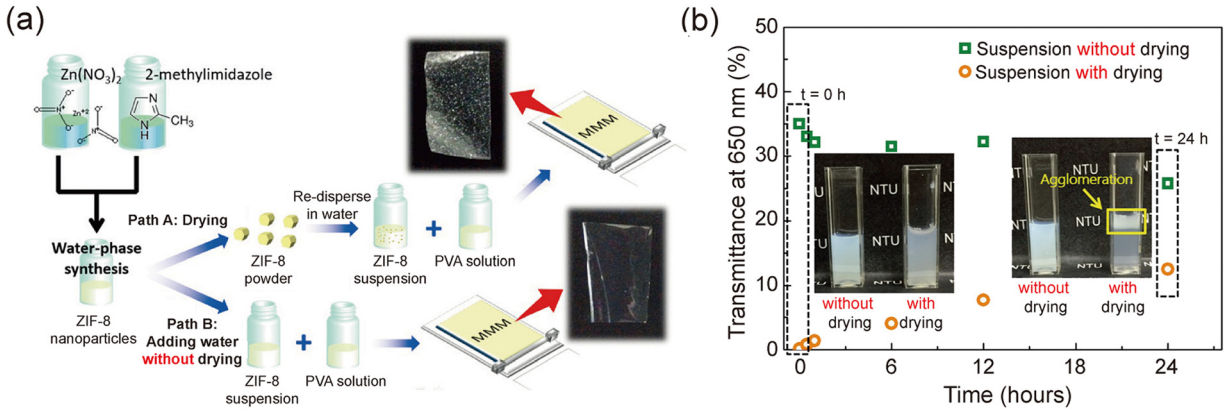

Fig. 21 (a) Schematic illustration of the preparation of MMMs from ZIF-8 suspensions with and without drying. (b) Transmittance of ZIF-8 suspensions as a function of standing time. Reproduced with permission from ref. 173. Copyright 2016, Wiley-VCH.

summarized here:[180] (1) controlling MOF growth kinetics by adjusting the crystallization temperature and time during conventional hydrothermal/solvothermal reactions; (2) choosing suitable solvent systems for MOF growth, such as mixed solvents with water or ethanol; (3) using surfactants, coordination modulators, or ionic-liquid microemulsions (ILMEs) during MOF crystallization; and (4) adopting a mechanochemical synthesis or microwave- or ultrasound-assisted synthesis approach. Moreover, the mechanical grinding of large micron-sized MOF crystals is the most widely used top-down method to fabricate MOF nanoparticles. These approaches offer substantial opportunities to produce high-quality MOF nanocrystals that can be applied as potential fillers in MMMs. For example, Nordin *et al.* prepared MMMs containing ZIF-8 nanoparticles with different sizes (100–500 nm) and explored their CO_2/CH_4 separation performance.[181] It was found MMMs with the smallest ZIF-8 nanoparticles ($\sim$100 nm) showed the highest CO_2/CH_4 selectivity. Smaller ZIF-8 fillers exhibited stronger interactions with the polymeric matrix, leading to enhanced interfacial compatibility and fewer interfacial defects.

MOFs can also be grown on external supports to fabricate composite filler materials with an improved dispersion status in MMMs. Graphene oxide (GO) is the most widely used support mainly due to its rich carboxylate groups offering excellent binding sites for the MOF growth and large surface area-to-volume-ratio promoting the filler distribution in the membrane. MOF nanoparticles are chemically anchored on GO planes once the growth process is finished, preventing the possible migration and aggregation of MOF nanoparticles in the membrane. For instance, UiO-66-NH_2@GO composite materials were successfully prepared by growing UiO-66-NH_2 nanoparticles on GO nanosheets under solvothermal conditions.[182] Contrary to the easy aggregation of pristine UiO-66-NH_2 nanoparticles in the membrane, UiO-66-NH_2@GO composite fillers showed better interactions with the polyimide matrix and an improved dispersion status in the membrane. Similarly, other MOF@GO composite materials, such as UiO-66@GO,[183] ZIF-8@GO,[184] and CNT-supported composites, such as ZIF-8@CNT,[185] MIL-101-NH_2@CNT,[186] have also been prepared and demonstrated better performance compared to pristine MOF materials in MMMs.

Another efficient strategy to improve interactions between MOF fillers and polymer chains is to use interfacial binders, mainly ionic liquids (ILs). ILs behave as interfacial wetting and binding agents to promote filler–polymer interactions by forming MOF–IL and IL–polymer interfaces, which can result in significantly reduced interfacial defects. Moreover, ILs demonstrate excellent thermal and chemical stability, low volatility, and high affinity for certain gases, such as CO_2 and H_2S. However, for polymers with large free volume, ILs can sometimes occupy the membrane free volume, leading to reduced membrane permeability. Therefore, careful design of choices of ILs, polymers, and MOF fillers is required to maximize the efficacy of ILs in MMMs. Lin *et al.* demonstrated that decorating micron-sized HKUST-1 fillers with an IL, 1-ethyl-3-methylimidazolium bis(trifluoromethylsulfonyl)imide (Emim[Tf_2N]), could be beneficial for preparing MMMs with better interfacial microstructures.[187] Pristine HKUST-1 microparticles exhibited poor interactions with the matrix polymer, leading to a "sieve-in-a-cage" morphology. In contrast, HKUST-1 fillers coated with the IL layer showed much better adhesion with polymer chains, which resulted in reduced interfacial voids in the MMMs.

3.2 Gas separation

The first-generation industrial membranes were developed for the separation of H_2 from the H_2/N_2 mixture during the ammonia production process in the late 1970s.[188] Since then, membranes with different configurations and module designs have been proposed for a wide range of gas separation applications, including natural gas sweetening, biogas upgrading, CO_2 capture from flue gas, H_2 purification, air separation, olefin/paraffin separation, and vapor/vapor separation.[189] The incorporation of MOF fillers into the polymeric matrix to prepare MMMs offer great opportunities in designing new membranes with outstanding separation performance. Owing to their adjustable structures and rich chemistry, MOF fillers can be customized for diversified separation processes. In this section,

recent state-of-the-art advances in MOF-based MMMs for gas separation will be outlined and discussed in detail.

3.2.1 H_2 purification. Membrane technology offers an energy-efficient alternative to conventional pressure swing adsorption for industrial H_2 purification. The incorporation of MOFs as fillers in the polymeric matrix to prepare MMMs has been proven successful in improving the membrane performance. MOFs with suitable aperture sizes and functional groups, such as ZIF-71,[190] ZIF-8,[191] ZIF-90,[192] ZIF-L,[193] functionalized UiO-66,[194] MIL-53-NH_2,[140] and CAU-21,[195] have been demonstrated effective in enhancing the membrane separation performance for H_2 purification. Al-Maythalony *et al.* demonstrated that the overall separation performance of MMMs could be improved by increasing the affinity between target gases and filler materials.[196] They adopted a post-synthetic modification (PSM) strategy to replace the benzimidazolate moieties in original ZIF-7 nanocrystals (nZIF-7) with benzotriazolate molecules to prepare PSM-nZIF-7 fillers with additional polar nitrogen atoms. These PSM-nZIF-7 fillers showed enhanced affinity with target gas molecules, therefore promoting the gas solubility in the corresponding MMMs. Impressively, PSM-nZIF-7-based MMMs demonstrated a H_2 permeability of 2020 barrer, nearly ten times that of the original nZIF-7-based MMMs (207 barrer), and a good H_2/CO_2 selectivity of 8, showing good potential for industrial H_2 purification. Meanwhile, Sánchez-Laínez *et al.* developed a PSM strategy to fabricate core–shell hybrid ZIFs and applied them as fillers in a PBI matrix for H_2/CO_2 separation.[197] ZIF-8 nanoparticles were post-modified with benzimidazole in DMF to produce hybrid ZIFs with ZIF-7 as the shell and ZIF-8 as the core. The benzimidazole moieties in the ZIF-7 shell improve the filler–polymer affinity, and ultrasmall pores in the ZIF-8 core enable a precise gas discrimination process in MMMs. The final MMMs containing ZIF-8@ZIF-7 core–shell hybrid fillers showed a high H_2 permeability of 1921 barrer and a H_2/CO_2 selectivity of ~12, outperforming the pure PBI membrane and MMMs containing either ZIF-7 or ZIF-8 fillers.

Another interesting study by Hess *et al.* suggested that ZIF-8 could be selectively grown inside polymer pores to form novel ZIF-8/polymer composite membranes for gas separation.[198] In their study, ZnO seed nanoparticles were first directed and immobilized in the pores of the PES matrix during a phase separation process, followed by the solvothermal treatment to produce ZIF-8 islands. Notably, these ZnO seed nanoparticles would only allow the growth of ZIF-8 islands within polymer pores and prevent the formation of continuous ZIF-8 membranes. Finally, post-treatment with dimethylacetamide (DMAc) vapor was conducted to allow the PES matrix to tightly fuse around ZIF-8 islands. Considering the simplicity of the whole membrane preparation process, it may enable the large-scale production of MOF-based membranes using the roll-to-roll coating technology. These ZIF-8/polymer composite membranes exhibited similar H_2/CO_2 separation performance but greatly increased mechanical stability compared to ZIF-8 polycrystalline membranes grown on porous polymeric supports. Moreover, these membranes could maintain their good H_2/CO_2 selectivity (~10) after bending tests owing to their high flexibility.

3.2.2 CO_2/N_2 separation. It has been reported that membranes with a CO_2 permeance of higher than 1000 GPU and a CO_2/N_2 selectivity of higher than 30 could be economically attractive for post-combustion CO_2 capture from coal-fired power plants.[199] Current pure polymeric membranes can hardly meet this goal. Therefore, MOFs have aroused great interest as potential fillers to boost the separation performance of membranes for efficient CO_2/N_2 separation. Various types of MOFs, including ZIFs,[200–203] the UiO-66 series,[137,204,205] the MIL series,[146,206,207] and the **SIFSIX** series,[208] have been investigated in MMMs for CO_2/N_2 separation. Among them, MOFs with size-selective pores and high CO_2 affinity are preferred because they can maximize the membrane separation performance in terms of permeability, selectivity, anti-swelling and anti-aging abilities.

To maximize the efficacy of MOF fillers in MMMs, it is highly desired to achieve sufficiently high loadings of MOF fillers to realize fast gas transport in membranes mainly through intrinsic pores or channels in the MOFs. For instance, Su *et al.* synthesized UiO-66-NH_2 nanoparticles *via* a microwave synthesis approach and incorporated them into the polysulfone matrix to prepare MMMs with filler loadings of up to 50 wt%.[137] A significant CO_2 permeability increase was observed for MMMs when the filler loading was increased from 30 wt% to 40 wt%. A closer examination of the membrane microenvironment by SEM revealed that a percolative network of UiO-66-NH_2 nanoparticles was formed in the MMMs at a filler loading of 40 wt% (Fig. 22a). Therefore, gas molecules not only passed through the polymeric matrix by the conventional solution-diffusion mechanism, but also directly permeated through intrinsic pores in the MOF percolation network. As a result, MMMs with a 40 wt% UiO-66-NH_2 loading demonstrated a CO_2 permeability of 46 barrer, seven times higher than that of the pure polysulfone membrane, with a comparable CO_2/N_2 selectivity of 26 (Fig. 22b). A closer examination of their gas transport properties revealed that the gas diffusion coefficients of the MMMs greatly increased when the filler loading was increased from 30 wt% to 40 wt%, validating the existence of dual transport pathways in the resultant membranes (Fig. 22c).

The chemical crosslinking between MOF fillers and the polymeric matrix has been demonstrated as a reliable strategy to improve the filler–polymer compatibility in MMMs. Compared to relatively weaker bonds, such as hydrogen bonds and π–π bonds,[205,206,209] stronger covalent bonds are more efficient in reducing interfacial defects for MMMs at high filler loadings. Yao *et al.* prepared a series of imidazolium based IL-decorated UiO-66 MOFs (UiO-66-IL-X, X = halide ion) and crosslinked them with polyurethane oligomers under mild conditions (ambient pressure and temperature) to fabricate MMMs for CO_2/N_2 separation.[210] The isocyanate groups in polyurethane oligomers could easily react with hydroxyl groups on UiO-66-IL-X nanoparticles, preventing the filler sedimentation and aggregation during the membrane preparation process. Owing to the strong covalent bonding between the fillers and the

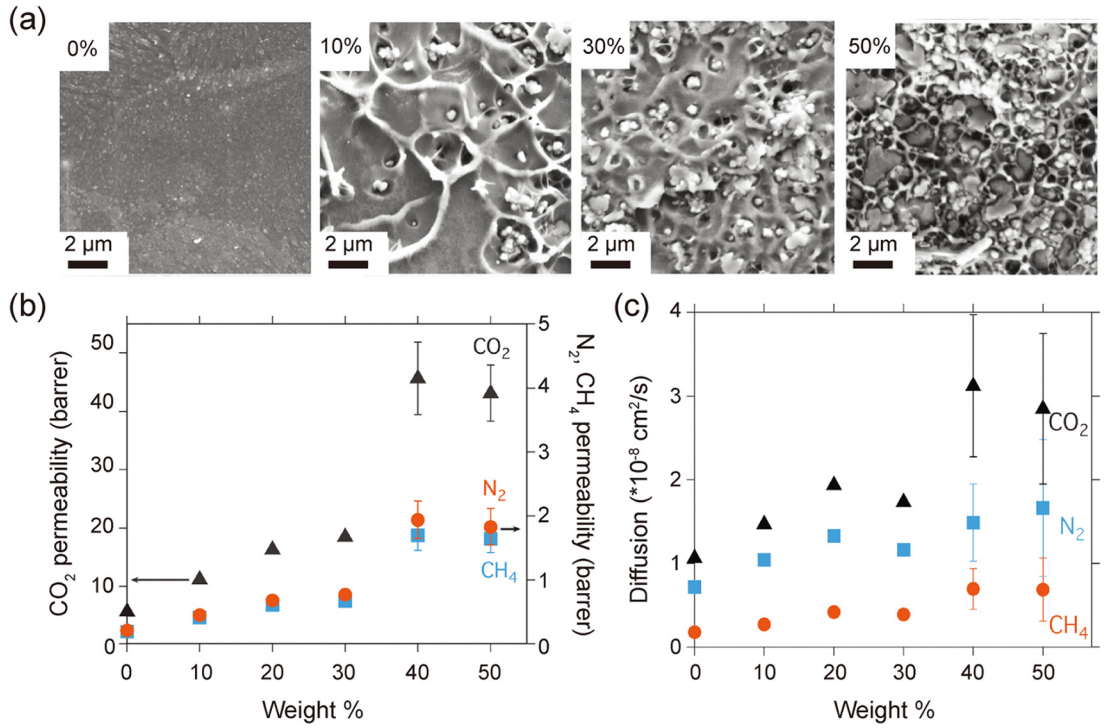

Fig. 22 (a) High magnification SEM cross-sectional images of membranes with different filler loadings. (b) The correlation between the pure gas permeabilities and filler loadings in UiO-66-NH_2-based MMMs. (c) The correlation between the gas diffusion coefficients and filler loadings in UiO-66-NH_2-based MMMs. Reprinted with permission from ref. 137. Copyright 2016 the Royal Society of Chemistry.

polymeric matrix, MMMs even with a 50 wt% MOF loading were still robust enough for mechanical property tests and maintained their structural integrity for CO_2/N_2 separation. The optimized MMMs with a 50 wt% MOF loading exhibited 490% and 380% increases in CO_2 permeance and CO_2/N_2 selectivity, respectively, compared to the pure polyurethane membrane.

Some MOFs can demonstrate reversible responses to external stimuli, such as pressure,[211] temperature,[212] light,[14] and electric fields,[15] which can enable them to be used as fillers to prepare smart MMMs with adjustable and controllable separation performance. Recently, several examples using light-responsive MOFs as potential fillers in MMMs for CO_2/N_2 separation have been reported.[213–215] Notably, these light-responsive MOFs all contain azobenzene moieties that can demonstrate reversible *cis* and *trans* isomerization under UV and visible light irradiation. For instance, Prasetya *et al.* synthesized two light-responsive MOFs, including JUC-62 and PCN-250 (PCN = porous coordination network), and added them into the Matrimid matrix to fabricate MMMs.[213] A noticeable CO_2 permeability change (5–9 wt%) was observed for MMMs containing light-responsive MOF fillers when the UV light source was switched on and off alternately. However, no CO_2 permeability change was found for a pure Matrimid membrane and MMMs with ZIF-8 fillers under the same conditions. Moreover, these MMMs with JUC-62 and PCN-250 fillers could maintain their light-responsive properties for two months, confirming their good long-term stability.

3.2.3 CO_2/CH_4 and $CO_2/H_2S/CH_4$ separation. The addition of MOFs with size-selective pores and high CO_2 affinity into polymeric matrixes to prepare MMMs for CO_2/CH_4 separation has aroused great interest over the past few decades. Up to now, a series of MOFs, such as ZIFs,[216,217] MILs,[218,219] MOF-74 series,[161] UiO-66 series,[220,221] **fcu**-MOFs and zeolite-like MOFs (ZMOFs),[222] have been explored as fillers to enhance the membrane performance for CO_2/CH_4 separation. Notably, the CO_2/CH_4 separation in the natural gas industry is often performed at high pressures (up to 60 bar). Under such harsh conditions, the dissolution of condensable gases, such as CO_2 and H_2S, in the polymeric matrix can severely swell polymer chains and reduce the membrane CO_2/CH_4 selectivity, leading to membrane plasticization. MOF fillers can induce polymer chain rigidification at their surfaces and even be crosslinked with polymer chains to improve the chain rigidity, therefore enhancing the membrane anti-plasticization ability.

To further improve the filler–polymer affinity in MMMs for CO_2/CH_4 separation, various strategies, such as introducing covalent and hydrogen bonding at the interface,[161,220,223] *in situ* growing MOFs in the membrane,[224] utilizing MOF nanosheets as fillers,[176] and adopting ILs as interfacial binders,[187] have been proposed and proved successful in preventing the filler aggregation and reducing interfacial defects in MMMs. For instance, Wang *et al.* proposed a novel approach to engineer the filler–polymer interface by grafting UiO-66-NH_2 fillers with polyimide brushes to obtain hybrid materials (UiO-66-NH_2@PI).[147] The abundant amino groups at the surface of UiO-66-NH_2 offered rich crosslinking sites for the coating of polyimide brushes through step-growth polymerization (Fig. 23a). UiO-66-NH_2@PI nanoparticles could be added into the polyimide

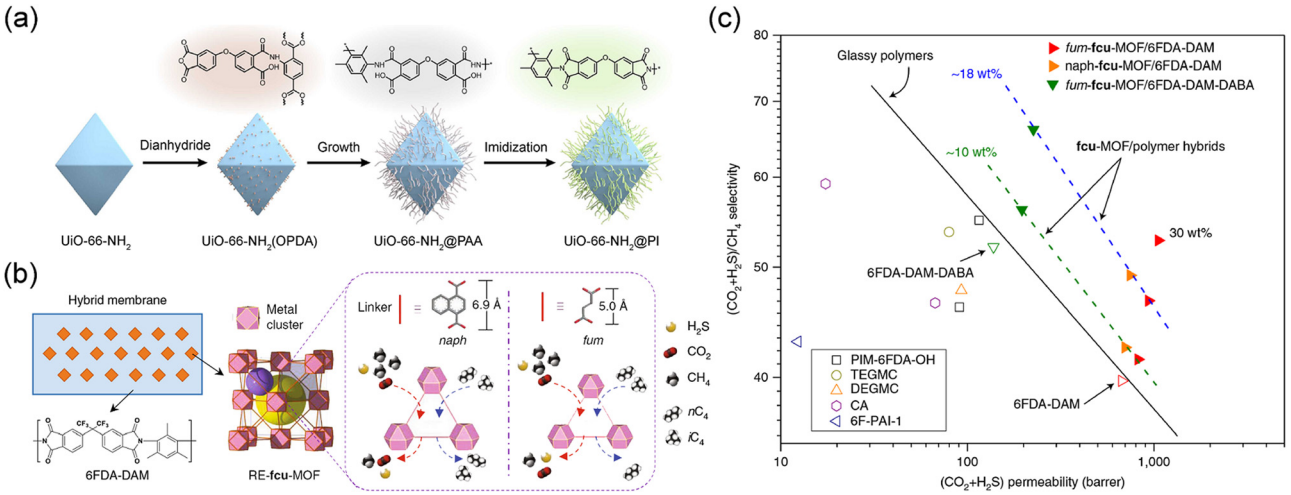

Fig. 23 (a) Schematic illustration of the synthetic procedure of UiO-66-NH_2@PI. (b) Schematic illustration of designing MMMs with RE-**fcu**-MOF with adjustable pores. (c) (CO_2 + H_2S)/CH_4 mixed-gas separation performance of the different membranes. Reprinted with permission from ref. 147. Copyright 2018 American Chemical Society, ref. 17, Copyright 2018, Nature Publishing Group, respectively.

matrix to prepare MMMs at a filler loading of 27 wt% without interfacial defects. Compared to traditional MMMs with original UiO-66-NH_2 MOF fillers, MMMs with UiO-66-NH_2@PI fillers showed improved ductility, reduced polymer chain mobility, and enhanced plasticization resistance against CO_2 under high pressures.

The existence of condensable H_2S in natural gas can severely deteriorate the separation performance of polymeric membranes because H_2S can dissolve in membranes and swell polymer chains. The research on MOF-based MMMs for CO_2/H_2S/CH_4 separation is rather limited owing to the acute toxicity of H_2S. Moreover, it is also a formidable challenge to design suitable MOF fillers that can simultaneously have size-selective pores and high chemical stability in a corrosive H_2S environment. Our group discovered that MMMs containing RE-**fcu**-MOFs could demonstrate high efficiency in simultaneously removing CO_2 and H_2S from natural gas.[17] These RE-**fcu**-MOFs possess tetrahedral and octahedral cages interconnected by triangular windows, and the dimensions of these windows can be precisely tuned by judicious choices of di-topic organic linkers (Fig. 23b). RE-**fcu**-MOF nanoparticles were incorporated with different glassy (6FDA-DAM and 6FDA-DAM-DABA) and rubbery (Pebax) polymeric matrixes to form a series of MMMs for the removal of CO_2 and H_2S from natural gas and the separation of butane isomers. Detailed analyses on gas transport properties in RE-**fcu**-MOFs revealed that the diffusivity coefficients of CO_2 and H_2S were much larger than that of CH_4, validating the molecular sieving ability of RE-**fcu**-MOFs. The optimized RE-**fcu**-MOF-based MMMs demonstrated a CO_2 and H_2S permeability of 580 and 470 barrer, respectively, with a (CO_2 + H_2S)/CH_4 selectivity of 53 for mixed gas separation, highlighting their great potential for efficient acid gas removal from natural gas (Fig. 23c). Subsequently, our group also explored three kinds of fluorinated MOFs with the same pyrazine (pyz) ligand, including $[Ni(NbOF_5)(pyz)_2]_n$ (NbOFFIVE-1-Ni), $[Ni(AlF_5)(pyz)_2]_n$ (AlFFIVE-1-Ni), and $[Cu(SiF_6)(pyz)_2]_n$ (**SIFSIX**-3-Cu), as fillers in MMMs.[225] The aperture sizes of the fluorinated MOFs could be precisely adjusted by the center metal (Ni or Cu) and the pillar ($[NbOF_5]^{2-}$, $[AlF_5]^{2-}$ or $[SiF_6]^{2-}$) to achieve a molecular sieving separation process for gas mixtures. Moreover, the NbOFFIVE-1-Ni and AlFFIVE-1-Ni crystals could maintain their good crystallinity when being exposed to pure and high-pressure H_2S over a long period of time, confirming their high stability in a corrosive H_2S environment. Therefore, these two MOFs were further explored in the 6FDA-DAM matrix for CO_2/H_2S/CH_4 separation. Simultaneous increases in CO_2 and H_2S permeability and (CO_2 + H_2S)/CH_4 selectivity were observed in MMMs compared to the pristine 6FDA-DAM membrane. The optimized MMMs showed CO_2 and H_2S permeabilities of 599 and 458 barrer, respectively, with a (CO_2 + H_2S)/CH_4 selectivity of 42 for mixed gas separation.

3.2.4 C_3H_6/C_3H_8 separation. It is estimated that membranes with a C_3H_6/C_3H_8 selectivity of greater than 10 and a C_3H_6 permeance of several hundred GPU could compete with distillation for C_3H_6/C_3H_8 separation in industry.[189] Some polymeric membranes can demonstrate good C_3H_6/C_3H_8 separation performance that surpasses the upper bound during single gas tests. Nevertheless, for mixed gas tests, C_3H_6 and C_3H_8 can easily dissolve in the membrane and swell polymer chains, resulting in severe membrane plasticization and reduced membrane selectivity. The incorporation of MOF fillers that demonstrate favorable interactions with polymer chains can lead to polymer chain rigidification at the filler surface, which will greatly improve the membrane anti-plasticization performance. Moreover, MOFs with ultrasmall pores, especially ZIFs, including ZIF-8[226] and ZIF-67,[227] can endow MMMs with a molecular sieving ability for efficient C_3H_6/C_3H_8 separation based on the minor kinetic diameter difference (0.20 Å) between these two gases.

Considering that C_3H_6 and C_3H_8 have different conformers due to the free rotation of their C–C bonds, our group prepared Zr-fum-**fcu**-MOFs with trefoil-like pores that can differentiate

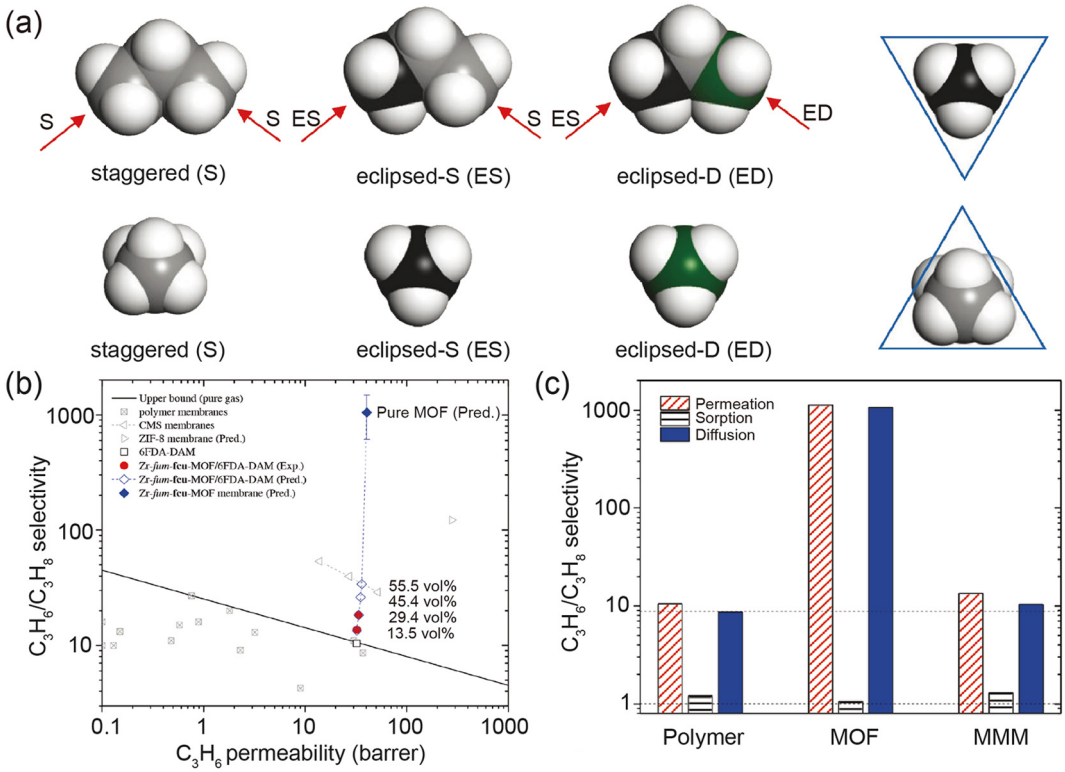

Fig. 24 (a) Typical conformers of a C_3H_8 molecule in space-filling (CPK) model. (b) The C_3H_6/C_3H_8 separation performance of MMMs with different filler loadings. (c) Permeation, sorption and diffusivity selectivity of C_3H_6/C_3H_8 of the polymer, MOF and MMM. Reprinted with permission from ref. 228. Copyright 2019 Wiley-VCH.

these conformers and incorporated them into the 6FDA-DAM matrix to improve the membrane C_3H_6/C_3H_8 selectivity by a conformation-controlled molecular sieving effect (Fig. 24).[228] Pure gas permeation data showed that MMMs with a 29 vol% Zr-fum-**fcu**-MOF loading exhibited 73% and 8% increase in C_3H_6/C_3H_8 selectivity and C_3H_6 permeability compared to the pure polymeric membrane, respectively. Detailed data analyses suggested that Zr-fum-**fcu**-MOF demonstrated a C_3H_6/C_3H_8 diffusivity selectivity of up to 1086, validating its ability to discriminate C_3H_6 and C_3H_8 by the conformation-controlled molecular sieving effect. Plasticization was also observed for MMMs when the testing pressure was increased to 483 kPa at 35 °C. Nevertheless, a simple increase in the membrane testing temperature from 35 °C to 55 °C could largely improve the membrane anti-plasticization ability.

Recently, another important finding in MMMs for efficient C_3H_6/C_3H_8 separation was made by Knebel *et al.* who fabricated high-performance MMMs with solution processable MOF fillers.[20] They demonstrated that ZIF-67 could be processed into porous liquid by outer surface functionalization with N-heterocyclic carbene molecules. These carbene-modified ZIF-67 nanoparticles could be easily dispersed in a polymeric matrix, allowing the fabrication of MMMs with high MOF filler loadings. MMMs with a carbene-modified ZIF-67 loading of up to 48 wt% still showed good mechanical strength with no visible filler agglomeration or sedimentation. In contrast, MMMs with a 35 wt% ZIF-67 loading were brittle and lost their structural integrity upon mechanical punching. With the addition of 48 wt% carbene-modified ZIF-67 fillers, MMMs showed a membrane C_3H_6 permeability of 93 barrer and a C_3H_6/C_3H_8 selectivity of 14, which are 324% and 153% higher compared to those of the pristine 6FDA-DAM membrane, respectively. This performance far exceeds the upper bound limit, highlighting the great potential of these high-performance membranes for industrial C_3H_6/C_3H_8 separation.

3.2.5 Other gas separation applications. There are also some other important gas separation applications in industry, such as SO_2 removal from flue gas (SO_2/N_2 separation) and ethylene purification from the ethylene/ethane mixture (C_2H_4/C_2H_6 separation). Owing to the different physicochemical properties of gas mixtures, membranes with specialized features are desired to maximize the separation efficiency. The adjustable pore size and geometry, rich chemical functionality, and good chemical and thermal stability endow MOFs with great potential to be applied as fillers in MMMs for the above-mentioned industrial gas separation applications. Specific prominent examples on MOF-based MMMs for these applications will be highlighted here.

SO_2 is considered as one of the most toxic air pollutants and it can result in poisonous acid rain and organosulfate aerosols. Currently, more than 90% of SO_2 comes from the combustion of fossil fuels. MOF-based MMM contactors have been shown to be promising for selective SO_2 removal from flue gas. MOFs with high porosity and rich SO_2 affinity sites are highly desired

to improve the membrane separation performance. For instance, Xin *et al.* designed and prepared MIL-101(Cr)-based MMM contactors for SO_2/N_2 separation.[229] With the incorporation of MIL-101(Cr) fillers, the resultant MMMs showed improved wetting resistance, higher gas permeation rates and enhanced SO_2 removal efficiency. Specifically, a MMM contactor with 15 wt% MIL-101(Cr) fillers showed a high SO_2 absorption flux of 1×10^{-3} mol m^{-2} s^{-1} and a good SO_2 removal efficiency of 90%. A similar phenomenon has also been found in MIL-125-NH_2-based MMM contactors,[230] highlighting the good potential of MOFs for efficient SO_2 removal.

As for the efficient separation of C_2H_4/C_2H_6 mixtures, conventional polymeric membranes can hardly achieve the separation goal owing to the severe membrane plasticization induced by the dissolution of condensable C_2H_4 and C_2H_6 molecules in membranes. These molecules can easily swell polymer chains at high pressures, resulting in largely reduced membrane selectivity. To enhance the membrane anti-plasticization performance, Bachman *et al.* proposed to crosslink these polymer chains by adding MOFs with coordinatively unsaturated metal sites as fillers in MMMs (Fig. 25).[144] A series of MOF-74 MOFs with different metal ions, including Mg, Mn, Co, Ni, were synthesized in a nanoparticle morphology and incorporated into the 6FDA-DAM matrix for C_2H_4/C_2H_6 separation. The strengths of filler–polymer interactions for these MOF-74 fillers follow the sequence Mg < Mn ≪ Co < Ni. Single gas permeation studies suggested that the incorporation of MOF-74 series MOF fillers into the 6FDA-DAM matrix could largely boost the membrane C_2H_4/C_2H_6 separation performance. Moreover, for the separation of the C_2H_4/C_2H_6 equimolar mixture, the pure 6FDA-DAM membrane demonstrated a plasticization pressure of ~10 bar, while MOF-74-Ni-based MMMs with a 25 wt% filler loading showed a plasticization pressure of greater than 20 bar. As a result, these MMMs still exhibited a good C_2H_4/C_2H_6 selectivity of 4 for mixed gas separation at a testing pressure of 20 bar, while the pure 6FDA-DAM membrane showed no selectivity under the same conditions. This study provides useful guidance on the rational design of good membranes with stable C_2H_4/C_2H_6 separation performance toward industrial applications.

3.3 Liquid separation

MOF-based MMMs have aroused great interest in various liquid separation applications owing to their exciting membrane separation performance and easy membrane preparation process. The homogeneous dispersion of porous MOF fillers with well-defined pores in the polymeric matrix can help to largely enhance the overall membrane separation performance. Moreover, MOF fillers can be chemically cross-linked with the polymeric matrix in MMMs, which can improve the membrane anti-swelling ability and operational stability in various liquids. Notably, MOFs with high water stability are preferred in MMMs for liquid separation in aqueous environments, such as water treatment and dehydration by pervaporation. In this section, recent advances in MOF-based MMMs for liquid separations with impressive performance are highlighted and discussed.

3.3.1 Water treatment. MOF-based MMMs often exhibit greatly enhanced separation performance for various water treatment applications, such as seawater desalination, dye removal, and heavy metal removal, compared to pristine polymeric membranes. The incorporation of MOF fillers into the polymeric matrix can offer additional transport pathways with a size-sieving ability, leading to improved membrane permeance and selectivity. Moreover, MOF-based MMMs sometimes can demonstrate better anti-fouling performance owing to the unique metal centers and organic linkers in the MOF structures. Therefore, there is ongoing interest in developing more MOF-based MMMs with good filler–polymer interfacial compatibility for water treatment.

Seawater desalination is of great importance for alleviating the water shortage in coastal areas by continuously producing drinkable water on a mass scale. Currently, thin film composite (TFC) membranes dominate the seawater desalination market due to their good separation performance and high mechanical and chemical stability. Despite the fact that TFC membranes demonstrate excellent salt rejections, it is still urgently required

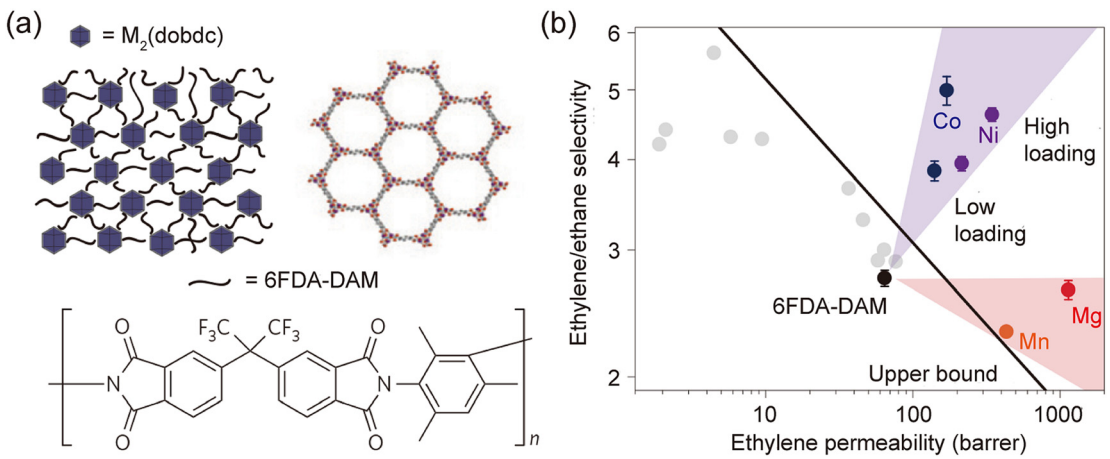

Fig. 25 (a) Illustration of nanocrystal-induced polymer rigidification, along with the structures of M_2(dobdc) and 6FDA-DAM. (b) Ethylene/ethane separation performance for M_2(dobdc)/6FDA-DAM membranes. Reprinted with permission from ref. 144. Copyright 2016 Nature Publishing Group.

to further improve their water permeance and rejections for other chemicals (*e.g.*, boron, selenium, and arsenic) to reduce the energy consumption for the production of drinkable water. Among various strategies for improving the performance of pristine TFC membranes, the introduction of MOF fillers into TFC membranes to fabricate TFN membranes is a facile and feasible approach. Since the pioneering work by Sorribas *et al.* on the investigation of MOF nanoparticles in TFN membranes,[231] a large number of MOFs, including ZIF-8,[232] ZIF-11,[233] MIL-53,[234] MIL-101,[231] UiO-66,[235] surface-functionalized HKUST-1,[236] CuBDC,[237] MOF-801,[238] and silver-based MOFs,[239,240] have been explored as fillers in TFN membranes for various applications with enhanced separation performance. For instance, Duan *et al.* applied hydrophobic ZIF-8 nanoparticles as fillers in TFN membranes for water desalination.[241] The pores in ZIF-8 with an aperture of 3.4 Å are ideal for the size-sieving separation of water molecules (2.8 Å) and hydrated sodium ions (7 Å). The addition of ZIF-8 fillers in the TFN membranes resulted in a good water permeance of $\sim$3 L m^{-2} h^{-1} bar^{-1} with a high NaCl rejection of 98%. Nevertheless, Van Goethem *et al.* discovered that the acid generated during the interfacial polymerization process could partially degrade acid-sensitive ZIF-8.[242] Therefore, the porosity of the original ZIF-8 fillers was lost in the final membranes. This finding strongly suggests that MOFs with excellent water stability should be used in TFN membranes for desalination.

Among various MOF materials explored for water-related separation applications, UiO-66 stands out as a promising candidate for membrane-based desalination owing to its excellent water stability and small apertures suitable for salt removal from seawater. Ma *et al.* pioneered the exploration of UiO-66 in TFN membranes for desalination under pressure retarded osmosis (PRO) and FO modes.[244] The hydrophilicity of the resultant TFN membranes was enhanced due to the existence of superhydrophilic UiO-66 nanoparticles on the membrane surface. TFN membranes with a UiO-66 filler loading of only 0.1 wt% showed 40% and 25% increases in water flux compared to pristine TFC membranes under PRO and FO modes, respectively. In addition to pristine UiO-66, UiO-66 series MOFs with different functional groups, especially UiO-66-NH_2, have also gained substantial attention as filler materials in TFN membranes. The amino (–NH_2) groups in UiO-66-NH_2 can further improve the membrane interfacial compatibility through either hydrogen bonding or covalent cross-linking with the polymeric matrix, enabling the homogeneous dispersion of MOF fillers in TFN membranes.[245,246] For instance, Zhu *et al.* cross-linked the amino groups in UiO-66-NH_2 with trimesoyl chloride (TMC) to ensure the firm immobilization of MOF nanocrystals in the polyamide layer (Fig. 26a).[243] A rough, fish-like surface was found in TFN membranes because the embedded UiO-66-NH_2 nanocrystals served as robust nodes to guide the growth of the polyamide layer (Fig. 26b). This unique structure showed higher surface area compared to the nodule structure in conventional TFC membranes, highlighting the existence of more water transport channels in the as-prepared TFN membranes. Moreover, the incorporation of UiO-66-NH_2 nanocrystals could increase the hydrophilicity of the polyamide layer, as reflected in dynamic water contact angle tests (Fig. 26c), which is beneficial for improving the water flux and the membrane fouling resistance. Therefore, the optimum TFN membranes showed a remarkable water permeability of 31 L m^{-2} h^{-1} bar^{-1} and a good Na_2SO_4 rejection of $\sim$98% (Fig. 26d).

MOF-based MMMs have also demonstrated promising potential for efficient dye removal from wastewater. The size-selective pores in the MOFs can permit the fast permeation of

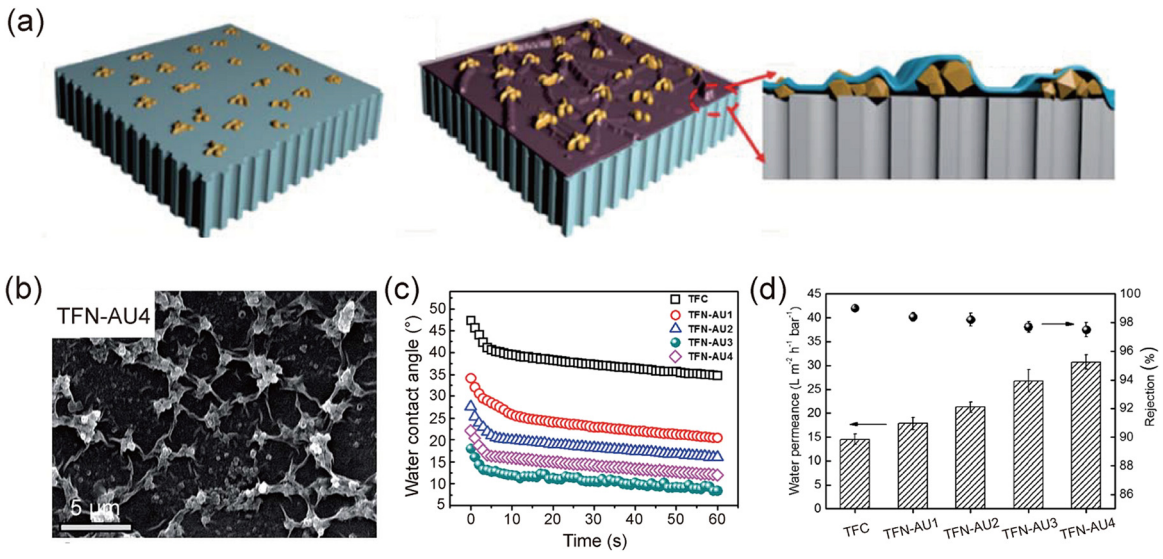

Fig. 26 (a) Schematic illustration of forming a crumpled polyamide surface by incorporating UiO-66-NH_2 nanoparticles, (b) SEM surface image of the TFN membrane with amino-functionalized UiO-66 fillers (TFN-AU4). (c) Dynamic water contact angle of the resultant membranes. (d) Separation performance of TFC and TFN membranes with different UiO-66-NH_2 loadings. Reprinted with permission from ref. 243. Copyright 2019 the Royal Society of Chemistry.

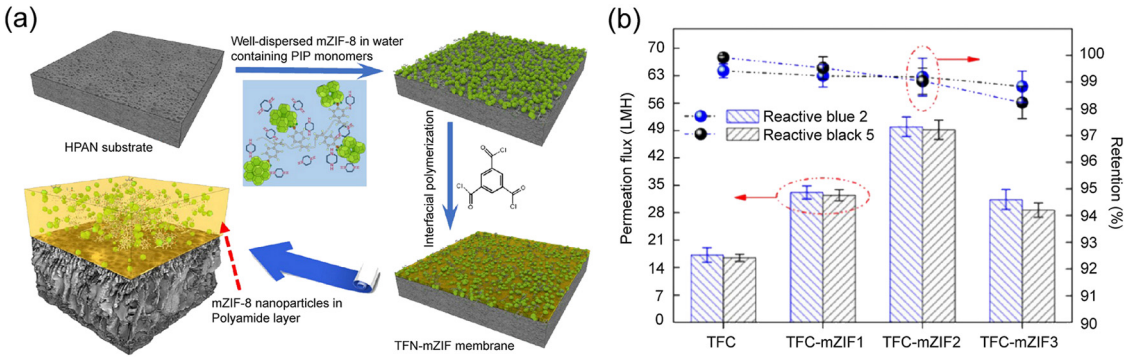

Fig. 27 (a) Schematic illustration of preparing TFN membranes containing mZIF-8 *via* an interfacial polymerization strategy. (b) Dye separation performance of mZIF-functionalized TFN membranes. Reprinted with permission from ref. 252. Copyright 2017 American Chemical Society.

water molecules and block the passage of dye molecules through the membrane. In recent years, a variety of examples involving different MOFs, including ZIF-8,[247] UiO-66,[248] IRMOF-3,[249] BUT-8(A),[250] BUT-203,[142] and MIL-100,[251] have successfully demonstrated the potential of MOFs in membranes for dye removal. For example, Zhu *et al.* added poly(sodium 4-styrenesulfonate) (PSS)-modified ZIF-8 (mZIF-8) fillers into the polyamide layer to prepare TFN membranes on HPAN substrates *via* an interfacial polymerization process.[252] These hydrophilic mZIF-8 fillers were homogeneously suspended in an aqueous solution containing piperazine (PIP) monomers, followed by polymerization with TMC in *n*-hexane to prepare TFN membranes (Fig. 27). These hydrophilic composite fillers showed better dispersibility in the polyamide matrix compared to pristine ZIF-8 fillers, facilitating the fabrication of TFN membranes with better dye removal performance. The as-prepared TFN membranes demonstrated a good water permeability of 15 L m^{-2} h^{-1} bar^{-1} and high rejections (99%) for reactive black 2 (RB 2) and reactive black 5 (RB 5).

3.3.2 Pervaporation. MOF-based MMMs can potentially show improved operational stability, permeability and/or selectivity, and anti-swelling performance compared to pure polymeric membranes for pervaporation applications. Up to now, various MOF materials, including HKUST-1,[253] ZIF series,[138,174,254,255] UiO series,[166,256,257] MIL series,[258,259] and MOF-801,[260] have been explored as fillers in MMMs for pervaporation applications. For instance, Zhang *et al.* modified ZIF-8 with EDA to obtain ZIF-8-NH_2 nanoparticles and applied them as fillers in the PVA matrix for pervaporation dehydration of ethanol.[138] These ZIF-8-NH_2 nanoparticles exhibited improved hydrophilicity and better dispersibility compared to pristine hydrophobic ZIF-8. With the addition of ZIF-8-NH_2 fillers, the resultant MMMs showed enhanced flux and separation factors, higher surface hydrophilicity, and better anti-swelling properties. The optimized MMM with a ZIF-8-NH_2 loading of 7.5 wt% demonstrated a high separation factor of 201 and a decent flux of 126 g m^{-2} h^{-1} for ethanol dehydration at 40 °C. A performance benchmarking study revealed that the as-prepared MMMs showed superior separation performance to most other PVA hybrid membranes.

To further facilitate the diffusion of water molecules in membranes, Cheng *et al.* designed and prepared hollow ZIF-8 (HZIF-8) nanospheres with well-designed hierarchical structures and incorporated them into the sodium alginate (SA) matrix to fabricate water-selective MMMs.[255] The micropores in the HZIF-8 nanosphere shells allowed the selective transport of water molecules and blocked the passage of ethanol molecules, leading to enhanced membrane selectivity. Moreover, the hollow structure of HZIF-8 permitted the rapid transport of water molecules, thus ensuring elevated membrane permeability. The resultant MMMs with a 6 wt% HZIF-8 loading displayed the optimum separation performance with a permeation flux of 2485 g m^{-2} h^{-1} and a separation factor of 1884 for ethanol dehydration, outperforming the pure SA membrane and those MMMs containing ZIF-8 nanocrystals.

To facilitate the diffusion of water molecules in membranes, hydrophilic MOFs with high water adsorption capacity have gained considerable attention as promising fillers in MMMs. Li *et al.* adopted hydrophilic MOF-801 as a filler material in the chitosan matrix to fabricate MMMs for dehydration of ethanol.[260] Simulation studies revealed that water molecules would preferentially occupy the cages and open window areas in MOF-801, hindering the diffusion of ethanol in the MOF structure. Therefore, the incorporation of MOF-801 into the chitosan matrix largely improved the membrane flux and separation factor by promoting the sorption and diffusion of water molecules while hindering the diffusion of ethanol molecules in the membranes. The resultant MMMs showed a high total flux of 1937 g m^{-2} h^{-1} and an excellent separation factor of 2156 for the dehydration of ethanol.

3.3.3 OSN. Compared to limited reports on defect-free MOF polycrystalline membranes for OSN, a great number of examples on MOF-based MMMs for OSN can be easily found in the literature.[248,261–265] Various MOFs, including ZIF-8,[264] ZIF-11,[233] UiO-66 and its derivatives,[266] MIL-68(Al),[233] and MIL-101(Cr),[267] have been explored as fillers in MMMs for OSN. Among them, ZIF-8 and UiO-66 series MOFs have gained most attention. Notably, the incorporation of MOF nanoparticles into the selective barrier layer of TFC membranes can lead to the formation of TFN membranes with improved flux compared to pristine TFC membranes. TFN membranes have demonstrated great potential in different OSN applications, such as concentrating or recycling organic solutes and purifying solvents.

ZIF-8 is one of the most widely studied MOF fillers in MMMs for OSN because of its well-defined pores, facile synthesis, and low cost. Considering that nanoparticle fillers often tend to aggregate in hybrid membranes at a high filler loading, Dai *et al.* tried to grow ZIF-8 nanoparticles on the outer surfaces of the macroporous resin microspheres (RMs) to prepare ZIF-8 core–shell microspheres (ZIF-8@RMs) to mitigate the filler aggregation in MMMs.[264] These ZIF-8@RMs showed good dispersion in the resultant MMMs, while the original ZIF-8 nanoparticles tended to aggregate in the membranes at the same filler loading. Consequently, these ZIF-8@RMs-based MMMs demonstrated improved dye rejections for dye/methanol mixed solution compared to the pristine polymeric membrane due to the selective micropores of ZIF-8 and minimized membrane interfacial defects in the MMMs. Moreover, it is highly desired to enhance filler–polymer interactions to prevent MOF aggregation in the MMMs. For example, the dispersion states of ZIF-8 in the MMMs could be impressively enhanced when the coordinative binding between ZIF-8 and the polymeric matrix was judiciously designed (Fig. 28a).[265] The resultant MMMs exhibited a two times higher flux for different solvents compared to the pristine polymeric membrane owing to the improved membrane porosity induced by ZIF-8 fillers.

UiO-66 series MOFs have also been extensively explored as promising fillers in MMMs for OSN. They possess subnanometer-sized pores that are suitable for separation at a molecular level. Moreover, they demonstrate excellent hydro- and solvent stability, which makes them attractive for liquid-based separation applications. For instance, Cheng *et al.* explored the construction of additional solvent paths in polyamide nanofiltration membranes *via* the addition of UiO-66 series MOFs with different functional ligands (UiO-66-$(CH_3)_2$, UiO-66-NH_2) and post-synthetic functionalization (UiO-66(Ti)) (Fig. 28b).[248] The pore sizes of these UiO-66 series MOFs (0.6–1.0 nm) are ideal for rejecting dyes while allowing the fast permeation of organic solvents during OSN processes. Consequently, the addition of these UiO-66 series MOFs into the polyamide layer could help to boost the membrane solvent permeance while retaining high rejections for dyes in different dye/solvent systems.

3.3.4 Other liquid separation applications. Efficient chiral and protein separations are of vital importance in the pharmaceutical and biological industries for the production of drugs with high purity. MOFs with designed functionalities and adsorption sites can demonstrate great potential in differentiating chiral compounds and proteins with similar sizes *via* an adsorption process. However, MOF crystalline powders are intrinsically brittle and can easily break down into tiny particles during industrial operations, leading to fast adsorbent loss and pipeline clogging. The incorporation of MOF particles into the polymeric matrix to yield MMMs can protect these fragile adsorbents and help to achieve a continuous separation of enantiomers and proteins. Recently, Wang *et al.* developed a thermally induced phase separation-hot pressing (TIPS-HoP) method to fabricate MMMs containing different MOFs to efficiently separate enantiomers and proteins.[251] The Zn-BLD MOF possesses chiral functional groups and its MMM with an 86 wt% filler loading showed an enantiomeric excess value of ~74% with a high acetonitrile permeance of 85 L m^{-2} h^{-1} bar^{-1}. Besides, the MIL-100(Cr) MOF demonstrates negative surface charge, which makes it suitable for protein separation through electrostatic attraction. Therefore, its MMM exhibited an excellent selective factor of 94 for the separation of protein bovine serum albumin (BSA) and protein bovine hemoglobin (BHb).

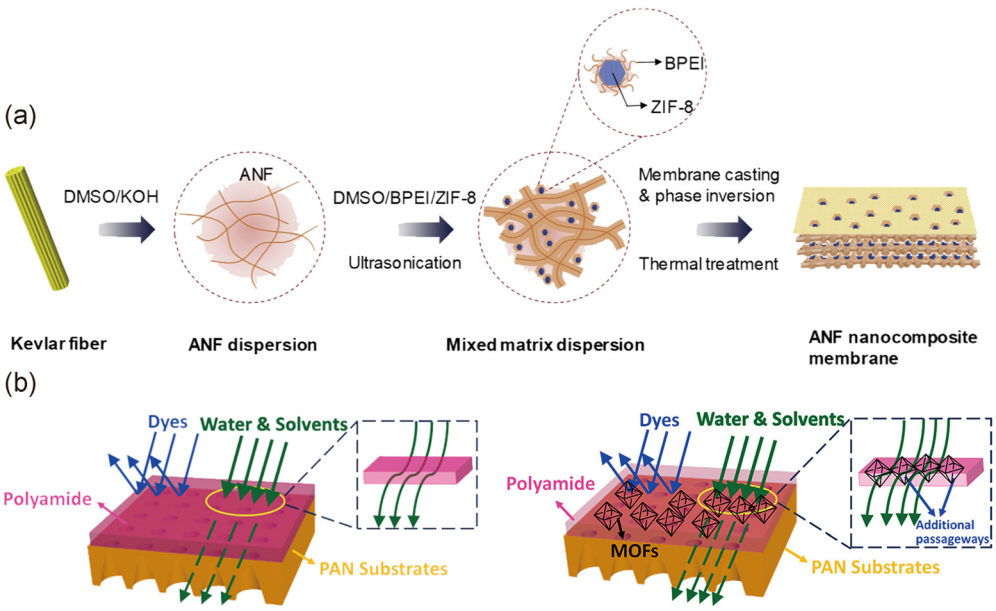

Fig. 28 (a) Schematic illustration of the preparation process of Kevlar aramid nanofiber (ANF) nanocomposite membranes. (b) Schematic illustration of dye rejection processes in pure polyamide membranes (left) and MOF/polyamide MMMs (right). Reprinted with permission from ref. 265. Copyright 2020 Elsevier, ref. 248. Copyright 2017 American Chemical Society, respectively.

Considering that chiral building blocks for direct MOF construction are usually expensive, Das *et al.* adopted inexpensive chiral molecules as dopants in MOF pores to induce chirality in the resultant MOFs and processed these chiral MOFs into MMMs for chiral separation.[268] A series of chiral amino alcohols, including (*R*)- or (*S*)-2-amino-1-butanol, (*R*)- or (*S*)-1-amino-2-propanol, (*R*)- or (*S*)-2-amino-3-methyl-1-butanol, and (*R*) or (*S*)-2-methyl-2,4-pentanediol, were selected as chiral dopants. The amino groups in these chiral amino alcohols could form hydrogen bonding with carboxyl groups in MOF ligands, thus enhancing the retention of dopants in the MOF pores during operation. For a proof of concept, these chirality-enriched MOF (CE-MOF) particles were added into the PIM-1 matrix to fabricate MMMs for the chiral separation of 2-amino-1-butanol. Nevertheless, the final MMMs demonstrated an enantiomeric excess value of 9%, which is much lower than that of CE-MOF particles (40%). Consequently, further optimizations, such as reducing the particle size of the CE-MOF and enhancing filler–polymer compatibility, should be conducted to improve the membrane performance. Similarly, a post-synthetic strategy can also be applied to induce chirality in achiral MOF nanocrystals.[269] Given that a large number of chiral MOFs reported in the literature,[270–272] it is anticipated that more MOF-based MMMs with good chiral separation performance will be prepared in the near future.

Another interesting yet important application for MOF-based membranes is their use as catalytic membrane reactors (CMRs). MOFs have demonstrated great potential in catalysis due to their abundant active sites and rich chemical functionality.[274] Owing to the high porosity of MOFs, MOF-based CMRs often show higher flux compared to pure polymeric membranes.[275,276] Moreover, MOFs can function as porous supports to load catalytic metal or metal oxide nanomaterials to prevent their aggregation during reactions. For example, HKUST-1 was loaded with Ag nanoparticles to prepare composite Ag@HKUST-1 crystals and incorporated into a TFC layer during interfacial polymerization to fabricate CMRs.[277] The resultant hybrid membranes exhibited both high catalytic activity for the degradation of a pesticide, 2,4-dichlorophenoxyacetic acid, and good rejection for low-molecular-weight components, showing substantial promise for agricultural wastewater treatment. Similarly, a composite Au-UiO-66/polymer membrane has been proved to be efficient for Knoevenagel condensation of 4-nitrobenzaldehyde with malononitrile and 4-nitrophenol reduction at ambient temperature, respectively.[278] Other hybrid systems, such as Cu-TiO_2/ZIF-8 and Cd-MOF/polymer, have also demonstrated impressive catalytic properties for different reactions.[279,280] Considering the vast number of MOFs with good porosity and active catalytic sites, these inspiring works open the avenue of designing next-generation CMRs with both good separation and catalytic performance.

4. MOF nanosheets in membrane applications

High-aspect-ratio molecular sieve nanosheets are desirable for the fabrication of thin molecular sieve membranes for energy-efficient separation.[281,282] MOF nanosheets with high aspect ratios could serve as the most appropriate building blocks for pure molecular sieve membranes[16] and/or high-performance MMMs.[13] The large external surface area of the nanosheets can significantly enhance the compatibility with the polymeric matrix, and the extremely short gas diffusion pathway with a precise molecular sieving effect of nanosheets enables them to act as superior separators or highly selective and energy-efficient separation membranes.

4.1 MOF nanosheet fabrication strategies

4.1.1 Top-down exfoliation. Top-down exfoliation involves the delamination of bulk layer-structured MOFs into MOF nanosheets. These layer-structured MOFs demonstrate relatively strong coordination bonds within layers, but relatively weak interactions between the neighbouring layers.[11,283] Therefore, the weak interlayer interactions can be facilely overcome by sonication-assisted exfoliation,[11] freeze–thaw exfoliation,[16] mechanical exfoliation,[284] chemical exfoliation,[285] and Li-intercalation exfoliation,[286,287] resulting in exfoliated 2D MOF nanosheets. Peng *et al.* reported that the layered $Zn_2(bim)_4$ MOF could be exfoliated into ultrathin 2D nanosheets by wet-ball milling and ultrasonication in a methanol/propanol mixture (Fig. 29a).[11] The shear forces generated during the ball milling process increased the diffusion of methanol molecules into interlayer space, and propanol molecules adsorbed on the surfaces of the exfoliated nanosheets, which helped to stabilized these nanosheets in the solvent. The atomic force microscopy (AFM) image analysis revealed that exfoliated 2D $Zn_2(bim)_4$ nanosheets demonstrated a single layer thickness. Moreover, the crystalline structure of these exfoliated nanosheets was confirmed by high-resolution transmission electron microscopy (TEM) analysis. Subsequently, MAMS-1, a layered MOF, was exfoliated into 2D nanosheets using a freeze–thaw method.[16] The abrupt solvent volume expansion and contraction during the freeze–thaw process weakened the van der Waals interactions within MAMS-1 interlayers, which triggered the exfoliation of MAMS-1 crystals. Therefore, ultrathin 2D MAMS-1 nanosheets could be obtained by repeating the freeze–thaw cycle several times. The obtained nanosheets exhibited an average lateral size of $\sim$10 μm and thickness of $\sim$4 nm, demonstrating aspect ratios of higher than 2800 (Fig. 29b).

Although top-down exfoliation methods have been proved to be useful in obtaining ultrathin 2D MOF nanosheets, they still have several limitations. For example, these methods are only applicable to layer-structured MOFs and not feasible for the production of uniform 2D MOF nanosheets in high yields (*e.g.*, $>$15%).[11,288] These exfoliated nanosheets have a strong tendency to reassemble/restack. Moreover, due to the strong external forces applied in the exfoliation process, the fabricated MOF nanosheets often contain structural defects,[289] which will adversely affect their separation performance for membrane-based applications.

4.1.2 Bottom-up synthesis. In contrast, bottom-up synthesis is highly desirable for the fabrication of homogeneous and well-dispersed 2D MOF nanosheets in high yields. Various methods were deployed for the bottom-up synthesis of 2D MOF nanosheets,

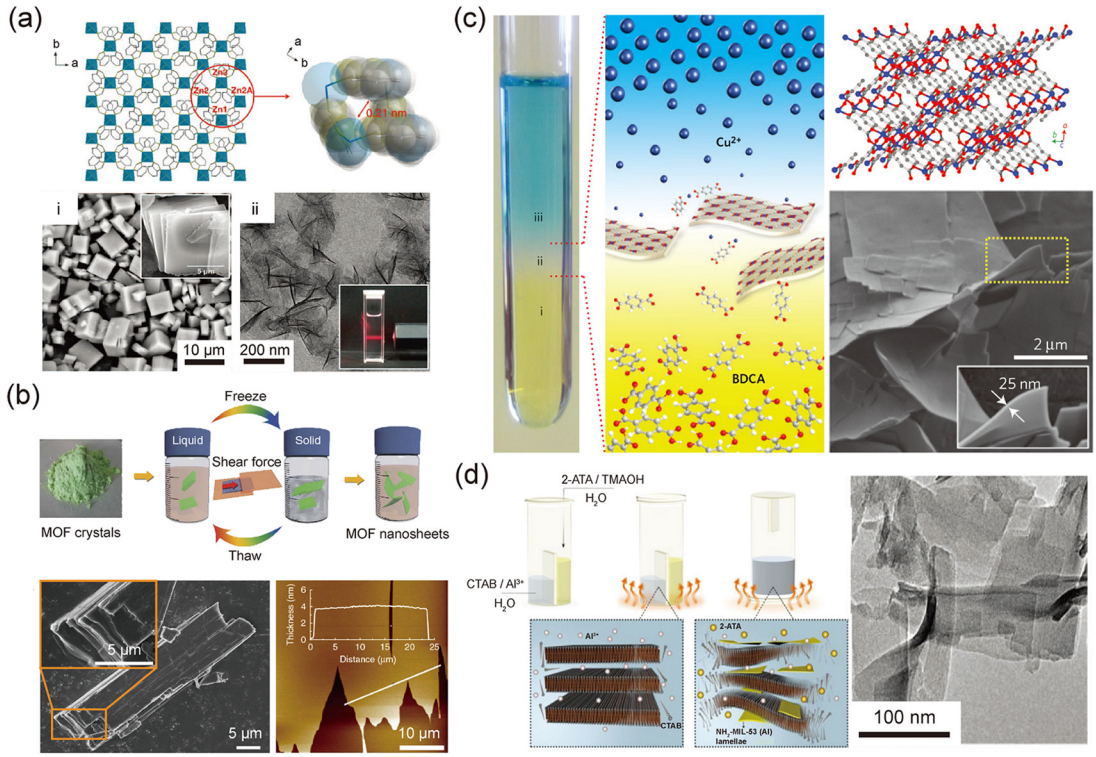

Fig. 29 (a) Crystal structure of $Zn_2(bim)_4$ MOF (top). SEM image of bulk $Zn_2(bim)_4$ crystals (bottom, i) and TEM image of $Zn_2(bim)_4$ nanosheets (bottom, ii). (b) Schematic illustration of the exfoliation of MAMS-1 crystals (top). SEM image of bulk MAMS-1 crystals (bottom, left) and AFM image of ultrathin MAMS-1 nanosheets (bottom, right). (c) Schematic illustration of the synthesis of CuBDC nanosheets (left). Crystal structure of CuBDC (right, top) and SEM image of CuBDC nanosheets (right, bottom). (d) Schematic illustration of the preparation of aluminium MOF nanosheets (left) and TEM image of the MOF nanosheets (right). Reprinted with permission from ref. 11. Copyright 2014 AAAS, ref. 16, Copyright 2017 Nature Publishing Group, ref. 13, Copyright 2015 Nature Publishing Group, ref. 273, Copyright 2018 Wiley-VCH, respectively.

including interfacial synthesis,[290] sonication-assisted synthesis,[291] three-layer synthesis,[13] surfactant-assisted synthesis,[273,292,293] modulated synthesis,[294,295] and direct synthesis.[296] For instance, a three-layer synthesis approach was found to be effective to fabricate CuBDC nanosheets with an average lateral dimension of 0.5–4 μm and thickness in the range of 5–25 nm, resulting aspect ratios of greater than 20 (Fig. 29c).[13] Interestingly, nanosheets of nonlayered aluminium MOFs could be successfully obtained in a surfactant-assisted synthesis process (Fig. 29d).[273] This synthesis process involved the use of two different aqueous solutions. Firstly, a metal precursor solution was obtained by dissolving $Al(NO_3)_3{\cdot}9H_2O$ and the cationic surfactant hexadecyltrimethylammonium bromide (CTAB). Secondly, the organic ligand precursor solution was obtained by dissolving 2-aminoterephthalic acid (2-ATA) in a basic solution containing tetramethylammonium hydroxide (TMAOH). Then, the mixtures were transferred into an autoclave which contained two separated compartments for two different precursor solutions. The autoclave was heated at 100 °C for 1 h before the precursor solutions were mixed together. Finally, the mixture was heated at 100 °C for 16 h. This two-step solvothermal reaction might favor the formation of oligomeric aluminium-containing structures. Zhao *et al.* reported another surfactant-assisted synthesis method to fabricate ultrathin Zn-TCPP (TCPP = tetrakis(4-carboxyphenyl)porphyrin) nanosheets with an average thickness of less than 10 nm.[292] Although the surfactant-assisted synthesis approach is useful to fabricate ultrathin 2D MOF nanosheets, one of its major drawbacks is that anchored or residual surfactants on the surfaces of the nanosheets may significantly deteriorate the performance of the nanosheets. Therefore, it still remains a formidable challenge to directly (surfactant/template-free) synthesize uniform 2D MOF nanosheets from the 3-periodic structure with a thickness below 50 nm.

A comparison of the two approaches, including top-down exfoliation and the bottom-up synthesis, is shown in Fig. 30. Although the top-down exfoliation method has been shown useful for producing nanosheets from MOFs with different structures, this method is still less attractive for the large-scale production of nanosheets with a high yield and good quality compared to the bottom-up synthesis method. Moreover, repetitive centrifugation is often required during the top-down exfoliation process to completely remove nanoparticles, resulting in high overall fabrication costs. Consequently, it is anticipated that the bottom-up synthesis method should deserve more attention for fabricating high-quality nanosheets for membrane-based applications.

4.2 MOF nanosheet membranes for H_2 purification

Energy-efficient gas separations are extremely important in many industries for clean energy production and environmental

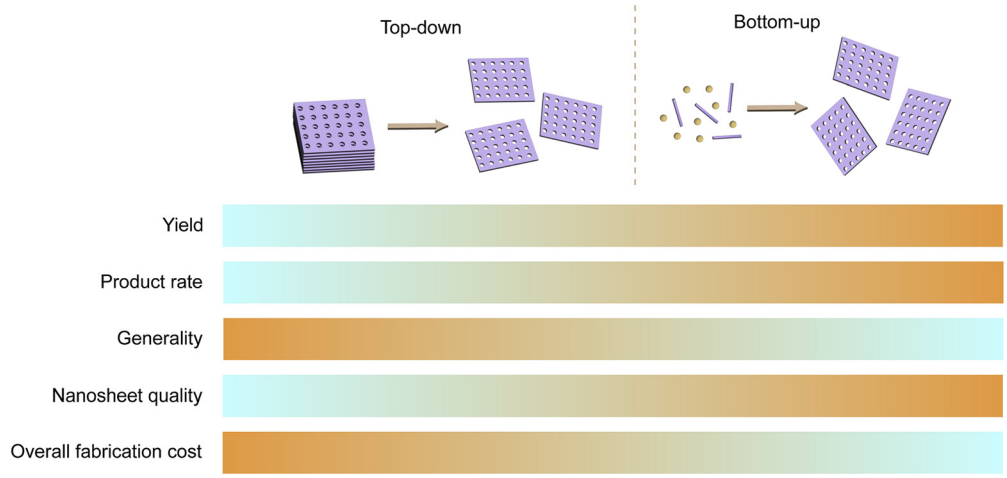

Fig. 30 Comparison of nanosheet fabrication approaches, including top-down exfoliation and bottom-up synthesis. Characteristics of these two approaches are qualitatively shown. Orange represents a strong characteristic and light blue represents a weak characteristic.

sustainability. H_2 separation/recovery from H_2/CO_2 mixtures is an important process in the syngas industry. However, the molecular size difference between H_2 and CO_2 is only 0.4 Å (H_2: 2.9 Å and CO_2: 3.3 Å), making this separation a significant challenge. 2D MOF nanosheets are promising candidates for highly selective and highly permeable molecular sieve membranes for gas separation. Defect-free ultrathin continuous pure MOF membranes based on 2D MOF nanosheets can offer a desired membrane platform to simultaneously achieve both high permeability and high selectivity owing to their ultrasmall thickness and well-defined pore structures, which effectively discriminate gas molecules based on differences in their size, shape, and chemical properties.

Peng *et al.* demonstrated successful fabrication of ultrathin $Zn_2(bim)_4$ nanosheets by the assistance of wet-ball milling and ultrasonic exfoliation.[11] Continuous ultrathin molecular sieving membranes were prepared by the deposition of these $Zn_2(bim)_4$ nanosheets onto porous α-Al_2O_3 supports *via* a hot-drop casting method. The membranes demonstrated excellent H_2/CO_2 separation performance with a H_2/CO_2selectivity of up to 290 and a good H_2 permeance of 760–3760 GPU (Fig. 31a). The ultrasmall pore aperture (0.21 nm) and extremely thin nanosheets are responsible for this extraordinary molecular discrimination. Small H_2 molecules could diffuse through the small pore of the nanosheets, while a small quantity of CO_2 could only pass through the interlayer gaps and/or defective sites in the nanosheet membranes. Following this encouraging finding, the same group developed a facile physical method to exfoliate bulk $Zn_2(Bim)_3$ crystals into 2D nanosheets and fabricated defect-free and sub-10-nm-thick continuous $Zn_2(Bim)_3$ nanosheet membranes.[297] The resultant membranes demonstrated impressive H_2/CO_2 separation performance with an excellent H_2/CO_2 selectivity of 166 and a good H_2 permeance of up to $\sim$2400 GPU. This remarkable separation performance primarily originated from the size exclusion properties of the $Zn_2(Bim)_3$ nanosheets (Fig. 31b).

Wang *et al.* reported ultrathin MAMS-1 nanosheet membranes with reversed thermo-switchable molecular sieving properties for H_2/CO_2 separation.[16] A 12-nm-thick MAMS-1 nanosheet membrane demonstrated a good H_2/CO_2 separation selectivity (34 ± 5) and a high H_2 permeance (6516 ± 900 GPU). Importantly, an even higher separation selectivity (235 ± 14) could be achieved by increasing the membrane thickness to 40 nm, but at the cost of reduced H_2 permeance (553 ± 228 GPU). MAMS-1 nanosheet membranes clearly demonstrated a cutoff between H_2 and CO_2, which is primarily attributed to the size exclusion properties of MAMS-1 nanosheets (Fig. 31c). Interestingly, during the membrane heating stage, the H_2 permeance decreased significantly along with the H_2/CO_2 selectivity. The membrane separation performance could be recovered after cooling the membrane. This thermo-switchable separation performance was induced by the adjustable aperture size of MAMS-1, which could inspire the design of other smart nanosheet membranes.

Li *et al.* reported a direct growth approach to prepare $Zn_2(blm)_4$ nanosheet membranes on hollow fiber supports by ZnO self-conversion and ammonia assistance (Fig. 32a).[298] Specifically, pre-deposited ZnO nanoparticles on porous hollow fiber supports were converted into 2D MOF nanosheets, and subsequently continuous $Zn_2(blm)_4$ membranes were formed. Ammonium hydroxide solution functioned as a modulator in this reaction. The as-prepared nanosheet tubular membranes were uniformly oriented, and their thicknesses were varied from 50 to 450 nm. These $Zn_2(blm)_4$ nanosheet membranes demonstrated a good H_2 permeance and an impressive H_2/CO_2 separation selectivity (Fig. 32b and c). More importantly, membrane modules based on hollow fibers are relevant to industrial gas separation processes.

4.3 MOF nanosheets in MMMs

It is to be noted that isotropic MOF fillers are often randomly oriented in MMMs.[36,37,299] The relatively small external surface areas of isotropic fillers (nanoparticles) in contrast to anisotropic fillers (nanosheets) largely restrain the interaction between MOF fillers and the polymeric matrix and often generate defective interfaces, which will limit the potency of MOF

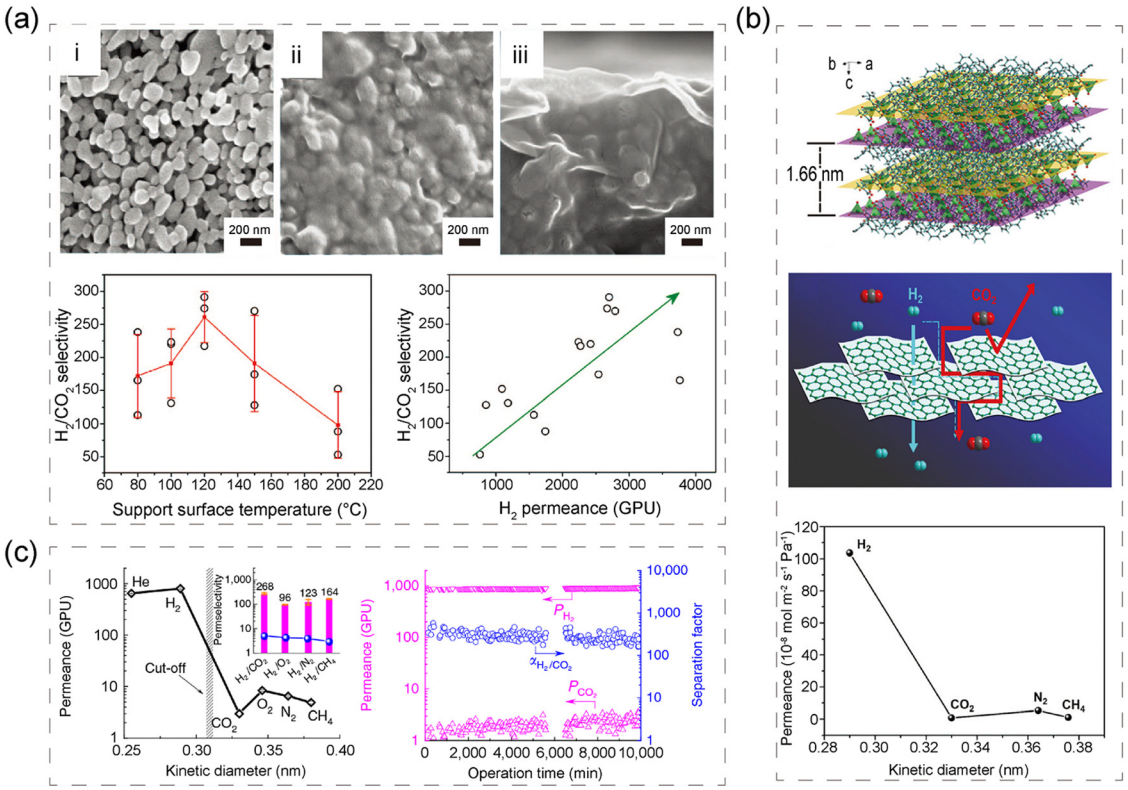

Fig. 31 (a) SEM images of the porous support (i), surface (ii), and cross-section (iii) of the $Zn_2(bim)_4$ nanosheet membrane (top). Gas separation performance of the as-prepared $Zn_2(bim)_4$ nanosheet membranes (bottom). (b) Crystal structure of $Zn_2(Bim)_3$ precursors (top), schematic illustration of the possible gas diffusion mechanism in $Zn_2(Bim)_3$ nanosheet membranes (middle), and gas separation performance of $Zn_2(Bim)_3$ nanosheet membranes (bottom). (c) Gas separation performance of MAMS-1 nanosheet membranes. Reprinted with permission from ref. 11. Copyright 2014 AAAS, ref. 297, Copyright 2017 Wiley-VCH, ref. 16, Copyright 2017 Nature Publishing Group, respectively.

fillers in MMMs. On the other hand, the orientation of nanoparticles with 1D channels/pores in the polymeric matrix can also play a pivotal role in determining the overall separation performance of MMMs.[225] As anticipated, among a large number of reported MMMs containing isotropic or near-isotropic MOFs, most of them exhibited relatively poor to moderate selectivity–permeability relationships.[36,37,299] In contrast, MMMs composed of MOF molecular sieve nanosheets with a desired orientation that can allow channels/pores to align parallelly to the gas diffusion direction are expected to exhibit impressive gas separation performance.

4.3.1 CO_2/CH_4 separation. Rodenas *et al.* demonstrated the advantage of using MOF nanosheets in MMMs.[13] For a comparative study, several MMMs were fabricated by blending Matrimid and CuBDC MOFs with 3 different morphologies: bulk crystals (b), nanocrystals (nc), and nanosheets (ns). The shear force generated during the membrane preparation process helped to align CuBDC nanosheets in the resultant MMMs. Therefore, CuBDC nanosheets were preferably oriented perpendicular to the gas diffusion direction. The nanosheet orientation in the polymeric matrix was thoroughly investigated using focused ion beam scanning electron microscopy (FIB-SEM) analyses (Fig. 33a and b). The dispersion of CuBDC nanosheets was homogeneous in the whole membrane, which was revealed by membrane cross-sectional analyses at various depths (Fig. 33c). The statistical orientation of the CuBDC nanosheets in the membrane was also investigated, and the histogram showed a maximum abundance of nanosheet orientation at angles close to 90° with respect to the gas pressure gradient (Fig. 33d). Consequently, the CO_2/CH_4 separation selectivity for nanosheet CuBDC (ns-CuBDC)-based MMMs exhibited 30–80% higher selectivity than that of the pure polymeric membrane, and 75–800% higher than that of the b-CuBDC-based MMMs.

Relatively highly permeable polymers (6FDA-DAM and PIM-1) were also selected as polymeric matrixes and blended with CuBDC nanosheets in the form of MMMs.[300] The mixed gas separation properties of the membrane with a 4 wt% ns-CuBDC loading in 6FDA-DAM showed a CO_2/CH_4 selectivity improvement from 30 to 45 but a CO_2 permeability decrease from 590 to 430 barrer. Similarly, the membrane with a 4 wt% ns-CuBDC loading in PIM-1 exhibited a CO_2/CH_4 selectivity increase from 17 to 22 but a CO_2 permeability decrease from 3100 to 2300 barrer. It should be noted that CuBDC nanosheets-containing MMMs always display a considerable CO_2 permeability decrease.[177] Thus, the concurrent enhancement of selectivity and permeability can hardly be achieved using CuBDC nanosheets.

Pustovarenko *et al.* reported the effects of filler morphology on MMM separation performance.[273] MMMs were fabricated using MIL-53(Al)-NH_2 with two different morphologies (nanoparticles

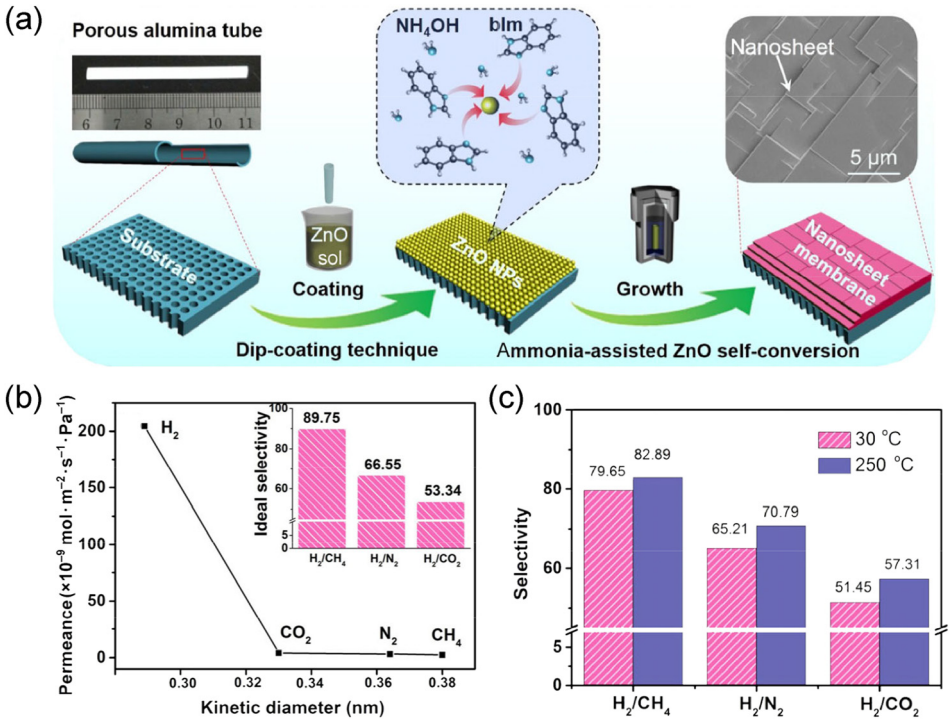

Fig. 32 (a) Scheme illustration of the preparation of 2D ZIF nanosheet membranes. (b) Single-gas performance of the 2D ZIF nanosheet membrane. (c) Mixed-gas selectivity of the 2D ZIF nanosheet membrane. Reprinted with permission from ref. 298. Copyright 2017 Tsinghua University Press and Springer-Verlag GmbH Germany.

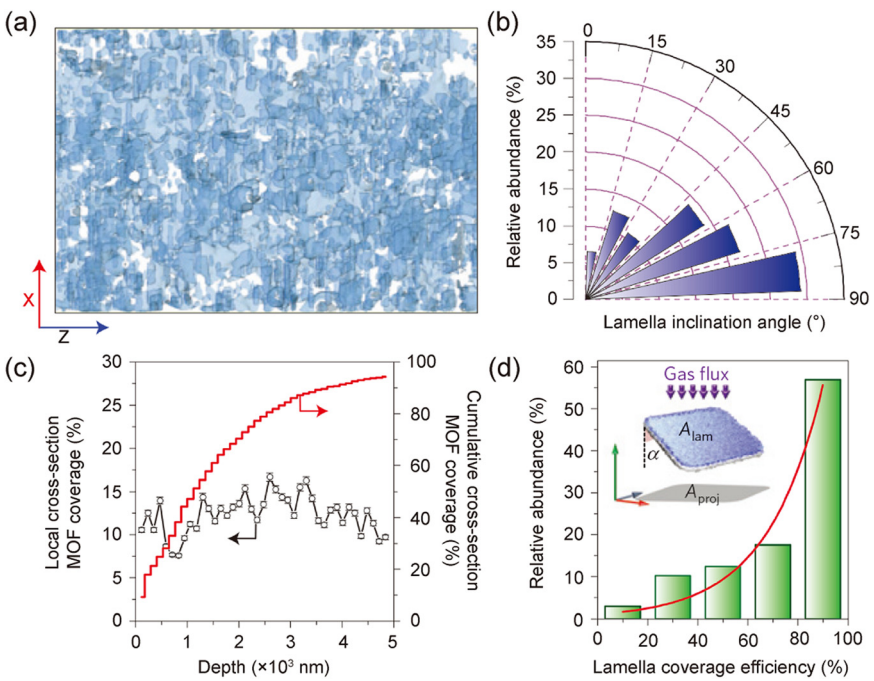

Fig. 33 (a) FIB-SEM analysis on the distribution of CuBDC nanosheets in the polyimide matrix. (b) The analysis of the orientation of CuBDC nanosheets in the membrane. (c) Summary of the coverage of the membrane by CuBDC nanosheets. (d) Histogram of the coverage efficiency of CuBDC nanosheets in the membrane. Reprinted with permission from ref. 13. Copyright 2015 Nature Publishing Group.

and nanosheets) as fillers and Matrimid as the polymeric matrix. The 1D channels of MIL-53(Al)-NH_2 were found to be parallel with the gas flux direction in nanosheet-based MMMs, which largely facilitated gas diffusion through the membrane. As expected, the

nanosheet-based MMM exhibited a higher CO_2 permeability in comparison to the nanoparticle-based MMM. Li *et al.* recently reported Pebax-based MMMs containing very thin α-Ni(im)$_2$ nanosheets.[301] The large external surface area of α-Ni(im)$_2$ nanosheets offered good compatibility with Pebax polymer. Therefore, the fabricated defect-free MMMs with a 2 wt% loading of α-Ni(im)$_2$ nanosheets exhibited a CO_2/CH_4 selectivity of 33 and a CO_2 permeability of 100 barrer. Overall, the separation selectivity was improved by 72% in MMMs without compromising the CO_2 permeability as compared with the pure Pebax membrane.

Recently, our group reported the rational design and fabrication of a series of MMMs with high loadings (up to ~60 wt%) of (001)-oriented AlFFIVE-1-Ni nanosheets for efficient $CO_2/H_2S/CH_4$ separation.[302] Bulk AlFFIVE-1-Ni crystals possess narrow 1D channels selectively allowing the diffusion of CO_2 and H_2S while blocking CH_4 based on their molecular size differences. By carefully controlling the concentration of the pillaring ligand, reaction temperature, and solvents, we could obtain high-quality AlFFIVE-1-Ni nanosheets with maximally exposed (001) facets. These nanosheets were uniformly and in-plane aligned throughout the membrane as confirmed by the FIB-SEM (Fig. 34a). The addition of AlFFIVE-1-Ni nanosheets could lead to concurrent enhancements of selectivity and permeability in different polyimide matrixes (Fig. 34b). Impressively, the pure (001)-AlFFIVE-1-Ni membrane demonstrated a theoretical CO_2/CH_4 selectivity of 354 and a CO_2 permeability of 2035 barrer based on the back-calculation using the Maxwell model. Moreover, the optimized MMM could maintain their outstanding separation

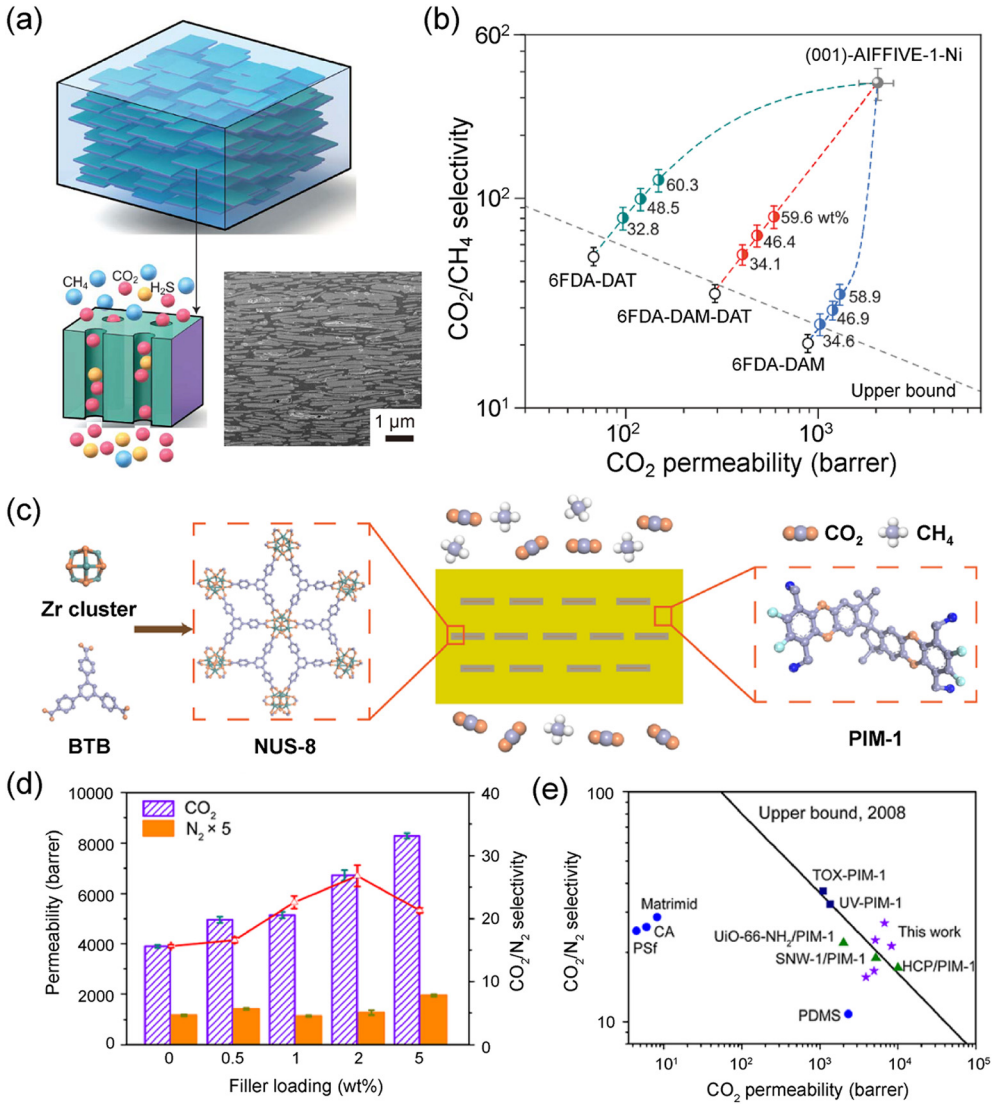

Fig. 34 (a) Schematic illustration of a (001)-oriented membrane with AlFFIVE-1-Ni nanosheets (top) and an efficient $CO_2/H_2S/CH_4$ separation process through 1D channels in the MOF (bottom, left). The FIB-SEM image of the AlFFIVE-1-Ni nanosheet-based MMM with a high loading of ~60 wt% (bottom, right). (b) CO_2/CH_4 separation performance of AlFFIVE-1-Ni nanosheet-based MMMs with various filler loadings. (c) Schematic illustration of the preparation of NUS-8 nanosheet-based MMMs. (d) CO_2/N_2 separation performance of MMMs with different filler loadings. (e) Comparison of the CO_2/N_2 separation performances of NUS-8 nanosheet-based MMMs with other membranes on the upper bound plot. Reprinted with permission from ref. 302, Copyright 2022 AAAS; ref. 176. Copyright 2018 American Chemical Society.

performance after a long-term stability test over 30 days. This work unambiguously confirms the great potential of utilizing 2D MOF nanosheets for construction of membranes with unprecedented separation performance.

4.3.2 CO_2/N_2 separation. Cheng *et al.* demonstrated the successful incorporation of chemically stable NUS-8 (NUS = National University of Singapore) nanosheets into the highly permeable PIM-1 matrix to obtain high-performance MMMs (Fig. 34c).[176] The high-aspect-ratio NUS-8 nanosheets offered large contacting areas with the PIM-1 matrix, which promoted the formation of good MMMs without interfacial defects. The MOF–polymer interfacial compatibility was substantially improved owing to the hydrogen bonding and π–π interactions between fillers and the polymeric matrix. The optimized MMMs exhibited impressive CO_2 separation performance with a CO_2 permeability of ~6500 barrer and a CO_2/N_2 selectivity of up to ~27, surpassing the Robeson upper bound (Fig. 34d and e). Moreover, the resultant MMMs demonstrated better anti-pressure and anti-aging performance compared to the pure PIM-1 membrane. This study revealed that the improved filler–polymer interfacial microstructure could play a critical role in promoting the long-term stability of MMMs for practical applications.

Feng *et al.* fabricated Pebax-based MMMs by blending ZIF-67 nanoflakes into the Pebax polymer.[303] The MMMs displayed a CO_2 permeability of 139.4 barrer and a single gas CO_2/N_2 selectivity of 73, which were 51% and 76% higher compared to those of the pure Pebax membrane, respectively. Recently, Deng *et al.* reported Pebax-based MMMs by using ZIF cuboid (ZIF-C) nanosheets with different thicknesses as fillers.[304] The membranes were evaluated for CO_2/N_2 separation in the presence of different relative humidities. Gas separation results showed that the incorporation of ZIF-C nanosheet fillers into the Pebax polymeric matrix could concurrently increase the membrane CO_2 permeability and CO_2/N_2 selectivity.

4.3.3 H_2/CO_2 separation. H_2/CO_2 separation in MMMs with MOF nanosheets is considerably scarce. Kang *et al.* incorporated a Cu MOF $[Cu_2(ndc)_2(dabco)]_n$ into the PBI polymer to prepare MMMs.[305] The impacts of different filler morphologies (bulk crystals, nanocubes, and nanosheets) on gas separation performances were thoroughly evaluated. It was observed that the MOF filler morphologies played a critical role in the membrane separation performance. Reducing the MOF crystal size from bulk crystals to nanocubes led to a more homogeneous distribution of MOF fillers in the polymeric matrix, which helped to improve the final membrane separation performance. Moreover, for nanosheet-based MMMs, their cross-sectional SEM images revealed that MOF nanosheets were partially oriented perpendicularly along the gas diffusion direction within the membrane. These MOF nanosheets allowed the passage of small H_2 molecules but hindered the diffusion of large CO_2 molecules, resulting in enhanced H_2/CO_2 selectivity in MMMs. The best H_2/CO_2 selectivity was achieved in the nanosheet-containing MMM with a 20 wt% loading.

In conventional MMMs, the polymeric matrix acts as a continuous phase, and this phase is always dominant compared to MOF fillers. Hence, both the selectivity and permeability of the MMMs are considerably reliant on the permeation properties of the polymer phase. Ma *et al.* reported an oriented and penetrated ZIF-7/polyimide MMM.[306] ZIF-7 sheets with a thickness of 20 μm were horizontally oriented and surrounded by the polyimide matrix. In the membrane, each ZIF-7 sheet penetrated both sides of the polyimide matrix. It was reported that the separation performance of the membrane was dominated by the penetrated ZIF-7 sheets rather than the polyimide matrix. Compared to conventional MMMs where fillers are fully embedded in the polymeric matrix, MMMs prepared in this work provide good guidance on how to fully exploit the potential of porous fillers to maximize the membrane separation performance.

Despite the fact that a large number of MOF nanosheets have been reported in the open literature, only limited MOF nanosheets, such as CuBDC, and MIL-53(Al)-NH_2, AlFFIVE-1-Ni, NUS-8, and α-Ni(im)$_2$ nanosheets, have been explored as fillers and displayed relatively moderate gas separation performance in MMMs. In the CuBDC case, often the CO_2/CH_4 selectivity was improved at the cost of reduced CO_2 permeability. On the other hand, MMMs with MIL-53(Al)-NH_2 often showed increased permeability, while their gas selectivity remained unchanged or barely improved. The weak interaction between gas molecules with layered MOF structures is a plausible reason for this moderate separation performance. To fabricate high-performance MMMs, efforts should be directed towards the production of high-aspect-ratio nanosheets from more complex and more interesting MOF structures with which target gas molecules can strongly interact. Besides, it is highly desired to develop non-exfoliation and non-surfactant-based synthesis methods to accelerate the large-scale production of high-quality MOF nanosheets.

5. Conclusions and outlook

Membrane-based separations are of great importance to human society and have attracted a wide range of attention from both the academic and industrial communities. MOFs represent a fascinating class of crystalline porous materials with great potential to function as new membrane materials for various separation applications. To date, three major types of MOF-based membrane configurations, including polycrystalline membranes, MMMs, and 2D nanosheet membranes, have been proposed for gas and liquid separations. This review has summarized different design and fabrication strategies for MOF-based polycrystalline membranes and MMMs with a special focus on evaluating the pros and cons of each strategy. Moreover, state-of-the-art advances on these membranes for key separations in industry have been discussed and analyzed in depth.

The strengths and weaknesses of these three types of MOF-based membranes for industrial separation applications are summarized based on our opinion and compared in Fig. 35. It is clear that MOF polycrystalline membranes and 2D nanosheet membranes can demonstrate better separation performance

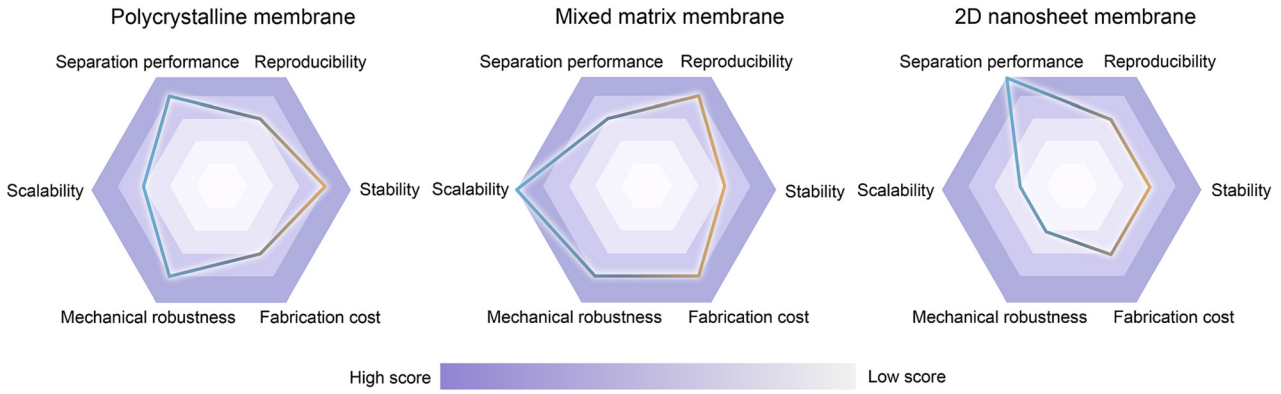

Fig. 35 A comparison of the strengths and weaknesses of the three types of MOF-based membranes for industrial separation applications in the form of a spider diagram. Purple represents a high score and white represents a low score.

compared to MOF-based MMMs. Nevertheless, from an engineering perspective, MMMs outperform the other types of membranes in terms of their good scalability and relatively low fabrication cost, showing the highest potential of commercialization at the current stage. Notably, as a novel class of MOF-based membranes, 2D MOF nanosheet membranes have demonstrated excellent separation performance owing to their ultrathin membrane thickness and size-selective pores. It is anticipated that future research efforts will be continuously devoted to the mass production of more 2D MOF nanosheet membranes with good membrane quality in an economic manner. Despite these exciting advances, MOF-based membranes with outstanding separation performance, easy mass production processes, good long-term stability, and low cost have yet to be realized. Here, we briefly outline some major issues that should be urgently addressed in order to facilitate the industrial implementation of MOF-based membranes.

Despite the vast number of MOF structures reported in the literature, the choices of MOFs with small pore size, high chemical stability, and good mechanical strength suitable for construction of membranes used under harsh industrial conditions are still rather limited. ZIF series, UiO-66 series, MIL series, and MOF-74 series MOFs are among the most widely explored MOF materials for membrane-based separation applications. The development of novel MOFs that can meet the strict requirements of industrial membranes deserves considerable attention. Reliable computational tools, such as grand canonical Monte Carlo (GCMC), density functional theory (DFT), and molecular dynamics (MD), can be adopted to assist the design of new MOF structures with size-selective pores or apertures for molecular sieving separation.[307–309] Moreover, it has been reported that more than 100,000 entries identified as MOFs have been saved in the Cambridge Structural Database (CSD).[310] It is impossible to experimentally examine all these materials for membrane applications. The newly developed machine learning methods offer powerful tools for screening MOFs with appropriate properties for membrane-based separation and predict their separation performance on a large scale.[311] For example, 12 723 experimentally synthesizable MOFs have been evaluated as membrane materials for D_2/H_2 separation, among which top 5 MOF membranes demonstrated one order of magnitude higher selectivity compared to previously reported nanoporous materials.[312] Therefore, it is anticipated that more efforts will be made towards advancing the development of machine learning in search of good MOF candidates for membranes. Moreover, in some cases, a single MOF material may not be able to fulfil the separation task, while the combination of MOFs with other materials that show distinct properties suitable for membrane separation, such as CNTs,[313] GO and rGO,[314,315] zeolites,[316] and COFs,[317] can provide better separation performance owing to the merits of different materials.

Another important challenge is related to the large-scale production of MOF-based membranes with acceptable fabrication cost. This cost mainly consists of two parts, including the cost of membrane materials and the cost incurred during the membrane production process. For the first part, although some MOFs are less cost-attractive compared to commercial polymers because of their expensive building blocks, they should still deserve attention as promising membrane candidates. In fact, the cost of membrane modules only accounts for a certain proportion of the total plant cost. For example, the cost of membrane modules only accounts 10–25% of the total plant cost in the gas separation industry, and other parts, such as large compressors, expensive valves, controllers, and instrumentation, account for the rest.[1] Therefore, the moderate increase in membrane cost is still acceptable as long as the membrane performance is outstanding. Moreover, tremendous efforts have been made to produce MOFs on a large scale, leading to the commercialization of some typical MOFs, including ZIF-8 (Basolite® Z1200), HKUST-1 (Basolite® C300), MIL-53(Al) (Basolite®A100), and Fe-BTC (Basolite® F300),[34] which may prompt the development of MOF-based MMMs. Beside the cost of MOF materials, the cost incurred during the membrane production process should also deserve considerable attention. As we mentioned in previous sections, various membrane preparation strategies, showing different pros and cons, have been proposed for the fabrication of MOF-based membranes with good separation performance. For example, for MOF polycrystalline membranes, conventional *in situ* solvothermal

growth and seed-assisted secondary growth often involve the use of large amounts of toxic solvents and require long reaction times. The solvent-free synthesis method and the FCDS strategy offer new opportunities in the mass production of MOF polycrystalline membranes in an economic way. Consequently, the development of mature membrane fabrication protocols with acceptable cost is of great importance for advancing the industrial implementation of MOF-based membranes.

It is also worth mentioning that most MOF-based membranes are tested under relatively ideal conditions in the literature, while industrial separations are often conducted under harsh and complex conditions. For example, for MOF polycrystalline membranes designed for natural gas upgrading, they are usually examined at low pressures (<10 bar), while current polymeric membranes widely used in the natural gas industry are operated at high pressures (*e.g.*, 60 bar). As the testing pressure increases, these MOF membranes may experience fast selectivity loss owing to possible cracks at grain boundaries induced by high pressure.[318] This is even more serious in 2D MOF membranes because their structural integrity may be completely destroyed at high pressures owing to the relatively weak mechanical strength of MOFs and the ultrathin membrane thickness.[319] Moreover, high-purity gases are adopted as the feed gases for membrane tests in laboratories, while industrial gases often consist of complex impurities (*e.g.*, water, C2–C6 hydrocarbons in natural gas),[2] which may condense on the membrane surface and block pores of MOFs, resulting in severe degradation of the membrane performance. Similarly, in liquid separation applications, a large number of factors, such as acidic/basic environments, complicated liquid mixtures, high temperature and pressure, can have pronounced effects on the membrane performance. The fascinating performance of MOF-based membranes acquired in laboratories could not be maintained when these membranes are operated in industries. It is therefore of paramount importance to perform membrane tests under more realistic conditions.

Despite these challenges, the rapid development of MOF-based membranes over the past years has strongly indicated the bright future of this class of membranes for diversified separation applications. Moreover, collaborative efforts between chemists, materials scientists, and chemical engineers will be continuously made to advance the development of MOF-based membranes with superior separation performance, good mechanical strength, acceptable cost, easy fabrication processes, and remarkable long-term stability, which will eventually facilitate their industrial implementation for energy-efficient separation applications.

Conflicts of interest

There are no conflicts of interest to declare.

Acknowledgements

The authors gratefully acknowledge financial support from the King Abdullah University of Science and Technology (KAUST).

References

1 R. W. Baker, *Ind. Eng. Chem. Res.*, 2002, **41**, 1393–1411.
2 R. W. Baker and B. T. Low, *Macromolecules*, 2014, **47**, 6999–7013.
3 W. J. Koros and C. Zhang, *Nat. Mater.*, 2017, **16**, 289–297.
4 L. M. Robeson, *J. Membr. Sci.*, 1991, **62**, 165–185.
5 L. M. Robeson, *J. Membr. Sci.*, 2008, **320**, 390–400.
6 H. Bux, F. Liang, Y. Li, J. Cravillon, M. Wiebcke and J. Caro, *J. Am. Chem. Soc.*, 2009, **131**, 16000–16001.
7 H. Guo, G. Zhu, I. J. Hewitt and S. Qiu, *J. Am. Chem. Soc.*, 2009, **131**, 1646–1647.
8 M. J. C. Ordoñez, K. J. Balkus, J. P. Ferraris and I. H. Musselman, *J. Membr. Sci.*, 2010, **361**, 28–37.
9 T.-H. Bae and J. R. Long, *Energy Environ. Sci.*, 2013, **6**, 3565–3569.
10 A. J. Brown, N. A. Brunelli, K. Eum, F. Rashidi, J. R. Johnson, W. J. Koros, C. W. Jones and S. Nair, *Science*, 2014, **345**, 72–75.
11 Y. Peng, Y. Li, Y. Ban, H. Jin, W. Jiao, X. Liu and W. Yang, *Science*, 2014, **346**, 1356–1359.
12 X. Liu, N. K. Demir, Z. Wu and K. Li, *J. Am. Chem. Soc.*, 2015, **137**, 6999–7002.
13 T. Rodenas, I. Luz, G. Prieto, B. Seoane, H. Miro, A. Corma, F. Kapteijn, F. X. Llabrés i Xamena and J. Gascon, *Nat. Mater.*, 2015, **14**, 48–55.
14 Z. Wang, A. Knebel, S. Grosjean, D. Wagner, S. Bräse, C. Wöll, J. Caro and L. Heinke, *Nat. Commun.*, 2016, **7**, 13872.
15 A. Knebel, B. Geppert, K. Volgmann, D. I. Kolokolov, A. G. Stepanov, J. Twiefel, P. Heitjans, D. Volkmer and J. Caro, *Science*, 2017, **358**, 347–351.
16 X. Wang, C. Chi, K. Zhang, Y. Qian, K. M. Gupta, Z. Kang, J. Jiang and D. Zhao, *Nat. Commun.*, 2017, **8**, 14460.
17 G. Liu, V. Chernikova, Y. Liu, K. Zhang, Y. Belmabkhout, O. Shekhah, C. Zhang, S. Yi, M. Eddaoudi and W. J. Koros, *Nat. Mater.*, 2018, **17**, 283–289.
18 C. Chen, A. Ozcan, A. O. Yazaydin and B. P. Ladewig, *J. Membr. Sci*, 2019, **575**, 209–216.
19 Y. Wang, H. Jin, Q. Ma, K. Mo, H. Mao, A. Feldhoff, X. Cao, Y. Li, F. Pan and Z. Jiang, *Angew. Chem., Int. Ed.*, 2020, **59**, 4365–4369.
20 A. Knebel, A. Bavykina, S. J. Datta, L. Sundermann, L. Garzon-Tovar, Y. Lebedev, S. Durini, R. Ahmad, S. M. Kozlov, G. Shterk, M. Karunakaran, I. D. Carja, D. Simic, I. Weilert, M. Klüppel, U. Giese, L. Cavallo, M. Rueping, M. Eddaoudi, J. Caro and J. Gascon, *Nat. Mater.*, 2020, **19**, 1346–1353.
21 S. Zhou, O. Shekhah, J. Jia, J. Czaban-Jóźwiak, P. M. Bhatt, A. Ramírez, J. Gascon and M. Eddaoudi, *Nat. Energy*, 2021, **6**, 882–891.
22 E. Fernandez, J. A. Medrano, J. Melendez, M. Parco, J. L. Viviente, M. van Sint Annaland, F. Gallucci and D. A. Pacheco Tanaka, *Chem. Eng. J.*, 2016, **305**, 182–190.
23 S. Escolástico, C. Solís, C. Kjølseth and J. M. Serra, *Energy Environ. Sci.*, 2014, **7**, 3736–3746.
24 D. Lee, L. Zhang, S. T. Oyama, S. Niu and R. F. Saraf, *J. Membr. Sci*, 2004, **231**, 117–126.

25 S. M. Saufi and A. F. Ismail, *Carbon*, 2004, **42**, 241–259.
26 N. Kosinov, J. Gascon, F. Kapteijn and E. J. M. Hensen, *J. Membr. Sci*, 2016, **499**, 65–79.
27 Y. Liu, Y. Ban and W. Yang, *Adv. Mater.*, 2017, **29**, 1606949.
28 L. Ansaloni, Y. Zhao, B. T. Jung, K. Ramasubramanian, M. G. Baschetti and W. S. W. Ho, *J. Membr. Sci.*, 2015, **490**, 18–28.
29 X. Li, Y. Cheng, H. Zhang, S. Wang, Z. Jiang, R. Guo and H. Wu, *ACS Appl. Mater. Interfaces*, 2015, **7**, 5528–5537.
30 H. Wu, X. Li, Y. Li, S. Wang, R. Guo, Z. Jiang, C. Wu, Q. Xin and X. Lu, *J. Membr. Sci.*, 2014, **465**, 78–90.
31 C. H. Park, J. H. Lee, J. P. Jung and J. H. Kim, *J. Membr. Sci*, 2017, **533**, 48–56.
32 R. Surya Murali, A. F. Ismail, M. A. Rahman and S. Sridhar, *Sep. Purif. Technol.*, 2014, **129**, 1–8.
33 S. Shahid and K. Nijmeijer, *J. Membr. Sci*, 2014, **470**, 166–177.
34 M. Rubio-Martinez, C. Avci-Camur, A. W. Thornton, I. Imaz, D. Maspoch and M. R. Hill, *Chem. Soc. Rev.*, 2017, **46**, 3453–3480.
35 W. Li, *Prog. Mater Sci.*, 2019, **100**, 21–63.
36 M. S. Denny, J. C. Moreton, L. Benz and S. M. Cohen, *Nat. Rev. Mater*, 2016, **1**, 16078.
37 J. Dechnik, J. Gascon, C. J. Doonan, C. Janiak and C. J. Sumby, *Angew. Chem., Int. Ed.*, 2017, **56**, 9292–9310.
38 X. Li, Y. Liu, J. Wang, J. Gascon, J. Li and B. Van, der Bruggen, *Chem. Soc. Rev.*, 2017, **46**, 7124–7144.
39 M. Shah, M. C. McCarthy, S. Sachdeva, A. K. Lee and H.-K. Jeong, *Ind. Eng. Chem. Res.*, 2012, **51**, 2179–2199.
40 S. Qiu, M. Xue and G. Zhu, *Chem. Soc. Rev.*, 2014, **43**, 6116–6140.
41 L. Sheng, C. Wang, F. Yang, L. Xiang, X. Huang, J. Yu, L. Zhang, Y. Pan and Y. Li, *Chem. Commun.*, 2017, **53**, 7760–7763.
42 Y. Liu, Z. Ng, E. A. Khan, H.-K. Jeong, C.-B. Ching and Z. Lai, *Microporous Mesoporous Mater.*, 2009, **118**, 296–301.
43 A. Huang, W. Dou and J. Caro, *J. Am. Chem. Soc.*, 2010, **132**, 15562–15564.
44 S. Zhou, Y. Wei, L. Zhuang, L.-X. Ding and H. Wang, *J. Mater. Chem. A*, 2017, **5**, 1948–1951.
45 Q. Liu, N. Wang, J. Caro and A. Huang, *J. Am. Chem. Soc.*, 2013, **135**, 17679–17682.
46 N. Wang, Y. Liu, Z. Qiao, L. Diestel, J. Zhou, A. Huang and J. Caro, *J. Mater. Chem. A*, 2015, **3**, 4722–4728.
47 X. Wu, W. Wei, J. Jiang, J. Caro and A. Huang, *Angew. Chem., Int. Ed.*, 2018, **57**, 15354–15358.
48 G. He, M. Dakhchoune, J. Zhao, S. Huang and K. V. Agrawal, *Adv. Funct. Mater.*, 2018, **28**, 1707427.
49 Y. Sun, Y. Liu, J. Caro, X. Guo, C. Song and Y. Liu, *Angew. Chem., Int. Ed.*, 2018, **57**, 16088–16093.
50 Y.-S. Li, F.-Y. Liang, H. Bux, A. Feldhoff, W.-S. Yang and J. Caro, *Angew. Chem., Int. Ed.*, 2010, **49**, 548–551.
51 H. Bux, A. Feldhoff, J. Cravillon, M. Wiebcke, Y.-S. Li and J. Caro, *Chem. Mater.*, 2011, **23**, 2262–2269.
52 R. Ranjan and M. Tsapatsis, *Chem. Mater.*, 2009, **21**, 4920–4924.
53 Y.-S. Li, H. Bux, A. Feldhoff, G.-L. Li, W.-S. Yang and J. Caro, *Adv. Mater.*, 2010, **22**, 3322–3326.
54 S. Hurrle, S. Friebe, J. Wohlgemuth, C. Wöll, J. Caro and L. Heinke, *Chem. – Eur. J.*, 2017, **23**, 2294–2298.
55 V. Chernikova, O. Shekhah, I. Spanopoulos, P. N. Trikalitis and M. Eddaoudi, *Chem. Commun.*, 2017, **53**, 6191–6194.
56 V. Chernikova, O. Shekhah, Y. Belmabkhout and M. Eddaoudi, *ACS Appl. Nano Mater*, 2020, **3**, 6432–6439.
57 J. Yao, D. Dong, D. Li, L. He, G. Xu and H. Wang, *Chem. Commun.*, 2011, **47**, 2559–2561.
58 Y. Hu, J. Wei, Y. Liang, H. Zhang, X. Zhang, W. Shen and H. Wang, *Angew. Chem., Int. Ed.*, 2016, **55**, 2048–2052.
59 W. Li, P. Su, Z. Li, Z. Xu, F. Wang, H. Ou, J. Zhang, G. Zhang and E. Zeng, *Nat. Commun.*, 2017, **8**, 406.
60 X. Ma, P. Kumar, N. Mittal, A. Khlyustova, P. Daoutidis, K. A. Mkhoyan and M. Tsapatsis, *Science*, 2018, **361**, 1008–1011.
61 O. Shekhah, R. Swaidan, Y. Belmabkhout, M. du Plessis, T. Jacobs, L. J. Barbour, I. Pinnau and M. Eddaoudi, *Chem. Commun.*, 2014, **50**, 2089–2092.
62 O. Shekhah and M. Eddaoudi, *Chem. Commun.*, 2013, **49**, 10079–10081.
63 R. Makiura, S. Motoyama, Y. Umemura, H. Yamanaka, O. Sakata and H. Kitagawa, *Nat. Mater.*, 2010, **9**, 565–571.
64 S. Motoyama, R. Makiura, O. Sakata and H. Kitagawa, *J. Am. Chem. Soc.*, 2011, **133**, 5640–5643.
65 S. Zhou, Y. Wei, L. Li, Y. Duan, Q. Hou, L. Zhang, L.-X. Ding, J. Xue, H. Wang and J. Caro, *Sci. Adv.*, 2018, **4**, eaau1393.
66 J. Hou, X. Hong, S. Zhou, Y. Wei and H. Wang, *AlChE J*, 2019, **65**, 712–722.
67 K. Eum, M. Hayashi, M. D. De Mello, F. Xue, H. T. Kwon and M. Tsapatsis, *Angew. Chem., Int. Ed.*, 2019, **58**, 16390–16394.
68 W. Wu, Z. Li, Y. Chen and W. Li, *Environ. Sci. Technol.*, 2019, **53**, 3764–3772.
69 M. J. Lee, H. T. Kwon and H.-K. Jeong, *Angew. Chem., Int. Ed.*, 2018, **57**, 156–161.
70 D. J. Babu, G. He, J. Hao, M. T. Vahdat, P. A. Schouwink, M. Mensi and K. V. Agrawal, *Adv. Mater.*, 2019, **31**, 1900855.
71 S. Zhou, O. Shekhah, A. Ramírez, P. Lyu, E. Abou-Hamad, J. Jia, J. Li, P. M. Bhatt, Z. Huang, H. Jiang, T. Jin, G. Maurin, J. Gascon and M. Eddaoudi, *Nature*, 2022, **606**, 706–712.
72 F. Cacho-Bailo, M. Etxeberría-Benavides, O. Karvan, C. Téllez and J. Coronas, *CrystEngComm*, 2017, **19**, 1545–1554.
73 S. Friebe, B. Geppert, F. Steinbach and J. Caro, *ACS Appl. Mater. Interfaces*, 2017, **9**, 12878–12885.
74 S. Friebe, A. Mundstock, K. Volgmann and J. Caro, *ACS Appl. Mater. Interfaces*, 2017, **9**, 41553–41558.
75 V. Chernikova, O. Shekhah and M. Eddaoudi, *ACS Appl. Mater. Interfaces*, 2016, **8**, 20459–20464.
76 J. Hou, Y. Wei, S. Zhou, Y. Wang and H. Wang, *Chem. Eng. Sci.*, 2018, **182**, 180–188.
77 M. N. Shah, M. A. Gonzalez, M. C. McCarthy and H.-K. Jeong, *Langmuir*, 2013, **29**, 7896–7902.

78 F. Cacho-Bailo, S. Catalán-Aguirre, M. Etxeberría-Benavides, O. Karvan, V. Sebastian, C. Téllez and J. Coronas, *J. Membr. Sci*, 2015, **476**, 277–285.
79 T. Hijikata, *Int. J. Hydrogen Energy*, 2002, **27**, 115–129.
80 M. Drobek, M. Bechelany, C. Vallicari, A. Abou Chaaya, C. Charmette, C. Salvador-Levehang, P. Miele and A. Julbe, *J. Membr. Sci.*, 2015, **475**, 39–46.
81 Y. Huang, D. Liu, Z. Liu and C. Zhong, *Ind. Eng. Chem. Res.*, 2016, **55**, 7164–7170.
82 X. Ma, Z. Wan, Y. Li, X. He, J. Caro and A. Huang, *Angew. Chem., Int. Ed.*, 2020, **59**, 20858–20862.
83 W. Li, P. Su, G. Zhang, C. Shen and Q. Meng, *J. Membr. Sci*, 2015, **495**, 384–391.
84 Y. Sun, C. Song, X. Guo, S. Hong, J. Choi and Y. Liu, *J. Membr. Sci*, 2020, **616**, 118615.
85 N. Wang, A. Mundstock, Y. Liu, A. Huang and J. Caro, *Chem. Eng. Sci.*, 2015, **124**, 27–36.
86 B. Ghalei, K. Wakimoto, C. Y. Wu, A. P. Isfahani, T. Yamamoto, K. Sakurai, M. Higuchi, B. K. Chang, S. Kitagawa and E. Sivaniah, *Angew. Chem., Int. Ed.*, 2019, **58**, 19034–19040.
87 J. Hou, P. D. Sutrisna, Y. Zhang and V. Chen, *Angew. Chem., Int. Ed.*, 2016, **55**, 3947–3951.
88 E. Shamsaei, Z.-X. Low, X. Lin, A. Mayahi, H. Liu, X. Zhang, J. Zhe Liu and H. Wang, *Chem. Commun.*, 2015, **51**, 11474–11477.
89 S. Zhang, B. Gui, T. Ben and S. Qiu, *J. Mater. Chem. A*, 2020, **8**, 19984–19990.
90 J. Zhu, H. Li, J. Hou, J. Liu, Y. Zhang and B. Van der Bruggen, *AlChE J.*, 2020, **66**, e16935.
91 K. Xie, Q. Fu, C. Xu, H. Lu, Q. Zhao, R. Curtain, D. Gu, P. A. Webley and G. G. Qiao, *Energy Environ. Sci.*, 2018, **11**, 544–550.
92 H. Yin, J. Wang, Z. Xie, J. Yang, J. Bai, J. Lu, Y. Zhang, D. Yin and J. Y. S. Lin, *Chem. Commun.*, 2014, **50**, 3699–3701.
93 Q. Hou, Y. Wu, S. Zhou, Y. Wei, J. Caro and H. Wang, *Angew. Chem., Int. Ed.*, 2019, **58**, 327–331.
94 R. W. Baker and K. Lokhandwala, *Ind. Eng. Chem. Res.*, 2008, **47**, 2109–2121.
95 A. Jomekian, R. M. Behbahani, T. Mohammadi and A. Kargari, *Microporous Mesoporous Mater*, 2016, **234**, 43–54.
96 Z. Rui, J. B. James, A. Kasik and Y. S. Lin, *AlChE J*, 2016, **62**, 3836–3841.
97 C. Kong, H. Du, L. Chen and B. Chen, *Energy Environ. Sci.*, 2017, **10**, 1812–1819.
98 H. Xia, H. Jin, Y. Zhang, H. Song, J. Hu, Y. Huang and Y. Li, *J. Membr. Sci*, 2022, **655**, 120611.
99 H. T. Kwon, H.-K. Jeong, A. S. Lee, H. S. An and J. S. Lee, *J. Am. Chem. Soc.*, 2015, **137**, 12304–12311.
100 C. Zhang, R. P. Lively, K. Zhang, J. R. Johnson, O. Karvan and W. J. Koros, *J. Phys. Chem. Lett.*, 2012, **3**, 2130–2134.
101 Q. Li, J. Li, X. Fang, Z. Liao, D. Wang, X. Sun, J. Shen, W. Han and L. Wang, *Chem. Commun.*, 2018, **54**, 3590–3593.
102 Q. Hou, S. Zhou, Y. Wei, J. Caro and H. Wang, *J. Am. Chem. Soc.*, 2020, **142**, 9582–9586.
103 N. T. Tran, J. Kim and M. R. Othman, *Sep. Purif. Technol.*, 2020, **233**, 116026.
104 C. Wang, F. Yang, L. Sheng, J. Yu, K. Yao, L. Zhang and Y. Pan, *Chem. Commun.*, 2016, **52**, 12578–12581.
105 K. Eum, K. C. Jayachandrababu, F. Rashidi, K. Zhang, J. Leisen, S. Graham, R. P. Lively, R. R. Chance, D. S. Sholl, C. W. Jones and S. Nair, *J. Am. Chem. Soc.*, 2015, **137**, 4191–4197.
106 K. Eum, C. Ma, D.-Y. Koh, F. Rashidi, Z. Li, C. W. Jones, R. P. Lively and S. Nair, *Adv. Mater. Interfaces*, 2017, **4**, 1700080.
107 Y. Yoo, V. Varela-Guerrero and H.-K. Jeong, *Langmuir*, 2011, **27**, 2652–2657.
108 F. Cao, C. Zhang, Y. Xiao, H. Huang, W. Zhang, D. Liu, C. Zhong, Q. Yang, Z. Yang and X. Lu, *Ind. Eng. Chem. Res.*, 2012, **51**, 11274–11278.
109 X. Zhang, Y. Li, C. Van Goethem, K. Wan, W. Zhang, J. Luo, I. F. J. Vankelecom and J. Fransaer, *Matter*, 2019, **1**, 1285–1292.
110 Q. Lyu, X. Deng, S. Hu, L.-C. Lin and W. S. W. Ho, *J. Phys. Chem. C*, 2019, **123**, 16118–16126.
111 H. Zhang, J. Hou, Y. Hu, P. Wang, R. Ou, L. Jiang, J. Z. Liu, B. D. Freeman, A. J. Hill and H. Wang, *Sci. Adv.*, 2018, **4**, eaaq0066.
112 S. Yuan, L. Feng, K. Wang, J. Pang, M. Bosch, C. Lollar, Y. Sun, J. Qin, X. Yang, P. Zhang, Q. Wang, L. Zou, Y. Zhang, L. Zhang, Y. Fang, J. Li and H.-C. Zhou, *Adv. Mater.*, 2018, **30**, 1704303.
113 S. Yuan, J.-S. Qin, C. T. Lollar and H.-C. Zhou, *ACS Cent. Sci*, 2018, **4**, 440–450.
114 N. C. Burtch, H. Jasuja and K. S. Walton, *Chem. Rev.*, 2014, **114**, 10575–10612.
115 C. Wang, X. Liu, N. Keser Demir, J. P. Chen and K. Li, *Chem. Soc. Rev.*, 2016, **45**, 5107–5134.
116 M. Ding, X. Cai and H.-L. Jiang, *Chem. Sci.*, 2019, **10**, 10209–10230.
117 J. H. Cavka, S. Jakobsen, U. Olsbye, N. Guillou, C. Lamberti, S. Bordiga and K. P. Lillerud, *J. Am. Chem. Soc.*, 2008, **130**, 13850–13851.
118 C. Serre, F. Millange, C. Thouvenot, M. Noguès, G. Marsolier, D. Louër and G. Férey, *J. Am. Chem. Soc.*, 2002, **124**, 13519–13526.
119 G. Férey, C. Mellot-Draznieks, C. Serre, F. Millange, J. Dutour, S. Surblé and I. Margiolaki, *Science*, 2005, **309**, 2040–2042.
120 K. S. Park, Z. Ni, A. P. Côté, J. Y. Choi, R. Huang, F. J. Uribe-Romo, H. K. Chae, M. O'Keeffe and O. M. Yaghi, *Proc. Natl. Acad. Sci. U. S. A.*, 2006, **103**, 10186–10191.
121 A. Cadiau, K. Adil, P. M. Bhatt, Y. Belmabkhout and M. Eddaoudi, *Science*, 2016, **353**, 137–140.
122 A. Cadiau, Y. Belmabkhout, K. Adil, P. M. Bhatt, R. S. Pillai, A. Shkurenko, C. Martineau-Corcos, G. Maurin and M. Eddaoudi, *Science*, 2017, **356**, 731–735.
123 X. Liu, C. Wang, B. Wang and K. Li, *Adv. Funct. Mater.*, 2017, **27**, 1604311.

124 V. K. Gupta and Suhas, *J. Environ. Manage.*, 2009, **90**, 2313–2342.
125 Z. Li, P. Yang, Z. Gao, M. Song, Q. Fang, M. Xue and S. Qiu, *Chem. Commun.*, 2019, **55**, 3505–3508.
126 J. R. Álvarez, E. Sánchez-González, E. Pérez, E. Schneider-Revueltas, A. Martínez, A. Tejeda-Cruz, A. Islas-Jácome, E. González-Zamora and I. A. Ibarra, *Dalton Trans.*, 2017, **46**, 9192–9200.
127 X. Wang, L. Zhai, Y. Wang, R. Li, X. Gu, Y. D. Yuan, Y. Qian, Z. Hu and D. Zhao, *ACS Appl. Mater. Interfaces*, 2017, **9**, 37848–37855.
128 J. Y. Chan, H. Zhang, Y. Nolvachai, Y. Hu, H. Zhu, M. Forsyth, Q. Gu, D. E. Hoke, X. Zhang, P. J. Marriot and H. Wang, *Angew. Chem., Int. Ed.*, 2018, **57**, 17130–17134.
129 M. C. Duke, B. Zhu, C. M. Doherty, M. R. Hill, A. J. Hill and M. A. Carreon, *Desalination*, 2016, **377**, 128–137.
130 Y. Zhu, K. M. Gupta, Q. Liu, J. Jiang, J. Caro and A. Huang, *Desalination*, 2016, **385**, 75–82.
131 X. Zhao, H. Zhang, S. Xu and Y. Wang, *AlChE J.*, 2019, **65**, e16620.
132 L. Zhai, X. Yu, Y. Wang, J. Zhang, Y. Ying, Y. Cheng, S. B. Peh, G. Liu, X. Wang, Y. Cai and D. Zhao, *J. Membr. Sci.*, 2020, **610**, 118239.
133 A. Kasik, J. James and Y. S. Lin, *Ind. Eng. Chem. Res.*, 2016, **55**, 2831–2839.
134 H. M. Tham, S. Japip, D. Hua and T.-S. Chung, *ChemSusChem*, 2018, **11**, 2612–2619.
135 D. Ma, G. Han, Z. F. Gao and S. B. Chen, *ACS Appl. Mater. Interfaces*, 2019, **11**, 45290–45300.
136 K. Huang, X. Dong, R. Ren and W. Jin, *AlChE J.*, 2013, **59**, 4364–4372.
137 N. C. Su, D. T. Sun, C. M. Beavers, D. K. Britt, W. L. Queen and J. J. Urban, *Energy Environ. Sci.*, 2016, **9**, 922–931.
138 H. Zhang and Y. Wang, *AlChE J.*, 2016, **62**, 1728–1739.
139 J. Gao, H. Mao, H. Jin, C. Chen, A. Feldhoff and Y. Li, *Microporous Mesoporous Mater.*, 2020, **297**, 110030.
140 E. V. Perez, G. J. D. Kalaw, J. P. Ferraris, K. J. Balkus and I. H. Musselman, *J. Membr. Sci.*, 2017, **530**, 201–212.
141 G. L. Han, Z. Chen, L. F. Cai, Y. H. Zhang, J. F. Tian, H. H. Ma and S. M. Fang, *Sep. Purif. Technol.*, 2019, **220**, 268–275.
142 L. Shu, L.-H. Xie, Y. Meng, T. Liu, C. Zhao and J.-R. Li, *J. Membr. Sci.*, 2020, **603**, 118049.
143 Z. Hu, Z. Kang, Y. Qian, Y. Peng, X. Wang, C. Chi and D. Zhao, *Ind. Eng. Chem. Res.*, 2016, **55**, 7933–7940.
144 J. E. Bachman, Z. P. Smith, T. Li, T. Xu and J. R. Long, *Nat. Mater.*, 2016, **15**, 845–849.
145 L. Xiang, L. Sheng, C. Wang, L. Zhang, Y. Pan and Y. Li, *Adv. Mater.*, 2017, **29**, 1606999.
146 Q. Xin, J. Ouyang, T. Liu, Z. Li, Z. Li, Y. Liu, S. Wang, H. Wu, Z. Jiang and X. Cao, *ACS Appl. Mater. Interfaces*, 2015, **7**, 1065–1077.
147 H. Wang, S. He, X. Qin, C. Li and T. Li, *J. Am. Chem. Soc.*, 2018, **140**, 17203–17210.
148 C. Wu, K. Zhang, H. Wang, Y. Fan, S. Zhang, S. He, F. Wang, Y. Tao, X. Zhao, Y.-B. Zhang, Y. Ma, Y. Lee and T. Li, *J. Am. Chem. Soc.*, 2020, **142**, 18503–18512.
149 Y. Cheng, Y. Ying, L. Zhai, G. Liu, J. Dong, Y. Wang, M. P. Christopher, S. Long, Y. Wang and D. Zhao, *J. Membr. Sci.*, 2019, **573**, 97–106.
150 Q. Qian, A. X. Wu, W. S. Chi, P. A. Asinger, S. Lin, A. Hypsher and Z. P. Smith, *ACS Appl. Mater. Interfaces*, 2019, **11**, 31257–31269.
151 J. Sánchez-Laínez, B. Zornoza, A. F. Orsi, M. M. Łozińska, D. M. Dawson, S. E. Ashbrook, S. M. Francis, P. A. Wright, V. Benoit, P. L. Llewellyn, C. Téllez and J. Coronas, *Chem. – Eur. J.*, 2018, **24**, 11211–11219.
152 Y. Fan, H. Yu, S. Xu, Q. Shen, H. Ye and N. Li, *J. Membr. Sci.*, 2020, **597**, 117775.
153 N. Tien-Binh, H. Vinh-Thang, X. Y. Chen, D. Rodrigue and S. Kaliaguine, *J. Mater. Chem. A*, 2015, **3**, 15202–15213.
154 M. L. Jue and R. P. Lively, *React. Funct. Polym.*, 2015, **86**, 88–110.
155 Z. P. Smith, J. E. Bachman, T. Li, B. Gludovatz, V. A. Kusuma, T. Xu, D. P. Hopkinson, R. O. Ritchie and J. R. Long, *Chem. Mater.*, 2018, **30**, 1484–1495.
156 A. M. Marti, S. R. Venna, E. A. Roth, J. T. Culp and D. P. Hopkinson, *ACS Appl. Mater. Interfaces*, 2018, **10**, 24784–24790.
157 B. Seoane, V. Sebastián, C. Téllez and J. Coronas, *CrystEngComm*, 2013, **15**, 9483–9490.
158 S. Park, M. R. Abdul Hamid and H.-K. Jeong, *ACS Appl. Mater. Interfaces*, 2019, **11**, 25949–25957.
159 R. Lin, L. Ge, L. Hou, E. Strounina, V. Rudolph and Z. Zhu, *ACS Appl. Mater. Interfaces*, 2014, **6**, 5609–5618.
160 N. Tien-Binh, D. Rodrigue and S. Kaliaguine, *J. Membr. Sci*, 2018, **548**, 429–438.
161 N. Tien-Binh, H. Vinh-Thang, X. Y. Chen, D. Rodrigue and S. Kaliaguine, *J. Membr. Sci.*, 2016, **520**, 941–950.
162 C. Satheeshkumar, H. J. Yu, H. Park, M. Kim, J. S. Lee and M. Seo, *J. Mater. Chem. A*, 2018, **6**, 21961–21968.
163 G. Yu, X. Zou, L. Sun, B. Liu, Z. Wang, P. Zhang and G. Zhu, *Adv. Mater.*, 2019, **31**, 1806853.
164 Y. Katayama, K. C. Bentz and S. M. Cohen, *ACS Appl. Mater. Interfaces*, 2019, **11**, 13029–13037.
165 J. Lee, C. Satheeshkumar, H. J. Yu, S. Kim, J. S. Lee, M. Seo and M. Kim, *ACS Appl. Nano Mater.*, 2020, **3**, 9356–9362.
166 H. Wang, S. Tang, Y. Ni, C. Zhang, X. Zhu and Q. Zhao, *J. Membr. Sci.*, 2020, **598**, 117791.
167 T. Zhu, X. Yu, M. Yi and Y. Wang, *ACS Sustainable Chem. Eng.*, 2020, **8**, 12664–12676.
168 Z. Wang, Y. Tian, W. Fang, B. B. Shrestha, M. Huang and J. Jin, *ACS Appl. Mater. Interfaces*, 2021, **13**, 3166–3174.
169 S. Shahid and K. Nijmeijer, *J. Membr. Sci.*, 2014, **459**, 33–44.
170 S. Ishaq, R. Tamime, M. R. Bilad and A. L. Khan, *Sep. Purif. Technol.*, 2019, **210**, 442–451.
171 S. Basu, A. Cano-Odena and I. F. J. Vankelecom, *Sep. Purif. Technol.*, 2011, **81**, 31–40.
172 E. A. Feijani, H. Mahdavi and A. Tavasoli, *Chem. Eng. Res. Des.*, 2015, **96**, 87–102.
173 Y.-H. Deng, J.-T. Chen, C.-H. Chang, K.-S. Liao, K.-L. Tung, W. E. Price, Y. Yamauchi and K. C.-W. Wu, *Angew. Chem., Int. Ed.*, 2016, **55**, 12793–12796.

174 P. Su, X. Zhang, Y. Li, H. Chen, Q. Meng and G. Zhang, *AIChE J.*, 2019, **65**, e16693.
175 B. Ghalei, K. Sakurai, Y. Kinoshita, K. Wakimoto, A. P. Isfahani, Q. Song, K. Doitomi, S. Furukawa, H. Hirao, H. Kusuda, S. Kitagawa and E. Sivaniah, *Nat. Energy*, 2017, **2**, 17086.
176 Y. Cheng, S. R. Tavares, C. M. Doherty, Y. Ying, E. Sarnello, G. Maurin, M. R. Hill, T. Li and D. Zhao, *ACS Appl. Mater. Interfaces*, 2018, **10**, 43095–43103.
177 Y. Cheng, X. Wang, C. Jia, Y. Wang, L. Zhai, Q. Wang and D. Zhao, *J. Membr. Sci.*, 2017, **539**, 213–223.
178 J. Wan, M. Nian, C. Yang, K. Ge, J. Liu, Z. Chen, J. Duan and W. Jin, *J. Membr. Sci.*, 2022, **642**, 119991.
179 E. A. Flügel, A. Ranft, F. Haase and B. V. Lotsch, *J. Mater. Chem.*, 2012, **22**, 10119–10133.
180 K. A. S. Usman, J. W. Maina, S. Seyedin, M. T. Conato, L. M. Payawan, L. F. Dumée and J. M. Razal, *NPG Asia Mater.*, 2020, **12**, 58.
181 N. A. H. M. Nordin, A. F. Ismail, A. Mustafa, R. S. Murali and T. Matsuura, *RSC Adv.*, 2014, **4**, 52530–52541.
182 M. Jia, Y. Feng, J. Qiu, X.-F. Zhang and J. Yao, *Sep. Purif. Technol.*, 2019, **213**, 63–69.
183 S. Castarlenas, C. Téllez and J. Coronas, *J. Membr. Sci.*, 2017, **526**, 205–211.
184 B. Chen, C. Wan, X. Kang, M. Chen, C. Zhang, Y. Bai and L. Dong, *Sep. Purif. Technol.*, 2019, **223**, 113–122.
185 Y. Zhang, Y. Tong, X. Li, S. Guo, H. Zhang, X. Chen, K. Cai, L. Cheng and W. He, *ACS Omega*, 2021, **6**, 18566–18575.
186 R. Lin, L. Ge, S. Liu, V. Rudolph and Z. Zhu, *ACS Appl. Mater. Interfaces*, 2015, **7**, 14750–14757.
187 R. Lin, L. Ge, H. Diao, V. Rudolph and Z. Zhu, *ACS Appl. Mater. Interfaces*, 2016, **8**, 32041–32049.
188 C. Z. Liang, T.-S. Chung and J.-Y. Lai, *Prog. Polym. Sci.*, 2019, **97**, 101141.
189 M. Galizia, W. S. Chi, Z. P. Smith, T. C. Merkel, R. W. Baker and B. D. Freeman, *Macromolecules*, 2017, **50**, 7809–7843.
190 S. Japip, Y. Xiao and T.-S. Chung, *Ind. Eng. Chem. Res.*, 2016, **55**, 9507–9517.
191 J. Sánchez-Laínez, B. Zornoza, S. Friebe, J. Caro, S. Cao, A. Sabetghadam, B. Seoane, J. Gascon, F. Kapteijn, C. Le Guillouzer, G. Clet, M. Daturi, C. Téllez and J. Coronas, *J. Membr. Sci.*, 2016, **515**, 45–53.
192 L. Diestel, N. Wang, A. Schulz, F. Steinbach and J. Caro, *Ind. Eng. Chem. Res.*, 2015, **54**, 1103–1112.
193 S. Kim, E. Shamsaei, X. Lin, Y. Hu, G. P. Simon, J. G. Seong, J. S. Kim, W. H. Lee, Y. M. Lee and H. Wang, *J. Membr. Sci.*, 2018, **549**, 260–266.
194 F. Xiang, A. M. Marti and D. P. Hopkinson, *J. Membr. Sci.*, 2018, **556**, 146–153.
195 C. Zhang, B. Liu, G. Wang, G. Yu, X. Zou and G. Zhu, *Chem. Commun.*, 2019, **55**, 7101–7104.
196 B. A. Al-Maythalony, A. M. Alloush, M. Faizan, H. Dafallah, M. A. A. Elgzoly, A. A. A. Seliman, A. Al-Ahmed, Z. H. Yamani, M. A. M. Habib, K. E. Cordova and O. M. Yaghi, *ACS Appl. Mater. Interfaces*, 2017, **9**, 33401–33407.
197 J. Sánchez-Laínez, A. Veiga, B. Zornoza, S. R. G. Balestra, S. Hamad, A. R. Ruiz-Salvador, S. Calero, C. Téllez and J. Coronas, *J. Mater. Chem. A*, 2017, **5**, 25601–25608.
198 S. C. Hess, R. N. Grass and W. J. Stark, *Chem. Mater.*, 2016, **28**, 7638–7644.
199 T. C. Merkel, H. Lin, X. Wei and R. Baker, *J. Membr. Sci.*, 2010, **359**, 126–139.
200 W. S. Chi, S. Hwang, S.-J. Lee, S. Park, Y.-S. Bae, D. Y. Ryu, J. H. Kim and J. Kim, *J. Membr. Sci.*, 2015, **495**, 479–488.
201 W. S. Chi, S. J. Kim, S.-J. Lee, Y.-S. Bae and J. H. Kim, *ChemSusChem*, 2015, **8**, 650–658.
202 S. Yu, S. Li, S. Huang, Z. Zeng, S. Cui and Y. Liu, *J. Membr. Sci.*, 2017, **540**, 155–164.
203 J. Yuan, H. Zhu, J. Sun, Y. Mao, G. Liu and W. Jin, *ACS Appl. Mater. Interfaces*, 2017, **9**, 38575–38583.
204 S. J. D. Smith, B. P. Ladewig, A. J. Hill, C. H. Lau and M. R. Hill, *Sci. Rep.*, 2015, **5**, 7823.
205 J. Shen, G. Liu, K. Huang, Q. Li, K. Guan, Y. Li and W. Jin, *J. Membr. Sci.*, 2016, **513**, 155–165.
206 M. Mubashir, Y. F. Yeong, K. K. Lau, T. L. Chew and J. Norwahyu, *Sep. Purif. Technol.*, 2018, **199**, 140–151.
207 B. Wang, Z. Qiao, J. Xu, J. Wang, X. Liu, S. Zhao, Z. Wang and M. D. Guiver, *Adv. Mater.*, 2020, **32**, 1907701.
208 S. R. Venna, A. Spore, Z. Tian, A. M. Marti, E. J. Albenze, H. B. Nulwala, N. L. Rosi, D. R. Luebke, D. P. Hopkinson and H. R. Allcock, *J. Membr. Sci.*, 2017, **535**, 103–112.
209 S. R. Venna, M. Lartey, T. Li, A. Spore, S. Kumar, H. B. Nulwala, D. R. Luebke, N. L. Rosi and E. Albenze, *J. Mater. Chem. A*, 2015, **3**, 5014–5022.
210 B.-J. Yao, L.-G. Ding, F. Li, J.-T. Li, Q.-J. Fu, Y. Ban, A. Guo and Y.-B. Dong, *ACS Appl. Mater. Interfaces*, 2017, **9**, 38919–38930.
211 B. Zornoza, A. Martinez-Joaristi, P. Serra-Crespo, C. Tellez, J. Coronas, J. Gascon and F. Kapteijn, *Chem. Commun.*, 2011, **47**, 9522–9524.
212 S. Ma, D. Sun, X.-S. Wang and H.-C. Zhou, *Angew. Chem., Int. Ed.*, 2007, **46**, 2458–2462.
213 N. Prasetya, A. A. Teck and B. P. Ladewig, *Sci. Rep.*, 2018, **8**, 2944.
214 N. Prasetya and B. P. Ladewig, *ACS Appl. Mater. Interfaces*, 2018, **10**, 34291–34301.
215 N. Prasetya, B. C. Donose and B. P. Ladewig, *J. Mater. Chem. A*, 2018, **6**, 16390–16402.
216 S. Hwang, W. S. Chi, S. J. Lee, S. H. Im, J. H. Kim and J. Kim, *J. Membr. Sci.*, 2015, **480**, 11–19.
217 X. Wu, W. Liu, H. Wu, X. Zong, L. Yang, Y. Wu, Y. Ren, C. Shi, S. Wang and Z. Jiang, *J. Membr. Sci.*, 2018, **548**, 309–318.
218 Q. Xin, T. Liu, Z. Li, S. Wang, Y. Li, Z. Li, J. Ouyang, Z. Jiang and H. Wu, *J. Membr. Sci.*, 2015, **488**, 67–78.
219 A. Sabetghadam, B. Seoane, D. Keskin, N. Duim, T. Rodenas, S. Shahid, S. Sorribas, C. L. Guillouzer, G. Clet, C. Tellez, M. Daturi, J. Coronas, F. Kapteijn and J. Gascon, *Adv. Funct. Mater.*, 2016, **26**, 3154–3163.
220 Z. Wang, H. Ren, S. Zhang, F. Zhang and J. Jin, *J. Mater. Chem. A*, 2017, **5**, 10968–10977.

221 L. Ma, F. Svec, T. Tan and Y. Lv, *ACS Appl. Nano Mater.*, 2018, **1**, 2808–2818.
222 G. Liu, Y. Labreche, V. Chernikova, O. Shekhah, C. Zhang, Y. Belmabkhout, M. Eddaoudi and W. J. Koros, *J. Membr. Sci.*, 2018, **565**, 186–193.
223 A. Kertik, L. H. Wee, M. Pfannmöller, S. Bals, J. A. Martens and I. F. J. Vankelecom, *Energy Environ. Sci.*, 2017, **10**, 2342–2351.
224 S. Shahid, K. Nijmeijer, S. Nehache, I. Vankelecom, A. Deratani and D. Quemener, *J. Membr. Sci.*, 2015, **492**, 21–31.
225 G. Liu, A. Cadiau, Y. Liu, K. Adil, V. Chernikova, I.-D. Carja, Y. Belmabkhout, M. Karunakaran, O. Shekhah, C. Zhang, A. K. Itta, S. Yi, M. Eddaoudi and W. J. Koros, *Angew. Chem., Int. Ed.*, 2018, **57**, 14811–14816.
226 S. H. Kunjattu, V. Ashok, A. Bhaskar, K. Pandare, R. Banerjee and U. K. Kharul, *J. Membr. Sci.*, 2018, **549**, 38–45.
227 H. An, S. Park, H. T. Kwon, H.-K. Jeong and J. S. Lee, *J. Membr. Sci.*, 2017, **526**, 367–376.
228 Y. Liu, Z. Chen, G. Liu, Y. Belmabkhout, K. Adil, M. Eddaoudi and W. Koros, *Adv. Mater.*, 2019, **31**, 1807513.
229 Q. Xin, K. An, Y. Zhang, M. Yun, S. Wang, L. Lin, H. Ye, X. Ding, H. Li and Y. Zhang, *J. Membr. Sci.*, 2021, **620**, 118908.
230 X. Li, Y. Zhang, Q. Xin, X. Ding, L. Zhao, H. Ye, L. Lin, H. Li and Y. Zhang, *Chem. Eng. J.*, 2022, **428**, 132595.
231 S. Sorribas, P. Gorgojo, C. Téllez, J. Coronas and A. G. Livingston, *J. Am. Chem. Soc.*, 2013, **135**, 15201–15208.
232 Z. Zhai, N. Zhao, W. Dong, P. Li, H. Sun and Q. J. Niu, *ACS Appl. Mater. Interfaces*, 2019, **11**, 12871–12879.
233 C. Echaide-Górriz, S. Sorribas, C. Téllez and J. Coronas, *RSC Adv.*, 2016, **6**, 90417–90426.
234 Y.-y Zhao, Y.-l Liu, X.-m Wang, X. Huang and Y. F. Xie, *ACS Appl. Mater. Interfaces*, 2019, **11**, 13724–13734.
235 L. Liu, X. Xie, S. Qi, R. Li, X. Zhang, X. Song and C. Gao, *J. Membr. Sci.*, 2019, **580**, 101–109.
236 Y. Lin, Y. Chen and R. Wang, *J. Membr. Sci.*, 2019, **589**, 117249–117261.
237 R. Dai, X. Zhang, M. Liu, Z. Wu and Z. Wang, *J. Membr. Sci.*, 2019, **573**, 46–54.
238 M. He, L. Wang, Y. Lv, X. Wang, J. Zhu, Y. Zhang and T. Liu, *Chem. Eng. J.*, 2020, **389**, 124452.
239 S. F. Seyedpour, A. Rahimpour and G. Najafpour, *J. Membr. Sci.*, 2019, **573**, 257–269.
240 A. Zirehpour, A. Rahimpour and M. Ulbricht, *J. Membr. Sci.*, 2017, **531**, 59–67.
241 J. Duan, Y. Pan, F. Pacheco, E. Litwiller, Z. Lai and I. Pinnau, *J. Membr. Sci.*, 2015, **476**, 303–310.
242 C. Van Goethem, R. Verbeke, M. Pfanmöller, T. Koschine, M. Dickmann, T. Timpel-Lindner, W. Egger, S. Bals and I. F. J. Vankelecom, *J. Membr. Sci.*, 2018, **563**, 938–948.
243 J. Zhu, J. Hou, S. Yuan, Y. Zhao, Y. Li, R. Zhang, M. Tian, J. Li, J. Wang and B. Van der Bruggen, *J. Mater. Chem. A*, 2019, **7**, 16313–16322.
244 D. Ma, S. B. Peh, G. Han and S. B. Chen, *ACS Appl. Mater. Interfaces*, 2017, **9**, 7523–7534.
245 X. Zhang, Y. Zhang, T. Wang, Z. Fan and G. Zhang, *RSC Adv.*, 2019, **9**, 24802–24810.
246 Y. Gong, S. Gao, Y. Tian, Y. Zhu, W. Fang, Z. Wang and J. Jin, *J. Membr. Sci.*, 2020, **600**, 117874–117881.
247 N. Wang, T. Liu, H. Shen, S. Ji, J.-R. Li and R. Zhang, *AlChE J.*, 2016, **62**, 538–546.
248 X. Cheng, X. Jiang, Y. Zhang, C. H. Lau, Z. Xie, D. Ng, S. J. D. Smith, M. R. Hill and L. Shao, *ACS Appl. Mater. Interfaces*, 2017, **9**, 38877–38886.
249 Z. Rao, K. Feng, B. Tang and P. Wu, *ACS Appl. Mater. Interfaces*, 2017, **9**, 2594–2605.
250 Y. Meng, L. Shu, L. Liu, Y. Wu, L.-H. Xie, M.-J. Zhao and J.-R. Li, *J. Membr. Sci.*, 2019, **591**, 117360–117368.
251 H. Wang, S. Zhao, Y. Liu, R. Yao, X. Wang, Y. Cao, D. Ma, M. Zou, A. Cao, X. Feng and B. Wang, *Nat. Commun.*, 2019, **10**, 4204.
252 J. Zhu, L. Qin, A. Uliana, J. Hou, J. Wang, Y. Zhang, X. Li, S. Yuan, J. Li, M. Tian, J. Lin and B. Van der Bruggen, *ACS Appl. Mater. Interfaces*, 2017, **9**, 1975–1986.
253 Y. Zhang, N. Wang, S. Ji, R. Zhang, C. Zhao and J.-R. Li, *J. Membr. Sci.*, 2015, **489**, 144–152.
254 G. Liu, Z. Jiang, K. Cao, S. Nair, X. Cheng, J. Zhao, H. Gomaa, H. Wu and F. Pan, *J. Membr. Sci.*, 2017, **523**, 185–196.
255 X. Cheng, Z. Jiang, X. Cheng, H. Yang, L. Tang, G. Liu, M. Wang, H. Wu, F. Pan and X. Cao, *J. Membr. Sci.*, 2018, **555**, 146–156.
256 Y. M. Xu, S. Japip and T.-S. Chung, *J. Membr. Sci.*, 2018, **549**, 217–226.
257 Y. M. Xu, S. Japip and T.-S. Chung, *J. Membr. Sci.*, 2020, **595**, 117571.
258 G. Wu, M. Jiang, T. Zhang and Z. Jia, *J. Membr. Sci.*, 2016, **507**, 72–80.
259 W. Zhang, Y. Ying, J. Ma, X. Guo, H. Huang, D. Liu and C. Zhong, *J. Membr. Sci.*, 2017, **527**, 8–17.
260 Q. Li, Q. Liu, J. Zhao, Y. Hua, J. Sun, J. Duan and W. Jin, *J. Membr. Sci.*, 2017, **544**, 68–78.
261 J. Campbell, R. P. Davies, D. C. Braddock and A. G. Livingston, *J. Mater. Chem. A*, 2015, **3**, 9668–9674.
262 J. Campbell, J. D. S. Burgal, G. Szekely, R. P. Davies, D. C. Braddock and A. Livingston, *J. Membr. Sci.*, 2016, **503**, 166–176.
263 X. Guo, D. Liu, T. Han, H. Huang, Q. Yang and C. Zhong, *AIChE J.*, 2017, **63**, 1303–1312.
264 J. Dai, S. Li, J. Liu, J. He, J. Li, L. Wang and J. Lei, *J. Membr. Sci.*, 2019, **589**, 117261.
265 Y. Li, J. Li, R. B. Soria, A. Volodine and B. Van der Bruggen, *J. Membr. Sci.*, 2020, **603**, 118002.
266 H. Liu, M. Zhang, H. Zhao, Y. Jiang, G. Liu and J. Gao, *RSC Adv.*, 2020, **10**, 4045–4057.
267 C. Echaide-Górriz, M. Navarro, C. Téllez and J. Coronas, *Dalton Trans.*, 2017, **46**, 6244–6252.
268 S. Das, S. Xu, T. Ben and S. Qiu, *Angew. Chem., Int. Ed.*, 2018, **57**, 8629–8633.
269 Y. Lu, H. Zhang, J. Y. Chan, R. Ou, H. Zhu, M. Forsyth, E. M. Marijanovic, C. M. Doherty, P. J. Marriott,

M. M. B. Holl and H. Wang, *Angew. Chem., Int. Ed.*, 2019, **58**, 16928–16935.
270 M. Zhang, Z.-J. Pu, X.-L. Chen, X.-L. Gong, A.-X. Zhu and L.-M. Yuan, *Chem. Commun.*, 2013, **49**, 5201–5203.
271 F. Song, C. Wang and W. Lin, *Chem. Commun.*, 2011, **47**, 8256–8258.
272 S. Lee, E. A. Kapustin and O. M. Yaghi, *Science*, 2016, **353**, 808–811.
273 A. Pustovarenko, M. G. Goesten, S. Sachdeva, M. Shan, Z. Amghouz, Y. Belmabkhout, A. Dikhtiarenko, T. Rodenas, D. Keskin, I. K. Voets, B. M. Weckhuysen, M. Eddaoudi, L. C. P. M. de Smet, E. J. R. Sudhölter, F. Kapteijn, B. Seoane and J. Gascon, *Adv. Mater.*, 2018, **30**, 1707234.
274 Q. Wang and D. Astruc, *Chem. Rev.*, 2020, **120**, 1438–1511.
275 Ó. de la Iglesia, S. Sorribas, E. Almendro, B. Zornoza, C. Téllez and J. Coronas, *Renewable Energy*, 2016, **88**, 12–19.
276 S. Sorribas, A. Kudasheva, E. Almendro, B. Zornoza, Ó. de la Iglesia, C. Téllez and J. Coronas, *Chem. Eng. Sci.*, 2015, **124**, 37–44.
277 L. F. Dumée, J. W. Maina, A. Merenda, R. Reis, L. He and L. Kong, *J. Membr. Sci.*, 2017, **528**, 217–224.
278 W.-L. Jiang, L.-G. Ding, B.-J. Yao, J.-C. Wang, G.-J. Chen, Y.-A. Li, J.-P. Ma, J. Ji, Y. Dong and Y.-B. Dong, *Chem. Commun.*, 2016, **52**, 13564–13567.
279 J. W. Maina, J. A. Schütz, L. Grundy, E. Des Ligneris, Z. Yi, L. Kong, C. Pozo-Gonzalo, M. Ionescu and L. F. Dumée, *ACS Appl. Mater. Interfaces*, 2017, **9**, 35010–35017.
280 Y. Jiang, J. Sun, X. Yang, J. Shen, Y. Fu, Y. Fan, J. Xu and L. Wang, *Inorg. Chem.*, 2021, **60**, 2087–2096.
281 K. Varoon, X. Zhang, B. Elyassi, D. D. Brewer, M. Gettel, S. Kumar, J. A. Lee, S. Maheshwari, A. Mittal, C.-Y. Sung, M. Cococcioni, L. F. Francis, A. V. McCormick, K. A. Mkhoyan and M. Tsapatsis, *Science*, 2011, **334**, 72–75.
282 M. Y. Jeon, D. Kim, P. Kumar, P. S. Lee, N. Rangnekar, P. Bai, M. Shete, B. Elyassi, H. S. Lee, K. Narasimharao, S. N. Basahel, S. Al-Thabaiti, W. Xu, H. J. Cho, E. O. Fetisov, R. Thyagarajan, R. F. DeJaco, W. Fan, K. A. Mkhoyan, J. I. Siepmann and M. Tsapatsis, *Nature*, 2017, **543**, 690–694.
283 J. N. Coleman, M. Lotya, A. O'Neill, S. D. Bergin, P. J. King, U. Khan, K. Young, A. Gaucher, S. De, R. J. Smith, I. V. Shvets, S. K. Arora, G. Stanton, H.-Y. Kim, K. Lee, G. T. Kim, G. S. Duesberg, T. Hallam, J. J. Boland, J. J. Wang, J. F. Donegan, J. C. Grunlan, G. Moriarty, A. Shmeliov, R. J. Nicholls, J. M. Perkins, E. M. Grieveson, K. Theuwissen, D. W. McComb, P. D. Nellist and V. Nicolosi, *Science*, 2011, **331**, 568–571.
284 A. Abhervé, S. Mañas-Valero, M. Clemente-León and E. Coronado, *Chem. Sci.*, 2015, **6**, 4665–4673.
285 Y. Ding, Y.-P. Chen, X. Zhang, L. Chen, Z. Dong, H.-L. Jiang, H. Xu and H.-C. Zhou, *J. Am. Chem. Soc.*, 2017, **139**, 9136–9139.
286 H.-S. Wang, J. Li, J.-Y. Li, K. Wang, Y. Ding and X.-H. Xia, *NPG Asia Mater.*, 2017, **9**, e354.
287 W.-J. Song, *Talanta*, 2017, **170**, 74–80.
288 P.-Z. Li, Y. Maeda and Q. Xu, *Chem. Commun.*, 2011, **47**, 8436–8438.
289 K. Kouroupis-Agalou, A. Liscio, E. Treossi, L. Ortolani, V. Morandi, N. M. Pugno and V. Palermo, *Nanoscale*, 2014, **6**, 5926–5933.
290 T. Kambe, R. Sakamoto, K. Hoshiko, K. Takada, M. Miyachi, J.-H. Ryu, S. Sasaki, J. Kim, K. Nakazato, M. Takata and H. Nishihara, *J. Am. Chem. Soc.*, 2013, **135**, 2462–2465.
291 S. Zhao, Y. Wang, J. Dong, C.-T. He, H. Yin, P. An, K. Zhao, X. Zhang, C. Gao, L. Zhang, J. Lv, J. Wang, J. Zhang, A. M. Khattak, N. A. Khan, Z. Wei, J. Zhang, S. Liu, H. Zhao and Z. Tang, *Nat. Energy*, 2016, **1**, 16184.
292 M. Zhao, Y. Wang, Q. Ma, Y. Huang, X. Zhang, J. Ping, Z. Zhang, Q. Lu, Y. Yu, H. Xu, Y. Zhao and H. Zhang, *Adv. Mater.*, 2015, **27**, 7372–7378.
293 S. C. Junggeburth, L. Diehl, S. Werner, V. Duppel, W. Sigle and B. V. Lotsch, *J. Am. Chem. Soc.*, 2013, **135**, 6157–6164.
294 L. Cao, Z. Lin, F. Peng, W. Wang, R. Huang, C. Wang, J. Yan, J. Liang, Z. Zhang, T. Zhang, L. Long, J. Sun and W. Lin, *Angew. Chem., Int. Ed.*, 2016, **55**, 4962–4966.
295 Y. Sakata, S. Furukawa, M. Kondo, K. Hirai, N. Horike, Y. Takashima, H. Uehara, N. Louvain, M. Meilikhov, T. Tsuruoka, S. Isoda, W. Kosaka, O. Sakata and S. Kitagawa, *Science*, 2013, **339**, 193–196.
296 M. Shete, P. Kumar, J. E. Bachman, X. Ma, Z. P. Smith, W. Xu, K. A. Mkhoyan, J. R. Long and M. Tsapatsis, *J. Membr. Sci*, 2018, **549**, 312–320.
297 Y. Peng, Y. Li, Y. Ban and W. Yang, *Angew. Chem., Int. Ed.*, 2017, **56**, 9757–9761.
298 Y. Li, L. Lin, M. Tu, P. Nian, A. J. Howarth, O. K. Farha, J. Qiu and X. Zhang, *Nano Res*, 2017, **11**, 1850–1860.
299 B. Seoane, J. Coronas, I. Gascon, M. E. Benavides, O. Karvan, J. Caro, F. Kapteijn and J. Gascon, *Chem. Soc. Rev.*, 2015, **44**, 2421–2454.
300 Y. Yang, K. Goh, R. Wang and T.-H. Bae, *Chem. Commun.*, 2017, **53**, 4254–4257.
301 C. Li, C. Wu and B. Zhang, *ACS Sustainable Chem. Eng.*, 2020, **8**, 642–648.
302 S. J. Datta, A. Mayoral, N. M. S. Bettahalli, P. M. Bhatt, M. Karunakaran, I. D. Carja, D. Fan, P. G. M. Mileo, R. Semino, G. Maurin, O. Terasaki and M. Eddaoudi, *Science*, 2022, **376**, 1080–1087.
303 S. Feng, M. Bu, J. Pang, W. Fan, L. Fan, H. Zhao, G. Yang, H. Guo, G. Kong, H. Sun, Z. Kang and D. Sun, *J. Membr. Sci.*, 2020, **593**, 117404.
304 J. Deng, Z. Dai, J. Hou and L. Deng, *Chem. Mater.*, 2020, **32**, 4174–4184.
305 Z. Kang, Y. Peng, Z. Hu, Y. Qian, C. Chi, L. Y. Yeo, L. Tee and D. Zhao, *J. Mater. Chem. A*, 2015, **3**, 20801–20810.
306 X. Ma, X. Wu, J. Caro and A. Huang, *Angew. Chem., Int. Ed.*, 2019, **58**, 16156–16160.
307 O. Kwon, J. Y. Kim, S. Park, J. H. Lee, J. Ha, H. Park, H. R. Moon and J. Kim, *Nat. Commun.*, 2019, **10**, 3620.
308 G. Avci, I. Erucar and S. Keskin, *ACS Appl. Mater. Interfaces*, 2020, **12**, 41567–41579.

309 C. E. Wilmer, M. Leaf, C. Y. Lee, O. K. Farha, B. G. Hauser, J. T. Hupp and R. Q. Snurr, *Nat. Chem.*, 2012, **4**, 83–89.
310 P. Z. Moghadam, A. Li, S. B. Wiggin, A. Tao, A. G. P. Maloney, P. A. Wood, S. C. Ward and D. Fairen-Jimenez, *Chem. Mater.*, 2017, **29**, 2618–2625.
311 S. Chong, S. Lee, B. Kim and J. Kim, *Coord. Chem. Rev.*, 2020, **423**, 213487.
312 M. Zhou, A. Vassallo and J. Wu, *J. Membr. Sci.*, 2020, **598**, 117675.
313 J. Ma, X. Guo, Y. Ying, D. Liu and C. Zhong, *Chem. Eng. J.*, 2017, **313**, 890–898.
314 P. Zhang, J.-L. Gong, G.-M. Zeng, B. Song, H.-Y. Liu, S.-Y. Huan and J. Li, *Chemosphere*, 2018, **204**, 378–389.
315 W. Li, Y. Zhang, P. Su, Z. Xu, G. Zhang, C. Shen and Q. Meng, *J. Mater. Chem. A*, 2016, **4**, 18747–18752.
316 K. Eum, S. Yang, B. Min, C. Ma, J. H. Drese, Y. Tamhankar and S. Nair, *ACS Appl. Mater. Interfaces*, 2020, **12**, 27368–27377.
317 J. Fu, S. Das, G. Xing, T. Ben, V. Valtchev and S. Qiu, *J. Am. Chem. Soc.*, 2016, **138**, 7673–7680.
318 H. Jin, A. Wollbrink, R. Yao, Y. Li, J. Caro and W. Yang, *J. Membr. Sci.*, 2016, **513**, 40–46.
319 N. C. Burtch, J. Heinen, T. D. Bennett, D. Dubbeldam and M. D. Allendorf, *Adv. Mater.*, 2018, **30**, 1704124.

